JETP Letters, Vol. 74, No. 10, 2001, pp. 481–485. From Pis'ma v Zhurnal Éksperimental'noĭ i Teoreticheskoĭ Fiziki, Vol. 74, No. 10, 2001, pp. 541–545.

On the Initial-Boundary Value Problems for Soliton Equations[1]

A. Degasperis[1, 2], S. V. Manakov[3], and P. M. Santini[1, 2]

[1] *Dipartimento di Fisica, Università di Roma "La Sapienza," I-00185 Roma, Italy*
e-mail: antonio.degasperis@roma1.infn.it, paolo.santini@roma1.infn.it
[2] *Istituto Nazionale di Fisica Nucleare, Sezione di Roma, I-00185 Roma, Italy*
[3] *Landau Institute for Theoretical Physics, Russian Academy of Sciences, ul. Kosygina 2, Moscow, 117334 Russia*
e-mail: manakov@itp.ac.ru

Received October 31, 2001

We present a novel approach to solving initial-boundary value problems on the segment and the half line for soliton equations. Our method is illustrated by solving a prototypal and widely applied dispersive soliton equation—the celebrated nonlinear Schroedinger equation. It is well known that the basic difficulty associated with boundaries is that some coefficients of the evolution equation of the (x) scattering matrix $S(k, t)$ depend on unknown boundary data. In this paper, we overcome this difficulty by expressing the unknown boundary data in terms of elements of the scattering matrix itself to obtain a nonlinear integrodifferential evolution equation for $S(k, t)$. We also sketch an alternative approach in the semiline case on the basis of a nonlinear equation for $S(k, t)$, which does not contain unknown boundary data; in this way, the "linearizable" boundary value problems correspond to the cases in which $S(k, t)$ can be found by solving a linear Riemann–Hilbert problem. © *2001 MAIK "Nauka/Interperiodica".*

PACS numbers: 02.30.Jr; 05.45.Yv

1. Initial-boundary value (IBV) problems for partial differential equations play an important role in applications to physics and, in general, to natural sciences.

Since the discovery of the inverse scattering (spectral) transform method to solve the IBV problem on the infinite line with vanishing boundary conditions for a class of distinguished nonlinear evolution equations, like the Korteweg de Vries (KdV), nonlinear Schrödinger (NLS), and sine Gordon (SG) equations (see, e.g., [1]), several attempts have been made to extend this method to the case of more complicated IBV problems, in which Dirichelet and/or Neumann boundary conditions are prescribed on the semi-infinite line or on the segment. It is well known that the basic difficulty associated with these problems is that the evolution equation of the traditional x-scattering matrix $S(k, t)$, as given by the Lax equations, cannot be integrated in most of the cases, because its coefficients depend on unknown boundary data.

Different approaches to the study of IBV problems for soliton equations have been developed during the last few years. In [2], an "elbow scattering" in the (x, t) plane was introduced to deal with the semiline problem for KdV, leading to a Gel'fand–Levitan–Marchenko formulation. In [3, 4] a different approach, based on a simultaneous x–t spectral transform, was introduced and rigorously developed [5, 6] to solve IBV problems for soliton equations on the semiline. It allows one to obtain a rigorous asymptotic behavior [7] and capture, in a natural way of the known cases of linearizable boundaries. In the case in which the Dirichelet condition $q(0, t)$ is given for the semiline problem for NLS, the unknown boundary $q_x(0, t)$ is obtained through a nonlinear Volterra equation, whose solution exists without a small norm assumption [5]. This approach also proved to be useful for treating linear equations on arbitrary convex polygonal domains [8–10].

In some distinguished cases of soliton equations corresponding to singular dispersion relations, like the stimulated Raman scattering (SRS) equations and the SG equation in light-cone coordinates, the evolution equation of the scattering matrix does not contain unknown boundary data. The SG equation on the semiline was treated using the x–t spectral transform [3, 6]; the SRS and the SG equations on the semiline were also treated using a more traditional x-transform method, respectively, in [11] and in [12]; the x-spectral data used in this last approach satisfy a nonlinear evolution equation of the Riccati type.

We finally remark that IBV problems for C-integrable equations were also considered [13]. In particular, for the Burgers equation, the problem reduces to that of solving a nonlinear Volterra equation.

In this paper, we present a novel approach to the solution of IBV problems on the segment and on the

[1] This article was submitted by the authors in English.

half line for soliton equations. In our approach, we overcome the difficulty associated with unknown boundaries using the analyticity properties of the spectral matrix, which allow one to express the unknown boundary data in terms of elements of the scattering matrix itself and obtain a closed nonlinear integrodifferential evolution equation of novel type for the spectral matrix $S(k, t)$. The approach is illustrated by the prototypal example of the NLS equation

$$iq_t + q_{xx} + c|q|^2 q = 0, \quad q = q(x, t), \tag{1}$$

where c is an arbitrary real parameter, which describes the amplitude modulation of a wave packet in a strongly dispersive and weakly nonlinear medium, but applies as well to most of the known examples of dispersive soliton equations in 1 + 1 dimensions, like the KdV and the modified KdV equations. When applied to the SG equation in light-cone coordinates, the spectral matrix used in our approach satisfies a linear evolution equation.

For the NLS Eq. (1), we consider the following basic IBV problems.

The NLS equation on the segment. We look for the solution $q(x, t)$ of the NLS Eq. (1) in the closed domain $0 \le x \le L$, $0 \le t \le T$ satisfying the initial condition $q(x, 0) = u(x)$ and one of the following three boundary conditions:

$$q(o, t) = v_0(t), \quad q(L, t) = v_L(t), \tag{2}$$

$$q_x(0, t) = w_0(t), \quad q_x(L, t) = w_L(t), \tag{3}$$

$$\begin{aligned} q(0, t) + a_0 q_x(0, t) &= f_0(t), \\ q(L, t) + a_L q_x(L, t) &= f_L(t), \end{aligned} \tag{4}$$

where a_0 and a_L are arbitrary real constants.

The problems on the half line $x \in [0, \infty)$ and on the line $x \in (-\infty, \infty)$ can obviously be viewed as limiting cases of the problem on the segment.

2. To solve the above problems, we make essential use of the fact that the NLS Eq. (1) is the integrability condition of the following system of linear 2×2 matrix equations (the well-known Lax pair) [14]:

$$\begin{aligned} &\text{a)} \quad \Psi_x = (ik\sigma_3 + Q)\Psi, \\ &\text{b)} \quad \Psi_t = (2ik^2\sigma_3 + \tilde{Q})\Psi + \Psi C, \end{aligned} \tag{5}$$

where $\sigma_3 = \mathrm{diag}(1, -1)$, C is an arbitrary x-independent matrix, and

$$\begin{aligned} Q(x, t) &= \begin{pmatrix} 0 & -c\bar{q}(x, t) \\ q(x, t) & 0 \end{pmatrix}, \\ \tilde{Q}(x, t) &= 2kQ - i\sigma_3 Q_x + iQ^2\sigma_3. \end{aligned} \tag{6}$$

As in the traditional spectral transform method, the Jost solutions $\Psi_+(x, t, k)$ and $\Psi_-(x, t, k)$ in Eqs. (5) are defined by the following conditions:

$$\Psi_-(0, t, k) = I, \quad \Psi_+(L, t, k) = e^{ikL\sigma_3} \tag{7}$$

and the scattering matrix $S(k, t)$ is introduced by the following relation:

$$\Psi_+(x, t, k) = \Psi_-(x, t, k)S(k, t). \tag{8}$$

It is well known that the Jost solutions and the scattering matrix have a unit determinant; it is also well known that, with Q given by Eq. (6), they have the following structures:

$$\begin{aligned} \Psi_\pm(x, k) &= \begin{pmatrix} \psi_{\pm 11}(k) & -c\overline{\psi_{\pm 21}(\bar{k})} \\ \psi_{\pm 21}(k) & \overline{\psi_{\pm 11}(\bar{k})} \end{pmatrix}, \\ S(k) &= \begin{pmatrix} \alpha(k) & -c\overline{\beta(\bar{k})} \\ \beta(k) & \overline{\alpha(\bar{k})} \end{pmatrix}. \end{aligned} \tag{9}$$

It is straightforward to show that $M := \Psi_+(x, t, k)e^{-ikx\sigma_3}$, $N := Y_-(x, t, k)e^{-ikx\sigma_3}$ and $S(k, t)$ are entire analytic functions of k. The first column of N is analytic in the lower half k plane (LHP) with asymptotic form

$$\begin{pmatrix} N_{11}(k) \\ N_{21}(k) \end{pmatrix} = \begin{pmatrix} 1 + O(k^{-1}) \\ q/2ik + O(k^{-2}) \end{pmatrix} \tag{10}$$

and grows exponentially like $e^{-2ikx}O(k^{-1})$ in the upper half plane (UHP), combining both behaviors (power-law decay and exponential oscillation) on the real axis. The first column of M is analytic in the UHP with the asymptotic expression (10) and grows exponentially in the LHP like $e^{2ik(L-x)}O(k^{-1})$, combining both behaviors (power-law decay and exponential oscillation) on the real axis. The analyticity properties and the asymptotic behavior of the second column follow from Eqs. (9). The scattering matrix $S(k, t) = M(0, t, k)$ shares the analyticity properties of M, and its asymptotic forms are written down below in some detail for future use.

$$\alpha(k) = \begin{cases} 1 + \dfrac{c}{2ik}\displaystyle\int_0^L dx|q|^2 + O(k^{-2}), & \mathrm{Im}k > 0 \\ e^{2ikL}\left(-\dfrac{c}{(2ik)^2}v_0 v_L + O(k^{-3})\right), & \mathrm{Im}k < 0; \end{cases} \tag{11}$$

$$\beta(k) = \begin{cases} \dfrac{1}{2ik}v_0 - \dfrac{1}{(2ik)^2}\beta_0 + O(k^{-3}), & \mathrm{Im}k > 0 \\ e^{2ikL}\left(-\dfrac{1}{2ik}v_L + \dfrac{1}{(2ik)^2}\beta_L + O(k^{-3})\right), & \mathrm{Im}k < 0, \end{cases} \tag{12}$$

where

$$\beta_0 = w_0 - c v_0 \int_0^L dx|q|^2 \quad \text{and} \quad \beta_L = w_L + c v_L \int_0^L dx|q|^2.$$

The direct problem is the mapping from the initial condition $q(x, 0) = u(x)$ to the elements $\alpha(k, 0)$, $\beta(k, 0)$ of the scattering matrix at $t = 0$.

The inverse problem is the mapping from the evolved elements $\alpha(k, t)$, $\beta(k, t)$ of the scattering matrix (or, more precisely, from the evolved spectral data) to the NLS field $q(x, t)$. This problem does not differ from the case of NLS on the line, and we refer to the classical literature [14, 1] for details.

3. The intermediate step, the t evolution of the scattering data, is where our approach introduces some important novelties. Using Eq. (5b), one can show that the time evolution of the scattering matrix $S(k, t) = \Psi_+(0, t, k)$ is governed by the following matrix equation:

$$\begin{aligned} S_t &= 2ik^2[\sigma_3, S] \\ &- \tilde{Q}(0, t, k)S - Se^{-ikL\sigma_3}\tilde{Q}(L, t, k)e^{ikL\sigma_3}, \end{aligned} \tag{13}$$

which takes the following form for the relevant components:

$$\begin{aligned} \alpha_t(k) &= c[i(|v_L|^2 - |v_0|^2)\alpha(k) \\ &+ (2kv_L + iw_L)e^{2ikL}\overline{\beta(\bar{k})} - (2k\bar{v}_0 - i\bar{w}_0)\beta(k)], \\ \beta_t(k) &= -4ik^2\beta(k) + (2kv_0 + iw_0)\alpha(k) \\ &- (2kv_L + iw_L)e^{2ikL}\overline{\alpha(\bar{k})} + ic(|v_L|^2 + |v_0|^2)\beta(k). \end{aligned} \tag{14}$$

This system of equations depends on known, as well as unknown, boundary data and cannot be used, as it is, to obtain $\alpha(k, t)$ and $\beta(k, t)$. This basic difficulty can be simply overcome using the analytic properties of α, β and their asymptotic expansions (11) and (12), which allow one to express the unknown boundary data in terms of known ones and α, β, thus obtaining the desired closed evolution equation. It is easy to show that the following formulas take place:

$$\begin{aligned} w_0(t) &= -\frac{2}{\pi}v_0(t)\int_{-\infty}^{\infty} dk[\alpha_+(k, t) - 1] \\ &+ \frac{4i}{\pi}\int_{-\infty}^{\infty} dk\left[k\beta_-(k, t) + \frac{iv_0(t)}{2} - \frac{iv_L(t)}{2}\cos 2kL\right], \\ w_L(t) &= \frac{2}{\pi}v_L(t)\int_{-\infty}^{\infty} dk[\alpha_+(k, t) - 1] \\ &+ \frac{4i}{\pi}\int_{-\infty}^{\infty} dk\Big[k\cos 2kL\beta_-(k, t) \\ &- ik\sin 2kL\beta_+(k, t) + \frac{iv_0(t)}{2}\cos 2kL - \frac{iv_L(t)}{2}\Big], \\ v_0(t) &= -\frac{2}{\pi}\int_{-\infty}^{\infty} dk\beta_+(k, t), \\ v_L(t) &= -\frac{2}{\pi}\int_{-\infty}^{\infty} dk[\cos 2kL\beta_+(k, t) - i\sin 2kL\beta_-(k, t)], \end{aligned} \tag{15, 16}$$

where $\alpha_\pm(k)$ ($\beta_\pm(k)$) are the even and odd parts of $\alpha(k)$ ($\beta(k)$) $\alpha_\pm(k) = (\alpha(k) \pm \alpha(-k))/2$, $\beta_\pm(k) = (\beta(k) \pm \beta(-k))/2$.

Therefore the t evolution of the scattering data corresponding to the initial-boundary value problems (2), (3), or (4) is given by the system of Eqs. (14) [with the initial conditions $\alpha(k, 0)$ and $\beta(k, 0)$ obtained from the direct problem], in which the unknown boundary data are replaced by Eqs. (15) or (16).

For example, the time evolution of $S(k, t)$ for the boundary condition (2) is given by Eq. (14) with $w_0(t)$ and $w_L(t)$ replaced by Eqs. (15), and so on.

Of course, our method of solution applies also to the *linear* Schrodinger equation. By analogy with this case, it is possible to prove that the solutions $\alpha(k, t)$ and $\beta(k, t)$ of the above nonlinear integrodifferential evolution equations are unique. This is in full agreement with PDE theory, in which the boundary values (2), (3), and (4) are necessary and sufficient to obtain one and only one solution $q(x, t)$ with given initial condition. It is interesting to note that, if we replaced not only the unknown boundary conditions, but also the assigned ones by their spectral representations, then the nonlinear evolutions would loose uniqueness and the solutions would depend on arbitrary functions of time (which could, therefore, be interpreted as the "illegitimately suppressed" boundary data).

The initial-boundary value problems for NLS on the semiline $x \in [0, \infty)$ are easily obtained from the above treatment in the limit $L \longrightarrow \infty$, assuming a sufficiently fast vanishing at $x \longrightarrow \infty$ of the relevant fields and, hence, setting $v_L = w_L = f_L = 0$.

In the semiline case, the first columns of $M(x, t, k)$ and $S(k, t)$ are analytic in the UHP. The asymptotic behavior of the scattering matrix reads

$$\begin{aligned} \alpha(k) &= 1 + \frac{c}{2ik}\int_0^{\infty} dx|q|^2 + O(k^{-2}), \quad \mathrm{Im}k \geq 0, \\ \beta(k) &= \frac{1}{2ik}v_0 - \frac{1}{(2ik)^2}\left(w_0 - cv_0\int_0^{\infty} dx|q|^2\right) + O(k^{-3}), \\ &\mathrm{Im}k \geq 0. \end{aligned} \tag{17}$$

The inverse problem is unchanged and the t evolutions of the scattering data corresponding to our initial-boundary value problems are given now by the equation

$$S_t = 2ik^2[\sigma_3, S] + \tilde{Q}(0, t, k)S, \tag{18}$$

which takes the following form for its relevant components:

$$\begin{aligned} \alpha_t(k) &= -c[i|v_0|^2\alpha(k) + (2kv_0 - i\bar{w}_0)\beta(k)], \\ \beta_t(k) &= -4ik^2\beta(k) + (2kv_0 + iw_0)\alpha(k) + ic|v_0|^2\beta(k) \end{aligned} \tag{19}$$

supplemented, respectively, by the following spectral representations of the unknown boundary data:

$$\begin{aligned} w_0(t) &= -\frac{2}{\pi}v_0(t)\int_{-\infty}^{\infty} dk[\alpha_+(k, t) - 1] \\ &+ \frac{4i}{\pi}\int_{-\infty}^{\infty} dk\left[k\beta_-(k, t) + \frac{iv_0(t)}{2}\right]; \end{aligned} \tag{20}$$

$$v_0(t) = -\frac{2}{\pi}\int_{-\infty}^{\infty} dk\beta_+(k, t); \tag{21}$$

$$\begin{aligned} v_0(t) &= -\frac{2}{\pi}\int_{-\infty}^{\infty} dk\beta_+(k, t), \\ w_0(t) &= \frac{1}{a_0}f_0(t) + \frac{2}{\pi a_0}\int_{-\infty}^{\infty} dk\beta_+(k, t). \end{aligned} \tag{22}$$

4. Here we describe, for the semiline case, an alternative approach. It is based on the equation

$$\begin{aligned} &(e^{-2ik^2t\sigma_3}S^{-1}(-k, t)[a_1I + 2ia_2k\sigma_3]S(k, t)e^{2ik^2t\sigma_3})_t \\ &= 4ke^{-2ik^2t\sigma_3}S^{-1}(-k, t) \\ &\times [a_1Q(0, t) + a_2Q_x(0, t)]S(k, t)e^{2ik^2t\sigma_3}, \end{aligned} \tag{23}$$

where a_1 and a_2 are arbitrary real parameters, which follows directly from Eq. (18). If we assign the boundary condition

$$a_1q(0, t) + a_2q_x(0, t) = f(t) \tag{24}$$

(which describes, due to the arbitrariness of the real parameters a_1 and a_2, all three IBV problems), Eq. (23), together with the analyticity properties of the scattering matrix, allows one to construct $S(k, t)$ through a nonlinear integral equation in both variables k and t. The main advantage of this approach is that Eq. (23) does not contain unknown boundary data; a discussion of this approach is beyond the scope of this paper and will be reported elsewhere.

Another advantage of this approach is that it captures in a natural way the known cases of linearizable boundary conditions [15–17] summarized by the equation $a_1q(0, t) + a_2q_x(0, t) = 0$. Indeed, in this case, the right-hand side of Eq. (23) is zero; therefore

$$\begin{aligned} &S^{-1}(-k, t)[a_1I + 2ia_2k\sigma_3]S(k, t) \\ &= e^{2ik^2t\sigma_3}(S^{-1}(-k, 0)[a_1I + 2ia_2k\sigma_3]S(k, 0))e^{-2ik^2t\sigma_3}, \end{aligned} \tag{25}$$

and, using the analyticity properties of $S(k, t)$, Eq. (25) can be interpreted as a linear RH problem for the columns of $S(k, t)$. Assuming, for simplicity, that the upper function $J(k) = (a_1 + 2ia_2k)\alpha(k, 0)\overline{\alpha(-\bar{k}, 0)} + c(a_1 - 2ia_2k)\beta(k, 0)\overline{\beta(-\bar{k}, 0)}$ has no zeros for $\mathrm{Im}\,k \geq 0$, the RH problem (25) can be expressed in terms of the following system of integral equations:

$$\begin{aligned} &\begin{pmatrix} \alpha(k, t) \\ \beta(k, t) \end{pmatrix} + \frac{1}{2\pi i}\int_{-\infty}^{\infty}\frac{dk'}{k' - (k + i0)}\gamma(k')e^{-4ik'^2t} \\ &\times\begin{pmatrix} -c\overline{\beta(k', t)} \\ \overline{\alpha(k', t)} \end{pmatrix} = \begin{pmatrix} 1 \\ 0 \end{pmatrix}, \end{aligned} \tag{26}$$

where

$$\begin{aligned} \gamma(k) &= [(a_1 + 2ia_2k)\alpha(k, 0)\beta(-k, 0) \\ &- (a_1 - 2ia_2k)\alpha(-k, 0)\beta(k, 0)]/J(-k), \end{aligned} \tag{27}$$

which allow one to construct $S(k, t)$ from the initial condition $S(k, 0)$ through a linear system of equations.

This work was carried out during several visits and meetings. We gratefully acknowledge the support of the Russian Foundation for Basic Research (project no. 01-01-00929), the INTAS (grant no. 99-1782), and the following Institutions: the University of Rome "La Sapienza" (Italy), the Istituto Nazionale di Fisica Nucleare (Sezione di Roma), the Landau Institute for Theoretical Physics, Moscow (Russia), and the Isaac Newton Institute, Cambridge (UK), within the programm "Integrable Systems."

REFERENCES

1. M. J. Ablowitz and H. Segur, *Solitons and the Inverse Scattering Transform* (SIAM, Philadelphia, 1981); S. P. Novikov, S. V. Manakov, L. P. Pitaevskii, and V. E. Zakharov, *Theory of Solitons: the Inverse Scattering Method* (Nauka, Moscow, 1980; Consultants Bureau, New York, 1984).
2. P. C. Sabatier, J. Math. Phys. **41**, 414 (2000).
3. A. S. Fokas, Proc. R. Soc. London, Ser. A **53**, 1411 (1997).
4. A. S. Fokas, J. Math. Phys. **41**, 4188 (2000).
5. A. S. Fokas, A. R. Its, and L. Y. Sung, Preprint (in preparation); private communication.

6. A. S. Fokas, *Integrable Nonlinear Evolution Equations on the Half-Line*, Preprint (October 2001).
7. A. S. Fokas and A. R. Its, Phys. Rev. Lett. **68**, 3117 (1992).
8. A. S. Fokas, Proc. R. Soc. London, Ser. A **457**, 371 (2001).
9. A. S. Fokas and B. Pelloni, Math. Proc. Cambridge Philos. Soc. (in press).
10. A. S. Fokas and B. Pelloni, Proc. R. Soc. London, Ser. A **454**, 654 (1998); A. S. Fokas and B. Pelloni, Phys. Rev. Lett. **84**, 4785 (2000).
11. J. Leon and A. V. Mikhailov, Phys. Lett. A **253**, 33 (1999).
12. J. Leon and A. Spire, nlin.PS/0105066.
13. F. Calogero and S. De Lillo, J. Math. Phys. **32**, 99 (1991); F. Calogero and S. De Lillo, Inverse Probl. **4**, L33 (1988).
14. V. E. Zakharov and A. B. Shabat, Zh. Éksp. Teor. Fiz. **61**, 118 (1971) [Sov. Phys. JETP **37**, 62 (1972)].
15. M. J. Ablowitz and H. Segur, J. Math. Phys. **16**, 1054 (1975).
16. E. K. Sklyanin, Funct. Anal. Appl. **21**, 86 (1987).
17. A. S. Fokas, Physica D (Amsterdam) **35**, 167 (1989).

JETP Letters, Vol. 74, No. 10, 2001, pp. 486–490. Translated from Pis'ma v Zhurnal Éksperimental'noĭ i Teoreticheskoĭ Fiziki, Vol. 74, No. 10, 2001, pp. 546–550.

Thermoelectric and Galvanomagnetic Properties of Chalcogens (Te, Se) at High Pressures Up To 30 GPa

V. V. Shchennikov and S. V. Ovsyannikov

Institute of Metal Physics, Ural Division, Russian Academy of Sciences, Yekaterinburg, 620219 Russia

Received September 19, 2001; in final form, October 15, 2001

The longitudinal and transverse Nernst–Ettingshausen effects have been measured at high pressures up to 30 GPa. The results of studying Te and Se in the region of metal–semiconductor phase transformations are presented as a demonstration of the possibilities of the given technique. In agreement with magnetoresistance data, it was found that the hole mobility grows with increasing pressure as a result of a decrease in the band gap width. Mechanisms of hole scattering at high pressures were determined. © *2001 MAIK "Nauka/Interperiodica".*

PACS numbers: 72.15.Gd; 72.20.My

The parameters of electronic structure of semiconductors, including estimates for the effective mass of charge carriers *m*, are commonly studied by measuring optical properties or galvanomagnetic effects, which are determined by the mobility of electrons and holes [1–4]. Galvanomagnetic effects are a more convenient tool for probing electron structure at high pressure *P* in the range from 0 to 100 GPa [5]. Alternative optical measurements in the infrared range are carried out less frequently because of the complexity of the experiment [6]. Thermomagnetic effects, as well as galvanomagnetic ones, also characterize the mobility μ of charge carriers and mechanisms of their scattering; however, they offer a number of advantages over the latter [7, 2]. Thus, not only do the values of the longitudinal and transverse Nernst–Ettingshausen (N–E) effects depend on the scattering parameters, but their signs depend as well [7, 2]. The transverse N–E effect strongly depends on the mobility in contrast to its galvanomagnetic analogue, the Hall effect, which does not depend on μ [2, 7]. Thus, studying thermomagnetic effects at ultrahigh pressures seems to be very topical; however, no such studies have been performed at *P* higher than 3 GPa, as judged from the available published data [3, 7, 8].

The goal of this work was to develop a procedure of thermomagnetic investigations at ultrahigh pressures. Semiconductors in which the mobility and, hence, the effective mass of charge carriers strongly vary with pressure are most interesting objects for such measurements. For the majority of known semiconductors, the effective mass of carriers *m* is proportional to the band gap width E_g, which corresponds to the general theoretical notions of the band theory [2–4]. At the same time, the behaviors of *m* for direct band gap and indirect band gap semiconductors must differ at $E_g \longrightarrow 0$, because the mass in the latter case is determined by different energy gaps. Two groups of direct gap semiconductor substances are well known: cubic InSb and HgTe crystals (the gap at the Γ point of the Brillouin zone), which have a region of structural stability up to 2 GPa [1, 8] and trigonal Te and Se crystals (the gap at the *H* point; this gap in Se becomes the smallest one at pressures higher than 5 GPa [1–4]). Elementary Te and Se semiconductors, whose band gap widths decrease down to zero [4, 5] and hole mobilities increase exponentially [5] in the ranges 0–4 and 0–25 GPa, were chosen as materials for investigations. Semiconductor tellurium samples had the hole concentration $p = 3 \times 10^{17}$ cm^{-3} at $T = 4.2$ K. The second material was gray amorphous Se. The crystal structure of samples was monitored by X-ray and neutron diffraction. Thermomagnetic effects in Te at atmospheric pressure were studied in [7], and no such data is available for Se because of the low mobility of holes [1, 4].

A high pressure up to 30 GPa was created with the use of chambers of synthetic superhard materials (diamond, boron nitride) [9, 10]. A schematic diagram of the arrangement of a sample in a high-pressure chamber and the placement of contacts are shown in Fig. 1. Procedures for studying thermopower (*S*) [9, 11, 12] and magnetoresistance (*MR*) [5, 13, 14] in such chambers at high pressures up to 30 GPa have been developed previously. The procedure for measuring the thermomagnetic N–E effect is in fact a combination of the first two procedures. Diamond anvils, whose thermal conductivity is several times higher than that of copper, were used for heat removal (Fig. 1) [9, 11–14]. In order to create a temperature gradient, one anvil was heated using a heating element; the temperature at fixed points of anvils was measured by thermocouples [11–14]. Measurements were performed in both steady-state and nonstationary thermal regimes [12] to exclude the effect of the heating element current on the thermomagnetic signal. The value of *P* in a quasi-hydrostatic

medium (catlinite) was estimated with an accuracy of ±10% by calibration plots constructed by phase transitions in Bi, ZnS, GaP, and other materials [9, 10]. Four different chambers with independent calibration were used. The working diameter of the anvils was from 0.6 to 1.0 mm. The anvils were both insulating (boron nitride, diamond) and conducting (synthetic diamond) [9, 11].

Samples were in the form of disks ~0.05–0.02 mm in thickness and ~0.3 mm in diameter (see Fig. 1). Because the length was considerably smaller than the width, the geometrical factor of magnetoresistance for such samples was approximately the same as for a Corbinaux disk (that is, the magnitude of the effect was a maximum), in which charge accumulation does not proceed because of the absence of side edges and the compensating Hall field does not arise [2]. Pressed contacts made of a platinum–silver band 5 μm in thickness and 0.1 mm in width [3–5] (the thermopower of this material is very small) or conducting diamond anvils were used to take *MR* and *S* signals. The current was supplied using a second pair of pressed contacts or through anvils. In the case of using anvils as electrodes, the error introduced into the thermopower was taken into account [12–14].

At fixed pressures (both for increasing and decreasing *P*), *S* and *MR* were simultaneously measured in a magnetic field *B* up to 2 T created in a vertebrate electromagnet. Closing the anvils produced no perceptible effects on *S*(*B*) and *MR*. Because the placement of contacts on a sample is not quite symmetric, a contribution of the Hall effect to the magnetoresistance (and vice versa) commonly exists. Therefore, special measures should be taken to compensate these contributions [2]. In our experiments, this was achieved by turning the chamber about its axis in the magnetic field. The measurements were carried out using a setup that simultaneously recorded all the experimental parameters and signals from a sample and accumulated them in an permanent memory, subsequently transferring the data to a computer [12].

Experimental plots of the thermoelectric signal and *MR* versus magnetic induction are shown in Fig. 2 for a Te sample at various positions of the chamber about its axis. The thermoelectric signal was a sum of components linear and quadratic in magnetic field, which we associated with thermomagnetic N–E effects [7, 2] (see Fig. 2). The contribution of the transverse effect was very high, but the transverse N–E effect (linear) transformed into the longitudinal effect (quadratic) upon rotating the chamber through 90°. This allowed both the longitudinal and transverse N–E effects to be measured separately from the same voltage contacts. The transverse effect was measured at the chamber position corresponding to a maximum signal. The contribution of the Hall effect to *MR* at two chamber positions corresponding to the longitudinal and transverse effects

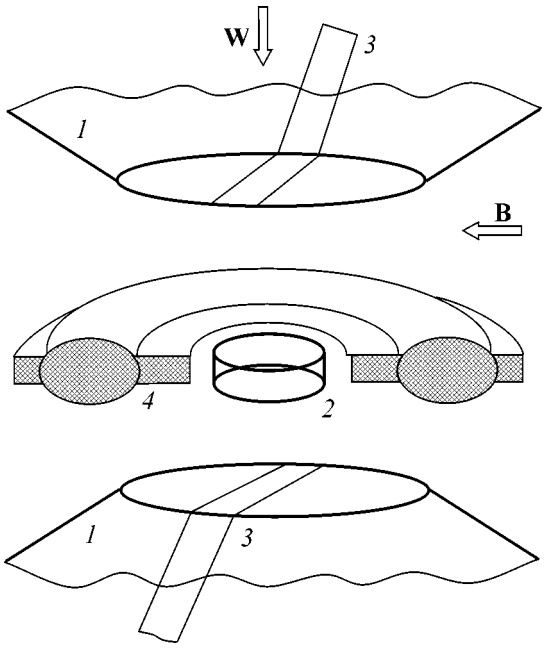

Fig. 1. Schematic diagram of the arrangement of a high-pressure chamber with a sample in a magnetic field *B*: (*1*) diamond anvils, (*2*) sample, (*3*) pressed voltage contacts, and (*4*) compressible catlinite insert. The directions of the magnetic field *B* and the heat flux *W* creating a temperature drop in a sample are shown.

was considerably lower and was detectable only upon algebraic subtraction of the *MR* curves measured experimentally (see Fig. 2). Similar curves were obtained in the other chambers for both Te and Se, regardless of the type of contacts and the material of anvils.

Mathematical expressions for the transverse *MR* and for the longitudinal and transverse N–E effects for a semiconductor with a standard band in weak magnetic fields take the following form [7, 2]:

$$MR \equiv \frac{\Delta\rho(B)}{\rho} = A_1(\mu B)^2, \quad (1)$$

$$\Delta S_{\parallel}(B) = A_2\left(\frac{k}{e}\right)(\mu B)^2, \quad (2)$$

$$Q = A_3 r\left(\frac{k}{e}\right)(\mu). \quad (3)$$

In Eqs. (1)–(3), ρ is the resistivity, *k* is the Boltzmann constant, *r* is the scattering parameter describing the dependence of the relaxation time τ of the momentum of charge carriers on the energy ε $\tau(\varepsilon) \approx (\varepsilon)^r$, and the A_1, A_2, and A_3 constants are functions of the scattering parameter and are determined by the Fermi integrals [2, 7]. In the case of scattering of charge carriers by acoustic vibrations of the lattice, which predominantly occurs at room temperature, the A_1, A_2, and A_3 constants

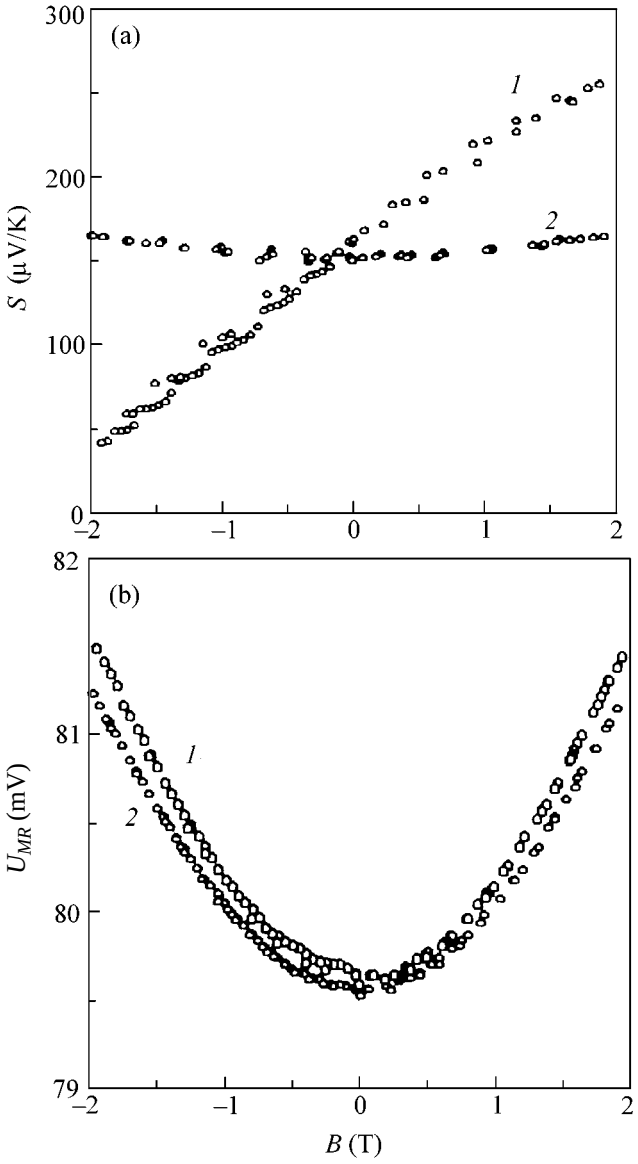

Fig. 2. Plots of (a) a thermoelectric and (b) magnetoresistance signals versus magnetic field for a Te sample measured in a chamber with boron nitride anvils at $T = 295$ K and fixed pressure ~1.5 GPa for two chamber positions in the magnetic field (curves *1* and *2*) differing by a rotation through 90°. Position *1* corresponds to the longitudinal N–E effect and position *2*, to the transverse N–E effect (two pairs of pressed contacts were used).

are equal to ~$9\pi/16(1 - \pi/4)$, $3\pi/8$, and $9\pi/16(1 - \pi/8)$, that is, of order ~1 [2]. The sign of the coefficient Q of the transverse N–E effect for scattering by acoustic phonons ($r = -1/2$) is negative, and, conversely, the longitudinal effect is positive (S increases in a magnetic field) [2, 7]. For the other limiting case, namely, scattering by impurity ions ($r = 3/2$), the signs of both effects are reversed [2, 7].

Electric fields $U_{\parallel}(B)$ and $\Delta U_{\perp}(B)$ are measured experimentally [2]:

$$\Delta U_{\parallel}(B)/\Delta x = \Delta S(B)\Delta T/\Delta x, \quad (4)$$

$$\Delta U_{\perp}(B)/\Delta y = BQ\Delta T/\Delta x. \quad (5)$$

Here, Δx and Δy are respectively the distances between the hot and cold ends of a sample (that is, the length) and between the voltage contacts in the direction perpendicular to the magnetic field and the heat flux (the distance by which the upper and lower voltage contacts or sample edges are displaced with respect to each other). Upon canceling Δx in the left- and right-hand parts, Eq. (4) gives the value of the longitudinal effect $\Delta S(B) = \Delta U_{\parallel}(B)/\Delta T$ that does not depend on the sample sizes. For the transverse N–E effect, the signal measured depends on the sizes; that is, it is proportional to both the coefficient Q and the ratio $\Delta y/\Delta x$: $\Delta S_{\perp}(B) = \Delta U_{\perp}(B)/\Delta T = QB(\Delta y/\Delta x)$.

The longitudinal and transverse thermomagnetic effects observed in our experiments depended quadratically and linearly on B in accordance with the theoretical expressions given by Eqs. (2) and (3). For Te, the longitudinal and transverse N–E effects grew with increasing P up to 4 GPa (Fig. 3) and then dropped. The drop was associated with the transition to a metal high-pressure phase (not shown in figure). The deviation of the transverse effect from linearity at $B \geq 1$ T (Fig. 3) is associated with the violation of the weak field condition $\mu B < 1$ due to an increase in mobility; in a strong field, Q is inversely proportional to B^2 [2, 7]. An increase in μ under pressure is also observed in the *MR* data (see Fig. 3c and [13, 15]). The mobility of holes in amorphous Se is very low; therefore, measurements in a magnetic field can be performed only under high pressure in the trigonal phase [14, 16]. For Se, the effects also increased up to the transition point at $P_t = 25$ GPa [4, 14, 16] and then decreased (Fig. 4). The transition to the metallic state was detected by a sharp decrease in the pressure coefficients S and ρ [13, 14, 16].

The measured transverse effect $\Delta S_{\perp} = \Delta U_{\perp}(B)/\Delta T$ involves the ratio $\Delta y/\Delta x$. Correspondingly, the values of μ calculated from it by Eq. (3) contain the same factor, whereas the mobilities determined from the longitudinal effect should not depend on the sample sizes. Actually, the values of μ obtained from *MR* and from the longitudinal N–E effect differed by no more than 20–30%, whereas the ratio of mobilities for the transverse effect attained 2–3 (Fig. 4). In order to determine the sign of the transverse N–E coefficient, the placement of voltage contacts should be known; however, it is accidental in our case. At atmospheric pressure, the sign of this effect in Te is negative [7], which corresponds to the scattering parameter $r = -1/2$. At high pressure, the sign is conserved. This indicates the behavior of the longitudinal N–E effect, which increases with the magnetic field (see Figs. 2, 3) (at $r = 3/2$, the sign of the longitudinal effect must be negative [2]. In a Se sample, a

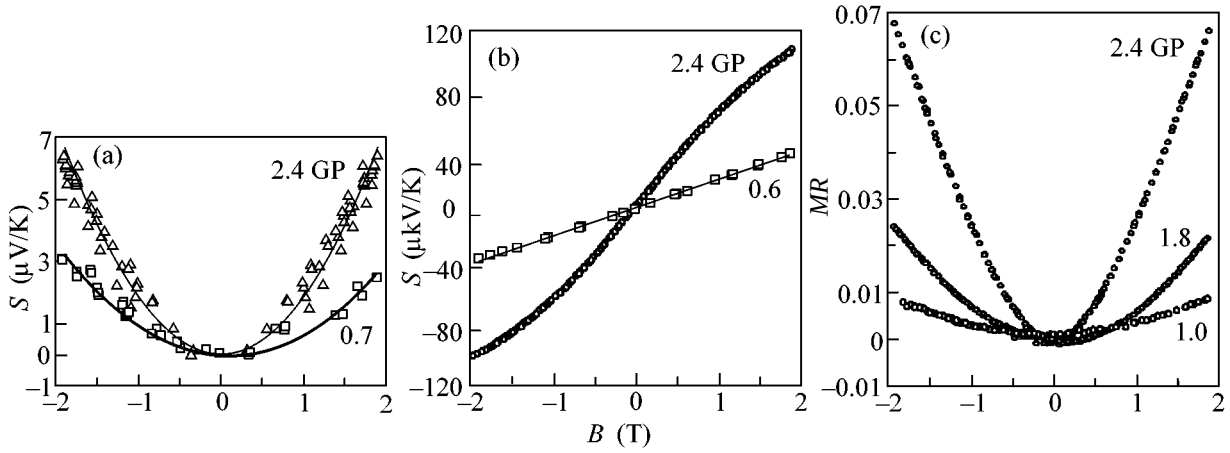

Fig. 3. (a) Longitudinal and (b) transverse N–E effects and (c) magnetoresistance of a Te sample measured in a synthetic-diamond chamber (with two pressed contacts) at T = 295 K and fixed pressure, GPa.

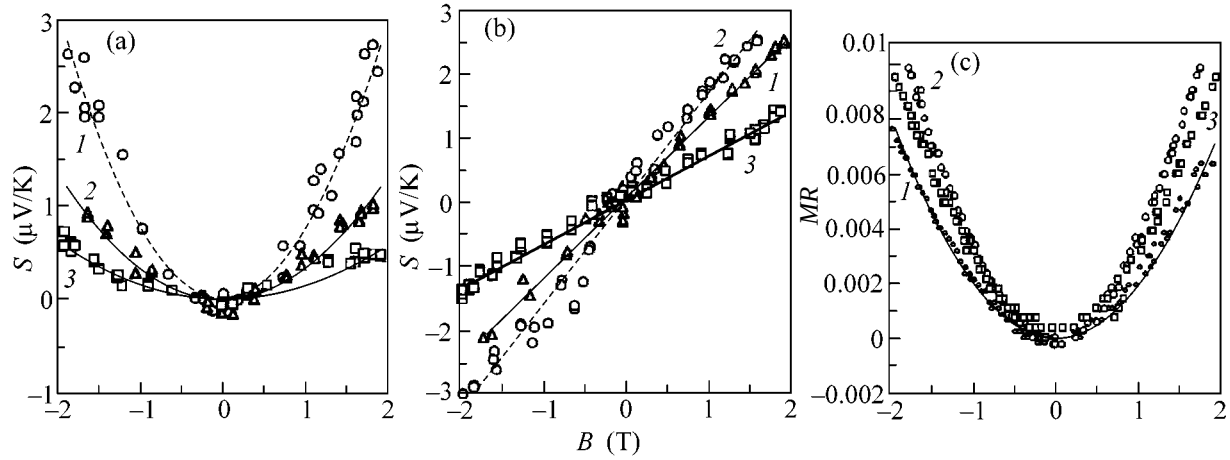

Fig. 4. (a) Longitudinal and (b) transverse N–E effects and (c) magnetoresistance of a Se sample measured in a synthetic-diamond chamber (with two pressed contacts) at T = 295 K and fixed pressure, GPa: (a) (*1*) 20, (*2*) 23, and (*3*) 26; (b) (*1*) 20, (*2*) 23, and (*3*) 29; (c) (*1*) 20, (*2*) 23, and (*3*) 26.

similar behavior of the longitudinal effect is observed in a magnetic field; hence, the sign of the transverse effect is also negative, and scattering by acoustic lattice vibrations is dominant at room temperature [1–4].

The mobilities evaluated from both thermomagnetic effects and from *MR* increased as P_t was approached, which was due to a decrease in E_g and a corresponding (for direct gap semiconductors) decrease in m [4, 13–16]. The decrease in the band gap width under pressure can be monitored by the decrease in the value of S, because this value is proportional to E_g [1–4, 13, 14] (see Fig. 2). The values of μ for Te and their pressure dependence are in agreement with the *MR* data obtained previously under hydrostatic pressures up to 1.5 GPa [15]. The increase in the mobility of holes in Se with increasing pressure is also in agreement with the *MR* data obtained in this work and with the data obtained in [13–15]. According to the available theoretical calculations, the electronic structure of Se and Te is identical, and this similarity must enhance with increasing pressure [1–4, 17]. It is evident from the results of this work (see Figs. 2–4) that the N–E effects and *MR* in Se and Te actually exhibit the same behavior in the region of semiconductor–metal transition under pressure [13–15], and the estimated mobilities are close in magnitude.

The studies performed allow the conclusion that the thermomagnetic (Nernst–Ettingshausen) effects are a convenient tool for studying the electronic structure of semiconductors under ultrahigh pressures and mechanisms of charge carrier scattering in high-pressure phases. The type of electronic structure (direct or indi-

rect gap in the electron spectrum) can be determined from experimental investigations of the $\mu(P)$ dependence at $E_g \sim 0$ obtained from thermomagnetic measurements [5]. The results of this work may have interesting practical applications, because thermomagnetic (galvanomagnetic) effects under certain conditions are a more efficient cooling technique than the conventional thermoelectric Peltier effect [2, 18].

This work was supported by the Russian Foundation for Basic Research, project no. 01-02-17203 and by the Russian Physical Society.

REFERENCES

1. I. M. Tsidil'kovskiĭ, *Electrons and Holes in Semiconductors* (Nauka, Moscow, 1972).
2. K. Seeger, *Semiconductor Physics* (Springer-Verlag, Berlin, 1973; Mir, Moscow, 1977).
3. I. M. Tsidil'kovskiĭ, *Conception of Effective Mass* (Ural. Otd. Ross. Akad. Nauk, Yekaterinburg, 1999).
4. V. V. Sobolev and A. M. Shirokov, *Electronic Structure of Chalcogens* (Nauka, Moscow, 1988).
5. V. V. Shchennikov, Phys. Status Solidi B **223**, 561 (2001).
6. M. Kobayashi, Phys. Status Solidi B **223**, 55 (2001).
7. I. M. Tsidil'kovskii, *Thermomagnetic Effects in Semiconductors* (Fizmatgiz, Moscow, 1960; Academic, New York, 1962).
8. M. M. Akselrod, K. M. Demchuk, and I. M. Tsidilkovskii, Phys. Status Solidi **27**, 249 (1968).
9. I. M. Tsidil'kovskiĭ, V. V. Shchennikov, and N. G. Gluzman, Fiz. Tekh. Poluprovodn. (Leningrad) **17**, 958 (1983) [Sov. Phys. Semicond. **17**, 604 (1983)].
10. V. V. Shchennikov and V. A. Smirnov, RF Patent No. 2050180 (1995).
11. V. V. Shchennikov and A. V. Bazhenov, Rev. High Pressure Sci. Technol. **6**, 657 (1997).
12. V. V. Shchennikov, A. Yu. Derevskov, and V. A. Smirnov, in *High Pressure Chemical Engineering*, Ed. by Ph. Rudolf von Rohr and Ch. Trepp (Elsevier, Amsterdam, 1996), p. 667.
13. V. V. Shchennikov, Fiz. Tverd. Tela (St. Petersburg) **42**, 626 (2000) [Phys. Solid State **42**, 641 (2000)].
14. V. V. Shchennikov and V. I. Osotov, Fiz. Tverd. Tela (St. Petersburg) **37**, 448 (1995) [Phys. Solid State **37**, 243 (1995)].
15. M. V. Glushkov, E. S. Itskevich, Yu. V. Kosichkin, *et al.*, Fiz. Tverd. Tela (Leningrad) **19**, 3580 (1977) [Sov. Phys. Solid State **19**, 2092 (1977)].
16. F. P. Bundy and K. J. Dunn, J. Chem. Phys. **71**, 1550 (1979).
17. B. A. Volkov, O. Pankratov, and S. V. Pakhomov, Zh. Éksp. Teor. Fiz. **86**, 2293 (1984) [Sov. Phys. JETP **59**, 1336 (1984)].
18. G. A. Ivanov, E. K. Iordanishvili, V. L. Naletov, *et al.*, in *Low Temperature Thermoelectric Materials*, Ed. by D. V. Gitsu (Akad. Nauk Moldavskoĭ SSR, Kishinev, 1970), p. 182.

Translated by A. Bagatur'yants

JETP Letters, Vol. 74, No. 10, 2001, pp. 491–494. Translated from Pis'ma v Zhurnal Éksperimental'noĭ i Teoreticheskoĭ Fiziki, Vol. 74, No. 10, 2001, pp. 551–555.

Formation of Two-Dimensional Lattices of Magnetic Domains in a Harmonic Magnetic Field

M. V. Logunov* and M. V. Gerasimov

Mordovia State University, ul. Bol'shevistskaya 68, Saransk, 430000 Russia

**e-mail: logunov@mrsu.ru*

Received October 17, 2001

New configurations of two-dimensional lattices of magnetic domains with symmetry described by the *P*2 and *Cmm*2 space groups are revealed in studying the formation of domain structures in a harmonic magnetic field. Two-dimensional lattices belonging to five space groups of the orthorhombic and hexagonal systems are observed in a single iron garnet film. Changes in the lattice configurations and in the lattice elements occur upon the variation of only one parameter of the applied magnetic field, namely, its frequency. © *2001 MAIK "Nauka/Interperiodica".*

PACS numbers: 75.70.Kw

Magnetic plates and films with a through domain structure are, in fact, two-dimensional objects in many respects. For such materials, the conditions for formation and the properties of stripe domain lattices with one-dimensional periodicity and of two-dimensional hexagonal lattices of magnetic bubbles have been studied in detail [1–3].

The observation and study of the new types of self-organization of magnetic moment in iron garnet films with a large uniaxial anisotropy constant were reported in [4–7]. Under the action of a unipolar pulsed magnetic field, the formation of reflective two-dimensional lattices of dumbbell-like, elliptic, and circular (bubble) magnetic domains was observed. Their symmetry under the static conditions corresponded to the *Pab*2, *Pmm*2, and *P*6 space groups, and in films with a strong orthorhombic anisotropy component, to the *P*2 group.

The spectrum of domain lattices observed under the action of a harmonic magnetic field is much more limited: it includes an array of paired ring domains with the *Cmm*2 symmetry and a hexagonal ring domain lattice with the *Pmm*6 symmetry [5, 7]. The conditions necessary for the formation of two-dimensional lattices of magnetic domains in both pulsed and harmonic fields are yet to be understood, while the attempts at realizing all these conditions in a single film have failed [7].

In this paper, we report the experimental observation of the formation of two-dimensional magnetic domain lattices belonging to five different space groups of the orthorhombic and hexagonal systems, namely, *P*2, *Pab*2, *P*6, *Cmm*2, and *Cmm*6 in a single film. The results are presented for an iron garnet single-crystal film of the composition $(Y, Bi)_3(Fe, Ga)_5O_{12}$ with crystallographic orientation (111), film thickness h = 7.8 μm, equilibrium period of the stripe domain structure P_0 = 32 μm, saturation magnetization M_s = 8.7 G, collapse field H_0 = 33 Oe, and uniaxial anisotropy field H_k = 7600 Oe. A harmonic magnetic field directed normally to the film surface was generated by a pancake coil 2 mm in diameter.

The static domain structures formed by applying a harmonic magnetic field for several seconds were observed using the Faraday effect and recorded by video tape (Fig. 1). As in [4, 6], the range of the magnetic field parameters for which the formation of two-dimensional structures was possible became broader after applying a small bias field $H < H_0$ normally to the film plane. It is remarkable that we observed the whole variety of domain structures, including new configurations of domain lattices, in a single sample under the action of a harmonic magnetic field with a constant amplitude $H_m \sim 2.5H_0$ by varying only a single parameter of the external action, namely, field frequency f.

The domain configurations shown in Fig. 1 were formed in the axially symmetric magnetic field generated by the pancake coil. Since the domain dimensions are small relative to the coil diameter, we present in Fig. 1 the micrographs of only that part of the domain structure which falls within the field of the microscope. The micrograph centers are shifted to the right and upward relative to the coil center to demonstrate the effect of field inhomogeneity, which increases as the coil turns are approached (Fig. 1b). The difference in the harmonic field strengths within the film area shown in Fig. 1 is less than 3%.

From our experiments it follows that, in the amplitude and frequency ranges corresponding to the formation of two-dimensional lattices of magnetic domains, the shape of the dynamic hysteresis loops has certain characteristic features. The quasistatic hysteresis loops are typical of low-coercive iron garnet films [8]. When the frequency of the harmonic field exceeds 50 kHz and

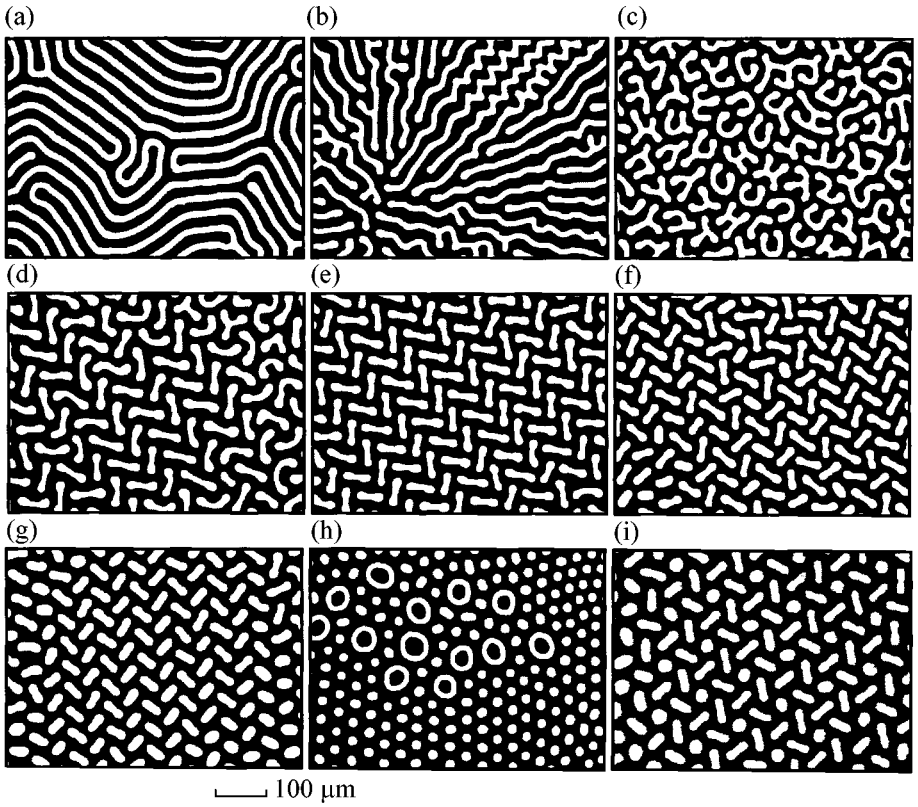

Fig. 1. Static domain structures formed in the same sample region (a–h) in the harmonic magnetic field with amplitude H_m = 77 Oe and frequency f and (i) in the pulsed field with amplitude H_p= 215 Oe and a pulse duration of 1.9 μs. The frequency f = (a) 0.1, (b) 60, (c) 70, (d) 80, (e) 90, (f) 100, (g) 120, and (h) 160 kHz. The bias magnetic field H = (a) 0, (b–h) 6, and (i) 8 Oe.

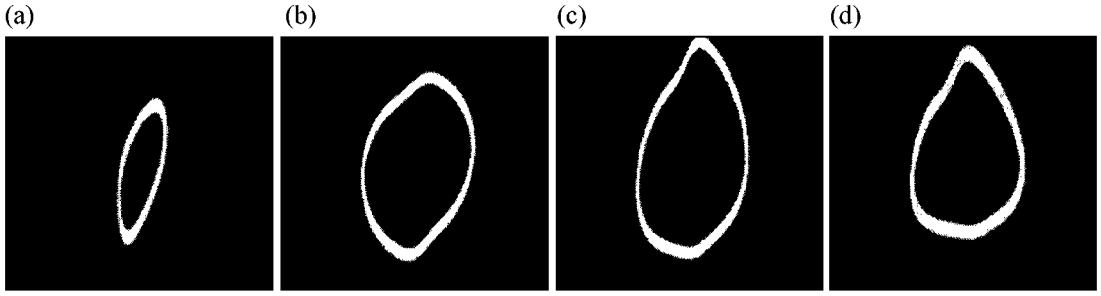

Fig. 2. Hysteresis loops of the iron garnet film in the harmonic field with frequency f = 100 kHz and amplitude H_m= (a) 34 and (b–d) 77 Oe. The bias field H = (a, b) 0, (c) 10, and (d) 20 Oe.

its amplitude is $H_m \le H_0$, the hysteresis loops become elliptic in shape because of the phase lag between the magnetization reversal signal and the variation of the magnetic field strength (Fig. 2a). An increase in the field amplitude to $H_m \sim 2.5H_0$ is accompanied by distortions of the elliptic loop (Fig. 2b). All dynamic hysteresis loops corresponding to the formation and transformation of two-dimensional domain lattices are minor hysteresis loops. They are asymmetric, as is seen upon applying the bias magnetic field (Fig. 2c). The asymmetry grows as the bias field increases (Fig. 2d).

Under the action of the harmonic magnetic field with a frequency of several tens or hundreds of hertz, a labyrinth domain structure, typical of quasistatically demagnetized iron garnets, is formed (Fig. 1a). As the field frequency increases to several kilohertz and higher, dynamic effects come into play; within a half-period of the field, the film is magnetized to saturation

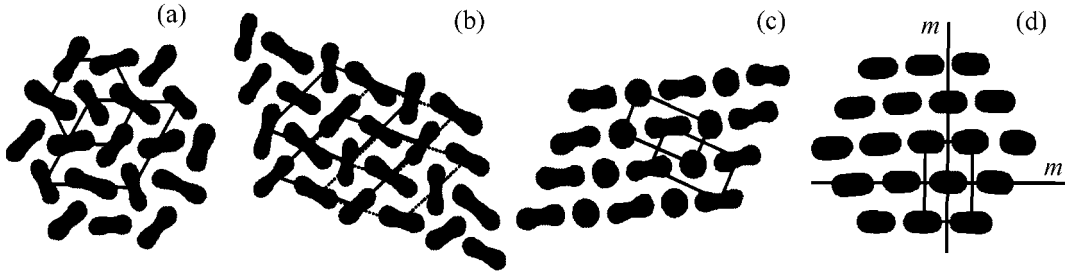

Fig. 3. Fragments of the static domain structures formed in the harmonic magnetic field with amplitude H_m = 77 Oe and frequency f = 100–110 kHz in the same region of the sample. The bias field H = 6 Oe. The unit cells and the mirror-reflection planes m are indicated in the patterns.

(because $H_m \sim 2.5H_0$), while the demagnetization process has no time to proceed quasistatically, and the start field in the hysteresis loop decreases. This occurs because of a high quality of the single-crystal film. Figure 1b shows that the region under observation contains no domain nucleation centers, and the domains grow from periphery toward the coil center. The quasiperiodic shape distortions and the ramification observed for part of the expanding domains indicate that the domain walls reach saturation velocity $V_s \sim 4$ m/s (according to the results of high-speed photography [9]) and the segments with different effective masses form in the domain walls [3].

As the field frequency increases further, the field half-period becomes insufficiently long for the labyrinth domains to completely collapse within this time. In this case, the domain walls with nonuniformly distributed effective masses only come closer to each other. This process is accompanied by breaking of labyrinth domains through the mechanism described in [10]. Within several periods of the applied magnetic field, a disordered array of short labyrinth domains of approximately equal lengths is formed (Fig. 1c). An increase in the field frequency leads to the transformation of the domain shape to a dumb-bell-like one and, then, to elliptic, circular, and ring shapes. These transformations are accompanied by the ordering in the domain arrangement (Figs. 1d–1h).

In the low-frequency region of the magnetic field range corresponding to the formation of two-dimensional domain lattices, we obtained two-dimensional lattices with the *Pab*2 symmetry (Fig. 1e), which were earlier observed only in a pulsed magnetic field [4–7]. Under the same external conditions, two-dimensional domain lattices of the *Pab*2 symmetry group can have different directions of domain alignment. This is caused by the smallness of the cubic and orthorhombic anisotropy components (more than an order of magnitude smaller than the uniaxial anisotropy).

Near the upper bound of the frequency range corresponding to the formation of two-dimensional domain lattices, a well-known hexagonal lattice of magnetic bubbles with the *Cmm*6 symmetry is formed. This lattice is observed in the region of maximal homogeneity of the magnetic field (at the coil center), while, near the coil turns, ring domains are concentrated (Fig. 1i). As the density of ring domains grows, they form a two-dimensional lattice, which is also characterized by the *Cmm*6 space group.

The widest variety of ordered two-dimensional lattices of magnetic domains is observed in a relatively narrow range of field frequencies between 100 and 110 kHz, where these lattices can coexist (Fig. 1f). In addition to the known configurations, new configurations of two-dimensional lattices with the *P*2 symmetry (Figs. 3a–3c) and the *Cmm*2 symmetry (Fig. 3d) are observed in this frequency range. This fact confirms the assumption [4] that the two-dimensional domain lattices may have different spatial symmetries.

The domain structures shown in Figs. 3a and 3c consist of two domain types differing in shape, dimensions, and orientation. Each of these domain types can be characterized by a two-dimensional lattice with a primitive unit cell *P*. The resulting two-dimensional lattice is obtained by combining the two lattices in such a way that their unit cells are shifted relative to each other by half the unit-cell parameters along the *X* and *Y* axes [11, 12]. In this case, one would expect the formation of a base-centered unit cell *C*. In fact, the structure observed in the experiment possesses a primitive cell and a twofold symmetry axis. Thus, the domain lattices shown in Figs. 3a and 3c are characterized by the two-dimensional *P*2 space group.

Figure 3b presents a fragment of the domain structure formed by four combined two-dimensional domain lattices. Their unit cells are orthorhombic and shifted relative to each other along the edges by half the parameters of the unit cell. The resulting domain configuration also belongs to the *P*2 space group.

The domain configurations observed in the experiment include some nonprimitive lattices [11, 12] (Fig. 3d). In the case of Fig. 3d, the domain structure corresponds to the arrangement of bricks according to the centered rectangle order. The corresponding two-dimensional lattice, whose elements are domains in the form of distorted ellipses, has a base-centered unit cell

C, mirror-reflection planes *m* passing through the domain centers and directed along the *X* and *Y* axes, and a twofold symmetry axis. The space group is *Cmm*2.

The mechanisms governing the formation of two-dimensional domain lattices in harmonic and pulsed magnetic fields are poorly understood. In [7], it was stated that the residual magnetization of the film is the critical parameter that determines the choice of one of the possible domain structure variants. It was found that the process of domain-structure formation is highly sensitive to the amplitude, duration, and shape of the pulses initiating the formation of two-dimensional domain lattices. The factors most adversely affecting the self-organization of magnetic moment were claimed to be the short (shorter than 0.5 μs) durations of the leading edge and (or) the trailing edge of the field pulse [4, 6].

Our experiments on studying the conditions for the formation of two-dimensional domain lattices in a harmonic magnetic field showed that the lattice formation processes are mainly affected by two field parameters: the amplitude H_m and the frequency f. The first parameter determines the magnetic field strength which is necessary to obtain a rarefied domain structure, to provide the conditions for domain rearrangement, and to produce noticeable inertial effects, which accompany the domain motion and play an important role in the formation of two-dimensional lattices [5, 6]. The second parameter determines the duration of the field half-period part t^* within which the domain walls move in the acting magnetic field $H_m \sim 2.5H_0$. In its turn, the time interval t^* determines the amplitude of domain-wall displacements and governs the domain collapse processes.

The upper and lower bounds of the frequency range corresponding to the formation of two-dimensional lattices, as well as the upper and lower bounds of the time t^*, differ by a factor of two. This result agrees well with the experimental data obtained by us in a pulsed magnetic field H_p. The processes of formation of two-dimensional domain lattices in a pulsed magnetic field were found to mainly depend on the bias field strength (0–15 Oe) and on the field pulse duration t_p. The value of t_p could also be varied by a factor of two (from 1.5 to 3 μs). It was found that the field pulse duration providing the conditions for the domain-lattice formation were half the corresponding values of t^* in the case of a harmonic field. This occurred because of the increase in the amplitude of domain-wall motion in the harmonic (bipolar) magnetic field, as compared to the pulsed (unipolar) field.

The durations of the leading and trailing edges of the field pulse were varied from 0.02 to 1 μs. In contrast to [4, 6], we observed no considerable effect of the pulse shape on the domain formation processes. Thus, if the durations of the leading and trailing edges of the field pulse are shorter than in [4–7] by more than an order of magnitude, the formation of two-dimensional domain lattices is possible. Note that the lattice with the *P*6 symmetry was the only two-dimensional lattice whose formation in the film under study was found to be more stable in a pulsed field than in the harmonic field (Fig. 1i).

The field pulse amplitude for which the formation of domain lattices was observed could be varied within a relatively wide interval beginning at a certain boundary value $H_p > 2H_0$. This result is largely explained by the form of the dependence of the domain wall velocity in the film on the pulsed field strength. Direct measurements by high-speed photography showed that the domain-wall saturation velocity V_s is reached in the field $H_p \ll H_0$ and remains virtually constant in the fields up to $H_p \sim 10H_0$. Most likely, the inertial effects also do not undergo any fundamental changes in the course of the domain-wall motion in the pulsed magnetic field range $2H_0 < H_p < 10H_0$.

We are grateful to V.I. Gerasimov for assistance in processing the experimental data. The work was supported by the Russian Foundation for Basic Research, project no. 98-02-03325.

REFERENCES

1. C. Kooy and U. Enz, Philips Res. Rep. **15**, 7 (1960).
2. T. H. O'Dell, *Magnetic Bubbles* (Macmillan, London, 1974; Mir, Moscow, 1978).
3. A. P. Malozemoff and J. C. Slonczewski, *Magnetic Domain Walls in Bubble Materials* (Academic, New York, 1979; Mir, Moscow, 1982).
4. F. V. Lisovskiĭ and E. G. Mansvetova, Pis'ma Zh. Éksp. Teor. Fiz. **55**, 34 (1992) [JETP Lett. **55**, 32 (1992)].
5. F. V. Lisovskiĭ and E. G. Mansvetova, Pis'ma Zh. Éksp. Teor. Fiz. **58**, 836 (1993) [JETP Lett. **58**, 784 (1993)].
6. F. V. Lisovskiĭ, E. G. Mansvetova, E. P. Nikolaeva, and A. V. Nikolaev, Zh. Éksp. Teor. Fiz. **103**, 213 (1993) [JETP **76**, 116 (1993)].
7. F. V. Lisovskiĭ, E. G. Mansvetova, and Ch. M. Pak, Zh. Éksp. Teor. Fiz. **108**, 1031 (1995) [JETP **81**, 567 (1995)].
8. A. Magni and G. Vertesy, Phys. Rev. B **61**, 3203 (2000).
9. M. V. Logunov, V. V. Randoshkin, and V. B. Sigachev, Prib. Tekh. Éksp., No. 5, 247 (1985).
10. T. J. Gallagher and F. B. Humphrey, Appl. Phys. Lett. **31**, 235 (1977).
11. N. V. Belov, *Outlines on Structural Crystallography and Fedorov Symmetry Groups* (Nauka, Moscow, 1986).
12. V. A. Koptsik, *Shubnik Groups: Handbook of Symmetry and Physical Properties of Crystal Structures* (Mosk. Gos. Univ., Moscow, 1966).

Translated by E. Golyamina

JETP Letters, Vol. 74, No. 10, 2001, pp. 495–497. Translated from Pis'ma v Zhurnal Éksperimental'noĭ i Teoretichesko ĭ Fiziki, Vol. 74, No. 10, 2001, pp. 556–559.

Thermionic Current in a Metal–Superconducting Semiconductor Junction

G. V. Kuznetsov

Shevchenko National University, Kiev, 284071 Ukraine

Received September 5, 2001; in final form, October 22, 2001

The transition of a semiconductor to a superconducting state leads to a decrease in the thermionic current in the metal–superconducting semiconductor junction in the range of voltages close to the potential barrier height. Changes in the current–voltage characteristic are determined by the temperature and the energy gap parameter of the superconductor. © *2001 MAIK "Nauka/Interperiodica".*

PACS numbers: 71.30.+h; 73.40.Ns

The tunneling mechanism of charge transport over a potential barrier is dominant for conventional metal–superconductor junction structures at low temperatures and for a sufficiently thin potential barrier at the interface [1]. The role of the overbarrier transport of charge carriers under these conditions is insignificant, and, hence, it has been scarcely investigated. At the same time, the possibility of a significant increase in the thermionic component of the total current through the junction appears in superconducting semiconductor materials with relatively wide and moderately high barriers. In particular, favorable conditions for the thermionic mechanism of charge transport can be accomplished in metal–high-T_c superconductor junction structures. Higher critical temperatures T_c of the transition of a high-T_c superconductor to the superconducting state, as well as typical processes of surface depletion of carriers (due to which the surface layer of an oxide superconductor can acquire semiconductor properties), favor an increase in the thermionic current component in metal–high-T_c superconductor junctions [2, 3]. In modern high-T_c superconductor materials, the tunnel and overbarrier components attain comparable values at $T < T_c$, and the thermionic mechanism can become predominant in junction structures of this type with a further increase in T_c and a decrease in the concentration of carriers.

An energy band diagram of a metal–*n*-type superconducting semiconductor junction is shown in Fig. 1, where φ_b is the potential barrier height, eV_b is the diffusion potential, eV_n is the difference in energy between the Fermi level and the conduction band bottom (positive in the case of a degenerate semiconductor), Δ is the energy gap parameter of the superconductor, and V is the bias on the junction. In comparison with a conventional metal–semiconductor junction, the modification of the model consists in the use of the density of states for the superconductor in the bulk of the semiconductor material at a temperature $T < T_c$.

In the theory of thermionic emission, it is suggested that the potential barrier height $\varphi_b \gg kT$ and the current flow through the junction does not disturb the thermodynamic equilibrium in the emission region [4]. Under these assumptions, the thermionic current I_{th} is determined by the difference between the carrier flux from the semiconductor to the metal and the opposite flux from the metal to the semiconductor, and it depends on only the height of the potential barrier rather than its shape. The description of the carrier transfer processes in the junction will be based on the assumptions common to superconducting junctions [1]. The probabilities of the transport of carriers from the superconducting semiconductor to the metal and from the metal to the semiconductor will be considered equal to each other and independent of the energy. Similarly, the densities of states in the metal and the nonsuperconducting semiconductor may be considered slowly varying functions and may be set equal to their value at the Fermi surface. Then, if the energy is reckoned from the conduc-

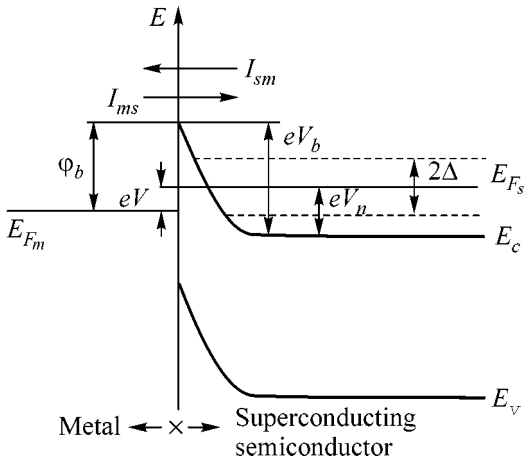

Fig. 1. Energy band diagram of a metal–superconducting semiconductor junction.

0021-3640/01/7410-0495$21.00 © 2001 MAIK "Nauka/Interperiodica"

tion band bottom ($E_c = 0$, Fig. 1) and all possible energies are taken into account, the maximum attainable density of the total current I_n through a metal–superconducting semiconductor junction can be described by the equation

$$I_n = \frac{G_n}{e}\left\{\int_{eV_n+\Delta}^{\infty} n_s(E)[f(E) - f(E-eV)]dE + \int_{0}^{eV_n-\Delta} n_s(E)[f(E) - f(E-eV)]dE\right\}, \quad (1)$$

where I_n is the maximum density of the total current in the junction, G_n is the conductivity of the junction in the nonsuperconducting state, $f(E) = \{1 + \exp[(E - eV_n)/kT]\}^{-1}$ and $f(E - eV) = \{1 + \exp[(E - eV_n + eV)/kT]\}^{-1}$ are the Fermi distribution functions in the semiconductor and the metal, and $n_s(E) = |E - eV_n|/[(E - eV_n)^2 - \Delta^2]^{1/2}$ is the superconductor structure of the density of states.

The current I_n in the general equation (1) is determined by the maximum possible flux of carriers in the junction under consideration. The problem of calculating the thermionic current is reduced to determining the overbarrier part of this flux and is solved by introducing the corresponding value of the minimal energy of passing carriers E_0 into one of the terms of Eq. (1) as the lower limit of integration. The explicit expressions for the current–voltage characteristic of a metal–superconducting semiconductor junction will be considered in more detail for various ranges of the applied external voltage V.

Voltage range $eV < \Delta - \Delta$. The carriers passing over the potential barrier in the voltage range $eV < \varphi_b - \Delta$ are characterized by the minimal energy $E_0 = eV_b = \varphi_b + eV_n - eV > eV_n + \Delta$, and the current through the junction depends on only the first term in Eq. (1). Consider only the case when $\Delta \gg \kappa T$. Then, the inequalities $\exp[(E - eV_n)/kT] \gg 1$ and $\exp[(E - eV_n + eV)/kT] \gg 1$ are fulfilled for the entire range of possible energies E. Therefore, the difference of the Fermi distribution functions can be written as $f(E) - f(E - eV) = [1 - \exp(-eV/kT)]\exp[-(E - eV_n)/kT]$. The effect of the superconducting state on the dependence of the current on the applied voltage will be taken into account restricting oneself to the first term in the series expansion of the function $n_s(E) \approx \{1 - [\Delta/(\varphi_b - eV)]\}^{-1/2}$ in the vicinity of the maximum energy of the potential barrier $eV_b = \varphi_b + eV_n - eV$. After substituting the values obtained into Eq. (1) and integrating from $E_0 = \varphi_b + eV_n - eV$ to ∞, the following equation will be obtained for the density of the current through the junction

$$I_{th} = \frac{A^*T^2}{\sqrt{1 - [\Delta/(\varphi_b - eV)]^2}} \times \exp\left(-\frac{\varphi_b}{kT}\right)\left[\exp\left(\frac{eV}{kT}\right) - 1\right]. \quad (2)$$

The designation $(kT/e)G_n = A^*T^2$ is used in this equation. This follows from the transformation of Eq. (2) at $\Delta \longrightarrow 0$ into the known equation for the thermionic current density in a conventional metal–semiconductor junction [4] $I_{th} = A^*T^2\exp(-\varphi_b/kT)[\exp(eV/kT) - 1]$, where $A^* = 4\pi em^*k^2/h^3$ is the Richardson constant for thermionic emission.

Voltage range $\varphi_b - \Delta \le eV \le \varphi_b + \Delta$. When the current is calculated in this voltage range, the values of both terms in Eq. (1) must be taken into account. After the change of the variable $x = E - eV_n - \Delta$ in the first term and $x = -E - eV_n - \Delta$ in the second, Eq. (1) is transformed to the form

$$I_{th} = \frac{G_n}{e}\left\{\exp\left(-\frac{\Delta}{kT}\right)\left[1 - \exp\left(-\frac{eV}{kT}\right)\right] + \exp\left(-\frac{\varphi_b + \Delta}{kT}\right)\left[\exp\left(\frac{eV}{kT}\right) - 1\right]\right\} \times \int_0^{\infty} \frac{x + \Delta}{\sqrt{x(x + 2\Delta)}}\exp\left(-\frac{x}{kT}\right)dx.$$

Here, $x_m = eV_n - \Delta \longrightarrow \infty$ is taken in the second term as the upper limit of integration, which is valid because of the rapid decrease of the Fermi function in a degenerate semiconductor at $E < eV_n$. The last integral can be found in tables of Laplace transformations [5]

$$\int_0^{\infty} \frac{(x + \Delta)\exp(-x/kT)}{\sqrt{x(x + 2\Delta/kT)}}dx = \Delta\exp\left(\frac{\Delta}{kT}\right)K_1\left(\frac{\Delta}{kT}\right),$$

where $K_1(\Delta/kT)$ is the first-order modified Bessel function of the second kind. At $\Delta \gg \kappa T$, the asymptotic expression $K_1(\Delta/kT) \approx (\pi kT/2\Delta)^{1/2}exp(-\Delta/kT)$ can be used for the Bessel function, and the final equation for the current density can be obtained after the substitution

$$I_{th} = A^*T^2\left(\frac{\pi\Delta}{2kT}\right)^{1/2}\exp\left(-\frac{\Delta}{kT}\right) \times \left[1 + \exp\left(-\frac{\varphi_b - eV}{kT}\right) - \exp\left(-\frac{eV}{kT}\right) - \exp\left(-\frac{\varphi_b}{kT}\right)\right]. \quad (3)$$

The maximum value of the ratio between the thermionic currents in the superconducting $I_{th}(S)$ and nonsuperconducting $I_{th}(N)$ states is attained at the voltage $eV = \varphi_b$. Using Eq. (3) and the expression for the current in a conventional metal–semiconductor junction, one can find that the $I_{th}(S)/I_{th}(N)$ ratio is determined by the value of $\Delta/\kappa T$ and is independent of the potential barrier height

$$\frac{I_{th}(S)}{I_{th}(N)} = \left(\frac{2\pi\Delta}{kT}\right)^{1/2}\exp\left(-\frac{\Delta}{kT}\right). \quad (4)$$

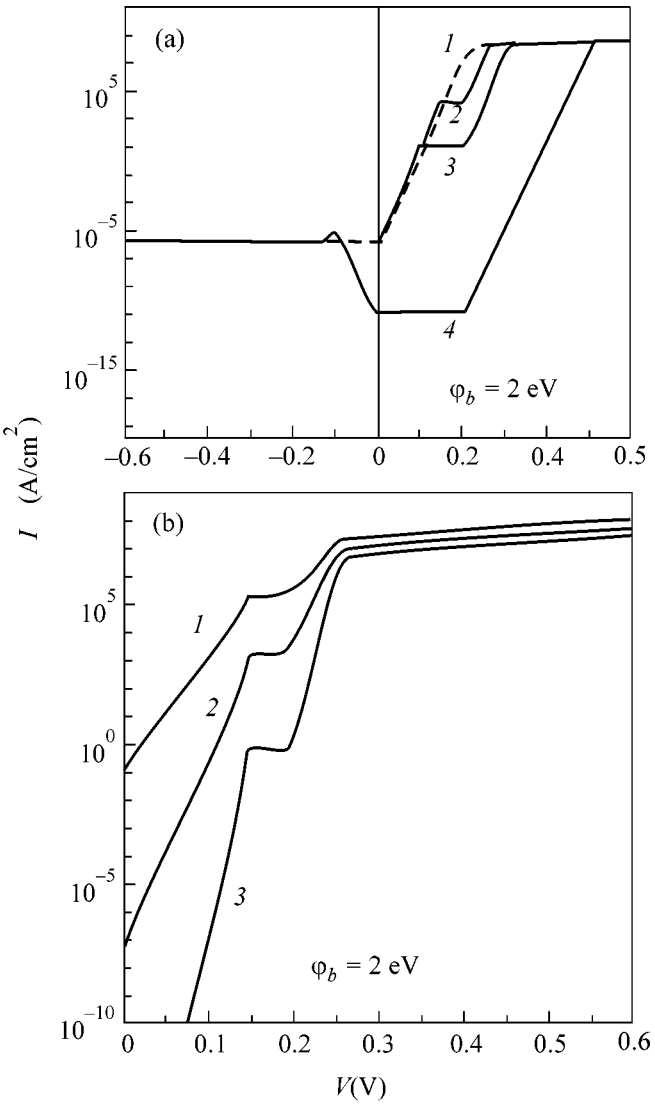

Fig. 2. Thermionic current in a metal–superconducting semiconductor junction: (a) φ_b = 0.2 eV, T = 77 K; (*1*) $\Delta/\varphi_b = 0$ (dashed line), (*2*) $\Delta/\varphi_b = 0.25$, (*3*) = 0.5, and (*4*) $\Delta/\varphi_b = 1.5$; (b) φ_b = 0.2 eV, Δ= 0.5 eV; (*1*) T = 150 K, (*2*) T = 77 K, and (*3*) T = 30 K.

Voltage range $eV > \varphi_b + \Delta$. The possible carrier energies in the voltage range $eV > \varphi_b + \Delta$ are determined by the relationship $0 \le E < eV_n - \Delta$. In this case, the current through the junction is determined by electrons arranged below the Fermi level of the semiconductor, and the contribution of the first term in Eq. (1) can be neglected. At $\Delta \gg \kappa T$, it is true for this range of energies E that $\exp[(E - eV_n)/kT] \ll 1$ and $\exp[(E - eV_n + eV)/kT] \gg 1$. Then, $f(E) - f(E - eV) = [1 - \exp(-eV/kT)]$. Integration from $E_0 = \varphi_b + eV_n - eV$ to $eV_n - \Delta$ gives the near-linear current–voltage characteristic in the voltage range $eV > \varphi_b + \Delta$

$$I_{th} = A^*T^2\left[1 - \exp\left(-\frac{eV}{kT}\right)\right]\sqrt{\left(\frac{eV - \varphi_b}{kT}\right)^2 - \left(\frac{\Delta}{kT}\right)^2}. \quad (5)$$

Voltage range $eV < 0$. The transition of the semiconductor to the superconducting state affects the dependence of the thermionic current on the inverse voltage only if the condition $\Delta > \varphi_b$ is fulfilled. Equations (2) and (3) obtained above do not depend on the sign of the applied voltage and can be used for describing the inverse branch of the current–voltage characteristic of the junction. The typical increase in the current at voltages $\varphi_b - \Delta$ is due to the occurrence of singularities in the density of states at the boundary of the superconductor energy gap.

The results of calculating the current–voltage characteristic of a metal–superconducting semiconductor junction at φ_b = 0.2 eV for various values of Δ are shown in Fig. 2a. Temperature changes in the current–voltage characteristic of a metal–superconducting semiconductor junction at φ_b = 0.2 eV and Δ = 0.05 eV are displayed in Fig. 2b.

The transition of the semiconductor to the superconducting state leads to the appearance of a singularity in the current–voltage characteristic caused by the absence of charge carriers in the energy range 2Δ. At $\Delta < \varphi_b$, changes occur only in the direct branch of the current–voltage characteristic in a region of voltages close to the potential barrier height, whereas changes are observed in both the direct and inverse branches at $\Delta > \varphi_b$. The decrease in the current becomes more significant with increasing energy gap parameter Δ and decreasing temperature T. The voltage corresponding to the maximum change in the thermionic current at the transition of the semiconductor to the superconducting state characterizes the potential barrier height at the metal–semiconductor interface $eV = \varphi_b$.

The thermionic mechanism of carrier transport considered above can be used for creating superconducting heterostructures with rectifying current–voltage characteristics and a zero resistance of the base area.

REFERENCES

1. E. L. Wolf, *Principles of Electron Tunneling Spectroscopy* (Clarendon, New York, 1985; Naukova Dumka, Kiev, 1990).
2. F. V. Komissinskiĭ, G. A. Ovsyannikov, and Z. G. Ivanov, Fiz. Tverd. Tela (St. Petersburg) **43**, 769 (2001) [Phys. Solid State **43**, 801 (2001)].
3. S. G. Lachenmann, I. Friedrich, A. Forster, *et al.*, Phys. Rev. B **56**, 14108 (1997).
4. S. M. Sze, *Physics of Semiconductor Devices* (Wiley, New York, 1981; Mir, Moscow, 1984), Part 1.
5. G. A. Korn and T. M. Korn, *Mathematical Handbook for Scientists and Engineers* (McGraw-Hill, New York, 1968; Nauka, Moscow, 1974).

Translated by A. Bagatur'yants

JETP Letters, Vol. 74, No. 10, 2001, pp. 498–501. Translated from Pis'ma v Zhurnal Éksperimental'noĭ i Teoreticheskoĭ Fiziki, Vol. 74, No. 10, 2001, pp. 560–564.

Double-Crystal X-ray Diffractometry in the Role of X-ray Standing-Wave Method

A. M. Afanas'ev[1], M. A. Chuev[1], R. M. Imamov[2], É. M. Pashaev[2], S. N. Yakunin[2], and J. Horvat[3]

[1] *Institute of Physics and Technology, Russian Academy of Sciences, Nakhimovskiĭ pr. 36, Moscow, 117218 Russia*

[2] *Shubnikov Institute of Crystallography, Russian Academy of Sciences, Leninskiĭ pr. 59, Moscow, 117333 Russia*

[3] *Research Institute of Technical Physics and Materials Science, H-1525 Budapest, Hungary*

Received October 25, 2001

It is shown that the atomic displacements (induced by foreign layers) comparable with or smaller than the interatomic distances can be detected in perfect multilayer systems by double-crystal X-ray diffractometry alone. It was earlier thought that the detection of displacements as small as those was accessible only to the specific methods such as the X-ray standing-wave method. The measurements were carried out on a GaAs/InAs/GaAs system, where InAs was a foreign layer. Its thickness did not exceed three monolayers, while the structure was of the insular type and represented a set of separate quantum dots. The displacement of the capping GaAs layer relative to the GaAs buffer was measured with an accuracy of less than 0.1 of the thickness of the atomic layer. © *2001 MAIK "Nauka/Interperiodica".*

PACS numbers: 68.49.Uv; 61.10.-i; 07.85.Nc

In recent years, the well-known method of double-crystal X-ray diffractometry (DXD) has experienced its second "birth" and has been transformed into a powerful and efficient tool for analyzing structure, composition, and quality of the thinnest layers in multilayer semiconducting systems placed not only at the surface of a structure but also in its bulk. This method is based on the measurement of diffraction reflection curves for X-ray incidence angles far from the Bragg peak (so-called method of truncated Bragg rods [1–4]). The central problem associated with the implementation of this method is that the coherent scattering must be separated from its diffuse component. To solve this problem, the triple-crystal X-ray diffractometry (TXD) technique was specially developed (see, e.g., [3]). However, this method proves to be rather cumbersome and requires substantially more prolonged measurements than does DXD. This restricts wide use of the TXD method in analysis of real multilayer structures and calls for the development of more efficient approaches. The way toward the solution of this problem is associated not with the development of a special apparatus but with recent advances in the technique of growing semiconducting multilayer systems. The interfaces between the layers in the real grown structures are rather sharp so the diffraction scattering amplitudes of different layers interfere, giving rise to a large number of well-resolved oscillations in the diffraction reflection curves [5].

The scheme of a double-crystal spectrometer designed for measuring the diffraction reflection curves or so-called rocking curves (RCs) over a wide range of deviations from the Bragg angle is shown in Fig. 1a. Contrary to the standard scheme, an additional slit is placed ahead of the detector. The role of this slit is quite important and consists of keeping, as far as possible, the detector out of the diffusively scattered X-ray component. In this case, the rotation of a crystal through an angle θ must be accompanied by the simultaneous turn of the detector and slit S_d through an angle 2θ in such a way that the diffracted rays fall on the detector. Figure 1b shows the RC measured for the (004) planes of the GaAs/InAs/GaAs structure (shown in the inset) using this scheme. One can see that the RC shows more than a hundred oscillations, allowing one to hope that the coherent and diffuse scattering components will be efficiently separated in the RCs and that vast information on the parameters of a multilayer system will be extracted. The presence oscillations in number as large as this is evidence primarily of the good quality of the grown structure. The InAs layer has a very small thickness of no more than three monolayers. Such layers, as known, are not homogeneous but form insular structures (so-called quantum dots). Nevertheless, one can see from the experimental RC (from the presence of a large number of oscillations) that the strains induced by these layers are "grown over" rather rapidly. The role of the InAs layer mainly consists of shifting the capping atomic layers relative to the buffer layer by a value u on the order of the interatomic distance (Fig. 2). The contribution to the diffraction scattering from this layer is quite small, so it can be ignored to a first approximation, whereas the shift induced by this layer in the capping and buffer layers gives rise to an additional phase shift

$$\Phi = K_h u \quad (1)$$

between their scattering amplitudes (K_h is the modulus of reciprocal lattice vector). It was previously assumed that information of this sort could be extracted only by special methods of the X-ray standing-wave type, in which the RC is measured simultaneously with measuring angular dependence of the photoelectron or photoluminescence yield accompanying X-ray diffraction (see, e.g., [3, 6]). It is the purpose of this work to demonstrate that small displacements induced in an atomic layer by a very thin foreign layers can be detected using double-crystal X-ray diffractometry alone in conjunction with a rather simple analysis.

A three-layer model comprised of layers with homogeneous thickness and absolutely sharp boundaries between them seems to be suitable as the first model for analysis (Fig. 2). Evidently, this model cannot be used for analysis of the entire RC. Indeed, the real grown layers are not homogeneous because of small changes in their interplanar spacing and in the degree of perfection. For this reason, this model cannot be used for analysis of the central portion of the curve in the close vicinity of the Bragg peak. Moreover, this model is sure to be unsuitable for analyzing far RC wings, because the diffraction scattering in these angular ranges depends substantially on the structure of interlayer boundaries. Nevertheless, one may assume that there is a certain range of intermediate angles where the model shown in Fig. 2 adequately describes the RC shape.

For a three-layer system with sharp boundaries and in the case of the ideal collimation of the incident beam, one can readily obtain the following rather simple expression for the diffraction reflection coefficient $R(\Delta\theta)$ over a wide range of angles away from the Bragg peak [3]:

$$R(\Delta\theta) = \left|\frac{1-\exp(i\Delta qL)}{\Delta\theta} f_c + \frac{\exp(i\Delta qL + i\Phi)}{\Delta\theta} f_s\right|^2 + R_b, \quad (2)$$

where $\Delta q = -(2\pi/\lambda) \times 2\cos\theta_B \Delta\theta$ is the momentum transfer without the reciprocal lattice vector; λ is the X-ray wavelength; $\Delta\theta$ is the deviation from the exact Bragg angle θ_B; L is the thickness of the capping layer; f_c and f_s are the static Debye–Waller factors of the capping and buffer layers, respectively; Φ is the phase given by Eq. (1); and R_b is the contribution from the diffuse-scattering background.

Let us introduce the reduced reflection intensity defined by the following expression:

$$\tilde{I}(\Delta\theta) = [R(\Delta\theta) - R_b](\Delta\theta)^2. \quad (3)$$

This quantity was introduced in [1] (see also the monograph [3]). Using Eq. (2), one can easily obtain the following rather simple expression for reduced intensity (3):

$$\tilde{I}(\Delta\theta) = B - A\sin(\Delta qL + \varphi), \quad (4)$$

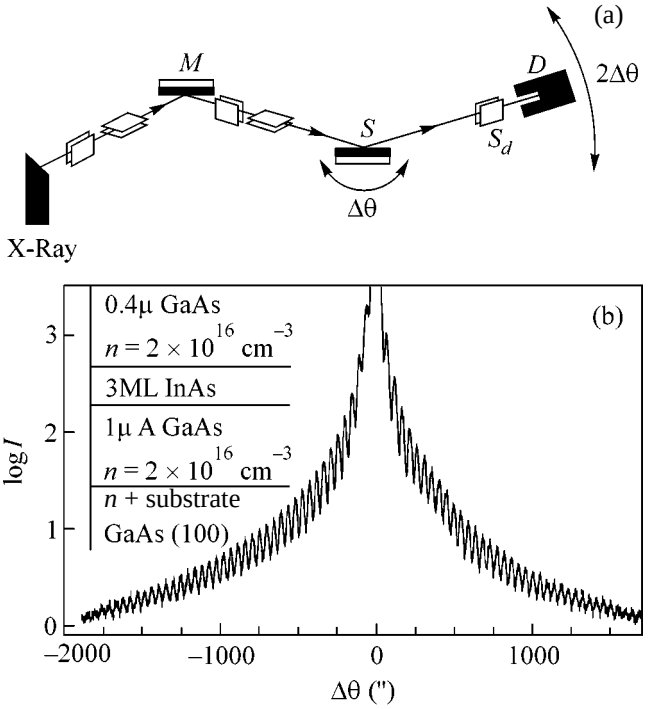

Fig. 1. (a) Scheme of a double-crystal X-ray diffractometer: (*M*) collimator block, (*S*) sample, (*D*) detector, and (S_d) slit ahead of the detector to reduce the background component. (b) Rocking curves: (dashes) experimental for the multilayer GaAs/InAs/GaAs structure shown in the inset and (solid line) calculated for a model with additional sublayers. The value of $\Delta\theta$ is given in seconds of arc.

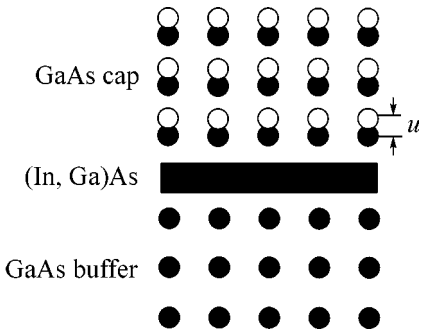

Fig. 2. Three-layer model of the structure.

where A and B are expressed in terms of the initial parameters Φ, f_c, and f_s:

$$A = 2f_c\sqrt{(f_c - f_s)^2 + 4f_s f_c \sin^2(\Phi/2)}, \quad (5)$$

$$B = f_c^2 + (f_c - f_s)^2 + 4f_s f_c \sin^2(\Phi/2), \quad (6)$$

$$\tan\varphi = \frac{f_c - f_s\cos\Phi}{f_s\sin\Phi}. \quad (7)$$

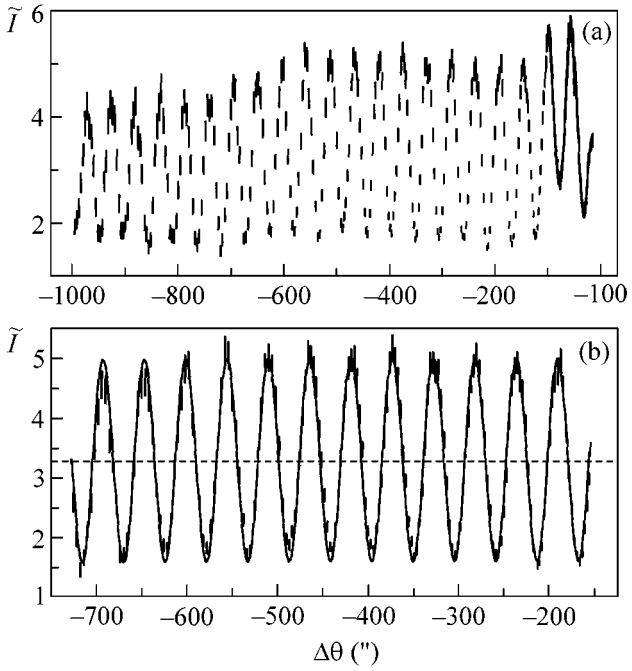

Fig. 3. (dashes) Reduced diffraction reflection intensity (a) in a wide angular range and (b) in the phase-informative range; the solid line is calculated using Eq. (4).

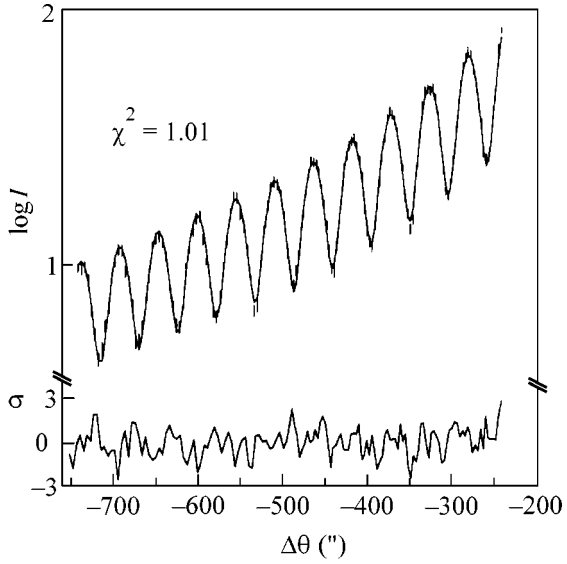

Fig. 4. Rocking curves in the phase-informative angular range: (dashes) experimental and (solid line) calculated using the three-layer model ($\chi^2 = 1.01$). The curve for the deviation (σ) of the calculated RC from the experimental RC is also shown in units of standard deviations.

One can see from Eq. (4) that the reduced intensity $\tilde{I}(\Delta\theta)$ is the sum of a constant and a sinusoid, whose period is determined by the cap thickness L, while the amplitude is determined by the phase Φ and the factors f_c and f_s. The substrate and the buffer layer are usually grown with a rather high degree of perfection so that the factors f_c and f_s are close to unity. In this case,

$$A \approx 4\sin(\Phi/2), \quad B \approx 1 + 4\sin^2(\Phi/2), \quad \varphi \approx \Phi/2; \tag{8}$$

i.e., the amplitude and phase of the sinusoid in Eq. (4), as well as its center line, are determined by the unknown phase Φ. We specially present here simple Eqs. (8) to demonstrate that the phase Φ can be determined in some cases by rather simple methods without the use of any time-consuming mathematics.

Let us now turn back to the experimental data presented in Fig. 1b. The reduced reflection intensity is shown in Fig. 3a for the left part of this curve. The oscillations in the angular range from approximately –700″ to –100″ closely resemble a pure sinusoid. The experimental curve for these angles is shown in Fig. 3b. It is superposed by the curve calculated using Eq. (4). One can see that this simple function describes the experiment very well. Therefore, a considerable portion of the reflection curve (about 200 experimental points) "works" for the phase information. The sinusoid parameters are L = 412 nm, A = 1.7, B = 3.3, and φ = 1.4. Using these data and Eqs. (4)–(7), one can easily calculate the phase Φ and the factors f_c and f_s determining the perfection of the capping and buffer layers, respectively.

However, it should be taken into account that one measures experimentally not the sample reflection curve but its convolution with the reflection curve of the collimator crystal. The corresponding quantity is

$$\bar{R}(\Delta\theta) = \int_{-\theta_s}^{\theta_s} R(\Delta\theta - \theta) R_m(\theta) d\theta, \tag{9}$$

where $R_m(\theta)$ is the reflection curve of the collimator crystal, and θ_s is determined by the geometry of the slit system. The experimental data presented in this work are obtained not for the quantity defined by Eq. (3) but for

$$\bar{I}(\Delta\theta) = [\bar{R}(\Delta\theta) - R_b](\Delta\theta)^2. \tag{10}$$

Simple analytic expressions of the type (4)–(7) do not apply to the reduced intensity defined by Eq. (10). In this case, one should use the fitting procedure that was described in [5]. As to the foregoing analysis with the use of Eqs. (4)–(7), it merely points to the fact that the simple three-layer model can be used to adequately describe the experimental data for angles ranging from –700″ to –150″. The semi-log plot of the RC measured in this angular range is shown in Fig. 4. The solid line in this figure is the best fit of the three-layer calculation to the experimental data. The goodness-of-fit test value χ^2 is very close to unity (1.01), indicating the good

quality of the fit. The deviation of the calculated RC from the experimental curve is also shown in Fig. 4:

$$\sigma(\Delta\theta) = [I_{calc}(\Delta\theta) - I_{exp}(\Delta\theta)]/s(\Delta\theta), \quad (11)$$

where $I_{calc}(\Delta\theta)$ and $I_{exp}(\Delta\theta)$ are, respectively, the calculated and the measured diffraction reflection intensities, and $s(\Delta\theta)$ is the measurement error. The quality of a fit is said to be good if σ falls within –3–3 [7]; in our case, this condition is nicely fulfilled. The corresponding layer parameters and their standard deviations are given in the first column of the table, the sinusoid parameters calculated using these data and Eqs. (5)–(7) are given in the second column, and the sinusoid parameters reproduced from the experimental data in Fig. 3b are given in the third column. It is seen that the parameters L, B, and φ of the sinusoid in Eq. (4) coincide well for two fitting variants, whereas the parameters A differ appreciably. This discrepancy points to the necessity of averaging over the collimator crystal reflection curve (9), because this will primarily reduce the oscillation amplitude in the resulting reflection curve.

It follows from the data obtained in this work that phase Φ is determined with a rather high accuracy (on the order of 10%), while the corresponding shift $u = 0.1a$ (a is the lattice parameter) of the capping layer relative to the buffer is equal to 0.56(5) Å. Therefore, the DXD method alone can be used to detect small shifts of the individual layers in the complex multicomponent systems, without invoking any additional phase-sensitive methods (e.g., X-ray standing-wave method). Note also that this example demonstrates that the role of special phase-sensitive methods in structural analysis may sometimes be strongly overstated. As a rule, these methods possess weaker luminosity compared to the usual DXD-type methods, which are usually thought to be incapable of directly determining the phases. However, the above analysis suggests that good statistics in the DXD method allows extraction of the phase information as well. Moreover, the main purpose of this work was to demonstrate that, in some cases, the phases can be directly determined using, for example, the DXD method alone.

Note that the experimental data presented in Fig. 1b, naturally, cannot be thoroughly analyzed within the framework of the simple three-layer model illustrated in Fig. 2. To do this, the model should be complicated through the introduction of additional sublayers near the interfaces. An appropriate analysis can be carried out using the approach developed in [5]. The solid line in Fig. 1b is calculated using the structural model with more than ten additional sublayers. The details of this analysis will be published elsewhere.

Structural parameters of layers and parameters of the sinusoid in Eq. (4)

Model Fig. 4		Model Fig. 3b
L = 411.9(2) nm		L = 412.4(2) nm
f_c = 0.77(2)	A = 2.5(1)	A = 1.65(2)
f_s = 1.00(2)	B = 3.43(4)	B = 3.32(1)
$\Phi = 0.90(8)\pi$	φ = 1.4(1)	φ = 1.46(2)

This work was supported by the Russian Foundation for Basic Research (project no. 00-02-17716) and the Russian Ministry of Industry, Science, and Technology [subprogram "Perspective Technologies and Micro- and Nanoelectronic Devices," state contract no. 204-8-(00)-P].

REFERENCES

1. S. S. Yakimov, V. A. Chaplanov, A. M. Afanas'ev, *et al.*, Pis'ma Zh. Éksp. Teor. Fiz. **39**, 3 (1984) [JETP Lett. **39**, 1 (1984)].
2. A. M. Afanas'ev, P. A. Alexandrov, R. M. Imamov, *et al.*, Acta Crystallogr. A **41**, 227 (1985).
3. A. M. Afanas'ev, P. A. Aleksandrov, and R. M. Imamov, *X-ray Diffraction Diagnostics of Submicron Layers* (Nauka, Moscow, 1989).
4. I. K. Robinson, Phys. Rev. B **33**, 3830 (1986).
5. A. M. Afanas'ev, M. A. Chuev, R. M. Imamov, *et al.*, Kristallografiya **42**, 514 (1997) [Crystallogr. Rep. **42**, 467 (1997)]; Kristallografiya **43**, 926 (1998) [Crystallogr. Rep. **43**, 872 (1998)]; A. M. Afanas'ev, M. A. Chuev, R. M. Imamov, and A. A. Lomov, Kristallografiya **45**, 715 (2000) [Crystallogr. Rep. **45**, 655 (2000)].
6. M. V. Koval'chuk and V. G. Kon, Usp. Fiz. Nauk **149**, 69 (1986) [Sov. Phys. Usp. **29**, 426 (1986)].
7. W. T. Eadie, D. Dryard, F. E. James, M. Roos, and B. Saboulet, *Statistical Methods and Experimental Physics* (North-Holland, Amsterdam, 1971; Atomizdat, Moscow, 1976).

Translated by V. Sakun

JETP Letters, Vol. 74, No. 10, 2001, pp. 502–506. From Pis'ma v Zhurnal Éksperimental'noĭ i Teoreticheskoĭ Fiziki, Vol. 74, No. 10, 2001, pp. 565–569.

Electron Spectral Functions of Two-Dimensional High-T_c Superconductors in the Model of Fermion Condensation[1]

V. A. Khodel and M. V. Zverev*

Russian Research Center Kurchatov Institute, pl. Kurchatova 1, Moscow, 123182 Russia

** e-mail: zverev@mbslab.kiae.ru*

Received November 1, 2001

Spectral functions of strongly correlated two-dimensional (2D) electron systems in solids are studied on the assumption that these systems undergo a phase transition, called fermion condensation, whose characteristic feature is flattening of the electron spectrum $\epsilon(\mathbf{p})$. Unlike the previous models, the decay of single-particle states in our study is properly taken into account. Results of our calculations are shown to be in qualitative agreement with ARPES data. The universal behavior of the ratio $\mathrm{Im}\Sigma(\mathbf{p}, \varepsilon, T)/T$ as a function of $x = \varepsilon/T$, uncovered in [3] for the single-particle states around the diagonal of the Brillouin zone, are found to be reproduced reasonably well. However, in our model this behavior is destroyed in vicinities of the van Hove points, where the fermion condensate resides. © *2001 MAIK "Nauka/Interperiodica".*

PACS numbers: 71.27.+a; 74.20.Mn

The single-particle (SP) dynamics of Fermi systems at near-zero temperatures T is known to depend crucially on the index ν, which characterizes the imaginary part of the mass operator, $\mathrm{Im}\Sigma(\varepsilon \longrightarrow 0) \sim \varepsilon^\nu$, the energy ε being measured from the chemical potential μ. In ordinary homogeneous Fermi liquids, such as nuclear matter and liquid ^{3}He, where the exclusion principle "leads the dance," the index ν equals 2, and the Fermi liquid can be treated as a gas of interacting "immortal" quasiparticles, the cornerstone of standard Fermi liquid theory (SFLT) [1]. After many successful years, SFLT is currently encountering serious difficulties in treating normal states of 2D high-T_c superconductors. The analysis of ARPES data shows that, even around the diagonals of the Brillouin zone, the index ν is unity [2, 3], while in the immediate vicinity of the van Hove points (vHP), the sharp ARPES peaks disappear altogether [4–6].

We propose that the solution of this challenging problem is associated with fermion condensation [7–17], a novel phase transition that generates a domain **C** of dispersionless states, called the fermion condensate (FC), whose energies $\epsilon(\mathbf{p})$ coincide with μ. As a rule, in strongly correlated anisotropic electron systems of high-T_c superconductors, the FC occupies vicinities of the vHP [8, 18], precisely the region where the Fermi liquid approach fails. States with the FC have been uncovered [7] as unconventional solutions for equations of Landau theory at $T = 0$. However, in dealing with spectral functions of strongly correlated Fermi systems, the basic equation of the fermion condensation $\epsilon(\mathbf{p} \in \mathrm{C}; n) = \mu$ should be rewritten as [18]

$$\epsilon^0_{\mathbf{p}} + \Sigma(\mathbf{p}, \varepsilon = 0; n) = \mu, \quad \mathbf{p} \in \mathrm{C}. \tag{1}$$

Beyond the FC phase-transition point, this equation does determine a new momentum distribution $n(\mathbf{p})$, differing from the conventional one $n_F(\mathbf{p}) = \theta(\mu - \epsilon(\mathbf{p}))$. The degeneracy of the SP spectrum at $T = 0$, a salient feature of the solution given by Eq. (1), is lifted by pairing correlations, which are ignored in writing this relation. In doing so, the BCS occupation numbers $v^2(\mathbf{p})$ coincide with $n(\mathbf{p})$ evaluated from Eq. (1), provided the BCS coupling constant is rather small [13]. For this reason, superfluid systems with and without the FC look more alike than normal ones, since, in normal states of conventional Fermi liquids, the damping makes no difference, whereas in normal states of systems with the FC, the damping becomes a real "weathermaker." Indeed, the relevant contribution to $\mathrm{Im}\Sigma_R(\mathbf{p}, \varepsilon)$ is given by [19]

$$\begin{aligned}\mathrm{Im}\Sigma_R(\mathbf{p}, \varepsilon) \sim \sum_{\mathbf{q}, \mathbf{p}_1} \iiint d\omega d\varepsilon_1 F(\varepsilon, \omega, \varepsilon_1, T) \\ \times \left|\Gamma(\mathbf{p}, \varepsilon, \mathbf{p}_1, \varepsilon_1, \mathbf{q}, \omega; n)\right|^2 \mathrm{Im}G_R(\mathbf{p} - \mathbf{q}, \varepsilon - \omega) \\ \times \mathrm{Im}G_R(-\mathbf{p}_1, -\varepsilon_1)\mathrm{Im}G_R(\mathbf{q} - \mathbf{p}_1, \omega - \varepsilon_1),\end{aligned} \tag{2}$$

where the factor

$$F(\varepsilon, \omega, \varepsilon_1, T) = \cosh\left(\frac{\varepsilon}{2T}\right) \times \left[\cosh\left(\frac{\varepsilon_1}{2T}\right)\cosh\left(\frac{\varepsilon - \omega}{2T}\right)\cosh\left(\frac{\omega - \varepsilon_1}{2T}\right)\right]^{-1},$$

[1] This article was submitted by the authors in English.

$|\Gamma|^2$ is the absolute square of the scattering amplitude properly averaged over spin variables, and G_R is the retarded Green's function with $\mathrm{Im}G_R(\mathbf{p}, \varepsilon) = -\gamma(\mathbf{p}, \varepsilon)[(\varepsilon - \sigma(\mathbf{p}, \varepsilon) - s(\mathbf{p}))^2 + \gamma^2(\mathbf{p}, \varepsilon)]^-$, where $\sigma(\mathbf{p}, \varepsilon) = \mathrm{Re}\Sigma_R(\mathbf{p}, \varepsilon) - \mathrm{Re}\Sigma_R(\mathbf{p}, \varepsilon = 0)$ and $s(\mathbf{p}) = \epsilon_p^0 + \mathrm{Re}\Sigma_R(\mathbf{p}, \varepsilon = 0) - \mu$.

We restrict ourselves to temperatures T markedly lower than the characteristic temperature T_f of destroying the FC, which allows the T dependence of η, the fraction of the Brillouin zone occupied by the FC, to be ignored. To simplify the problem, we replace the function $\gamma(\mathbf{p}, \varepsilon)$ by a set of functions of the single variable ε; e.g., in the FC region, $\gamma(\mathbf{p} \in \mathrm{C}, \varepsilon)$ is reduced to $\gamma_\mathrm{C}(\varepsilon)$. The complementary region of momentum space, in which the dispersion of the spectrum $\epsilon(\mathbf{p})$ has a nonzero value, is composed of two subregions. The first one, adjacent to the FC domain and henceforth denoted by T, is a transition region, in which the same decay processes as in the FC region are still kinematically allowed. The second subregion, denoted by M, is located around diagonals of the Brillouin zone. Here, some of these processes are either kinematically forbidden or at least strongly suppressed. Correspondingly, $\gamma(\mathbf{p} \in \mathrm{T}, \varepsilon) \longrightarrow \gamma_\mathrm{T}(\varepsilon)$, $\gamma(\mathbf{p} \in \mathrm{M}, \varepsilon) \longrightarrow \gamma_\mathrm{M}(\varepsilon)$. To close the set of equations of the problem, the amplitude $\Gamma(n)$ should somehow be specified. Bearing in mind that η is small, we neglect the FC contributions to Γ, replacing it by $\Gamma(n_F)$. In this work, we continue to examine a scenario of [18] when the fermion condensation precedes the antiferromagnetic phase transition and employ the same amplitude $\Gamma(\mathbf{p}, \mathbf{p}_1; n_F)$ as in [20, 18], $\Gamma(\mathbf{p}, \mathbf{p}_1; n_F) \sim [\beta^2 + \kappa^2(\mathbf{p} - \mathbf{p}_1 - \mathbf{Q})^2]^{-1}$, where $\mathbf{Q} = (\pi, \pi)$ is taken.

We start with the case $\varepsilon \gg T$, and set $T = 0$ in the integral (2), thus dropping all T-dependent contributions. First we evaluate $\gamma_\mathrm{C}(\varepsilon \longrightarrow 0)$. In this case, (i) contributions from processes involving only the FC states prevail (see below), (ii) the quantity $|\Gamma(n_F)|^2 \sim \beta^{-4}$ can be factored out of the integral (2), and (iii) the quantity $s(\mathbf{p} \in \mathrm{C}, T)$, which vanishes over the FC region at $T = 0$, can be verified to remain small compared to leading terms in Eq. (2) and thus can be neglected. As a result, the energy and momentum integrations in Eq. (2) separate. Taking for certainty $\varepsilon > \mathrm{O}$ and omitting numerical factors, we are left with

$$\gamma_\mathrm{C}(\varepsilon \longrightarrow 0) \sim \beta^{-4}\eta^2 \times \int_0^\varepsilon \int_0^\omega A_\mathrm{C}(\varepsilon - \omega)A_\mathrm{C}(-\varepsilon_1)A_\mathrm{C}(\omega - \varepsilon_1)d\omega d\varepsilon_1, \quad (3)$$

where $A_\mathrm{C}(\varepsilon) = \mathrm{Im}G_R(\mathbf{p} \in \mathrm{C}, \varepsilon)$. To proceed, we insert $\gamma_\mathrm{C}(\varepsilon \longrightarrow 0) \sim \varepsilon^{\nu_\mathrm{C}}$ into the Kramers–Krönig relation to obtain $\sigma_\mathrm{C}(\varepsilon \longrightarrow 0) \sim \varepsilon^{\nu_\mathrm{C}}$. We then substitute γ_C and σ_C into A_C and find $A_\mathrm{C}(\varepsilon \longrightarrow 0) \sim \varepsilon^{-\nu_\mathrm{C}}$. Finally, upon inserting this result into Eq. (3), we arrive at $\nu_\mathrm{C} = 1/2$ [16]. More precisely, one obtains $\gamma_\mathrm{C}(\varepsilon \longrightarrow 0) \sim \beta^{-1}(\eta\varepsilon_F^0\varepsilon)^{1/2}$ and

$$G_R(\mathbf{p} \in \mathrm{C}, \varepsilon \longrightarrow 0) \sim e^{-i\pi/4}[\gamma_\mathrm{C}(\varepsilon \longrightarrow 0)]^{-1} \sim e^{-\pi i/4}\beta(\eta\varepsilon_F^0\varepsilon)^{-1/2}. \quad (4)$$

This result can be shown to hold even if the momentum dependence of the quantities $\gamma_\mathrm{C}(\mathbf{p}, \varepsilon)$ and $\sigma_\mathrm{C}(\mathbf{p}, \varepsilon)$ is properly taken into account to ensure the correct momentum distribution $n(\mathbf{p})$. We see that, in the FC region, the conventional structure of the Green's function is destroyed, the familiar pole being replaced by a branch point at $\varepsilon = 0$.

Now we are in position to discuss the impact of the damping on the topological charge N of a system with the FC introduced by Volovik [8]. Recall that in 2D systems this charge is given by the integral

$$N = \oint_L \frac{dl}{2\pi i} G(\mathbf{p}, \varepsilon = i\Omega)\partial_l G^{-1}(\mathbf{p}, \varepsilon = i\Omega) \quad (5)$$

taken along the contour L embracing the Fermi line in the 3D space (p_x, p_y, Ω). If one neglects the ε dependence of $\Sigma(\mathbf{p}, \varepsilon)$, then the FC Green's function $G(\mathbf{p} \in \mathrm{C}, \varepsilon) = [\varepsilon + \mu - \epsilon_\mathbf{p}^0 - \Sigma(\mathbf{p}, \varepsilon)]^{-1}$ becomes $1/\varepsilon$ and, upon inserting this expression for G into the integral (5), one finds $N = 1/2$, implying that systems with the FC form a separate class of normal Fermi liquids [8]. What happens to the topological charge N if the energy dependence of the mass operator is incorporated and $G = 1/\varepsilon$ is replaced by the Green's function (4)? After performing simple integration, we are again led to the previous result $N = 1/2$ [8], in spite of the dramatic alteration of the Green's function itself that occurs in the FC region.

In the transition region T, the decay into the FC states is not kinematically forbidden. Accordingly, $\gamma_\mathrm{T}(\varepsilon \longrightarrow 0) \sim \beta^{-1}(\eta\varepsilon_F^0\varepsilon)^{1/2}$, while the function $s(\mathbf{p} \in \mathrm{T})$ already differs from zero. Requiring it to vanish at the boundaries of the FC region, along with its first derivative, one finds that in the region T, the conventional structure of the Green's function is recovered, but in the vicinity of the FC domain, SP excitations appear to be ill-defined, since the pole of $G(\mathbf{p}, \varepsilon)$ is located close to the imaginary energy axis.

In the region M, dominant contributions to $\mathrm{Im}\Sigma_R(\varepsilon)$ come from a process associated with the generation of three states: two from the FC region and one from the M

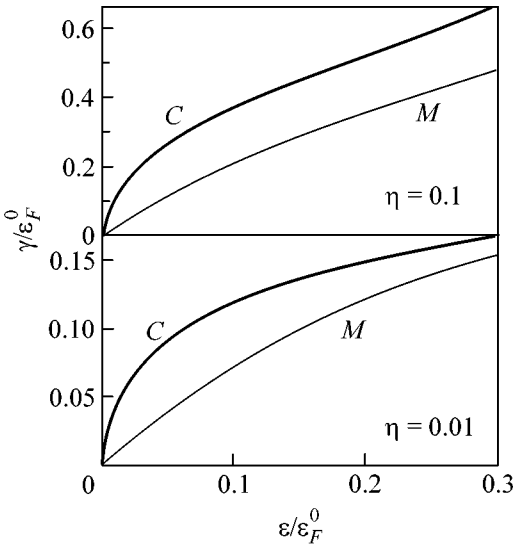

Fig. 1. The damping of the SP states (solid lines) in the vicinity of the vHP and (thin lines) around the diagonals of the Brillouin zone, as calculated with the scattering amplitude $\Gamma(\mathbf{p}, \mathbf{p}_1) = (N(0))^{-1}[\beta^2 + \kappa^2(\mathbf{p} - \mathbf{p}_1 - \mathbf{Q})^2]^{-1}$, where $N(0)$ is the density of states and $\beta = 0.2$; $\eta =$ (upper panel) 0.1 and (lower panel) 0.01. Damping is measured in ε_F^0.

region. In this case, the formula for finding $\gamma_M(\varepsilon \longrightarrow 0)$ reads

$$\gamma_M(\varepsilon \longrightarrow 0) \sim \beta^{-4} \sum_{\mathbf{p}, \mathbf{p}_1}^{0\ 0} \int\int_{\varepsilon\ \omega} A_C(-\varepsilon_1) A_C(\omega - \varepsilon_1) \times [1 - \theta(\mathbf{p})] P_C(\mathbf{p} - \mathbf{p}_1) A_M(\mathbf{p}, \varepsilon - \omega) d\omega d\varepsilon_1, \quad (6)$$

where $P_C(\mathbf{q}) = \sum_{\mathbf{p}} \theta(\mathbf{p})\,\theta(\mathbf{p} - \mathbf{q})$ and $\theta(\mathbf{p}) = 1$ if $\mathbf{p} \in$ C and vanishes otherwise. It is seen that, in this case, the momentum and energy integrations do not separate. However, one can take advantage of the fact that the spectrum $\xi_M(\mathbf{p}) = \epsilon_M(\mathbf{p}) - \mu$ is proportional to $(p - p_F)$ and introduce $\xi_M(\mathbf{p})$ as a new variable. Then, after simple integration, we are led to the result $\nu_M = 1$, postulated in the model of a marginal Fermi liquid [21]. Evaluation of the η dependence of relevant quantities in the M region yields $\gamma_M(\varepsilon \longrightarrow 0) \sim \beta^{-2}\eta^{1/2}\varepsilon$ and $\sigma_M(\varepsilon \longrightarrow 0) \sim \beta^{-2}\eta^{1/2}\varepsilon \ln|\varepsilon|$.

These results can be applied to the case $\varepsilon \sim T$, where, according to Eq. (4), the leading term in the FC Green's function has the form $G_R(\mathbf{p} \in \text{C}, \varepsilon) \sim e^{-i\pi/4}[\gamma_C(\varepsilon, T)]^{-1}$. Upon inserting this expression into Eq. (3), one finds that the damping $\gamma_C(x, T)$, where $x = \varepsilon/T$, can be displayed as $\gamma_C(x, T) = \gamma_C \sqrt{T\varepsilon_F^0}\, D(x)$, where the constant γ_C specifies the compound, while the dimensionless quantity $D(x)$ obeys the universal integral equation

$$D(x) = \cosh\frac{x}{2} \times \iint \frac{dydz}{\cosh\frac{y}{2}\cosh\frac{x-z}{2}\cosh\frac{z-y}{2} D(-y) D(x-z) D(z-y)}. \quad (7)$$

With this result, the damping $\gamma_M(x, T)$ is calculated straightforwardly:

$$\gamma_M(x, T) = \gamma_M T \cosh\frac{x}{2} \times \iint \frac{dydz}{\cosh\frac{y}{2}\cosh\frac{x-z}{2}\cosh\frac{z-y}{2} D(-y) D(z-y)}, \quad (8)$$

the constant γ_M being a characteristic of the given compound. The function $\gamma_M(x, T)/T$ starts out of the origin as a parabolic function $\gamma_M(x, T)/T \sim 1 + 0.1x^2$. The asymptotic regime $\gamma_M(x, T)/T \sim x$, stemming from Eq. (6), is attained at $x \sim 2.5$.

Equations (7) and (8) hold even in superfluid states as long as the gap value remains less than the damping $\gamma_C(T)$. On the other hand, they are violated if the energy attains values for which contributions to $\gamma(\varepsilon)$ that were omitted from Eqs. (3) and (6) become comparable to the terms that were retained. A leading correction $\delta\gamma_C(\varepsilon)$ to the integral (3) comes from the final states, which involve one hole (particle) belonging to the region T. Equation (6), with the single replacement $s(\mathbf{p} \in \text{M}) \longrightarrow s(\mathbf{p} \in \text{T})$, can be employed to estimate this contribution.

We find $\delta\gamma_C(\varepsilon \longrightarrow 0) \sim \beta^{-1}\varepsilon$, which is independent of the η value. Estimation of other corrections to $\gamma(\varepsilon)$ is carried out along the same lines, justifying the identification of (3) and (6) as paramount contributions to $\text{Im}\Sigma_R(\mathbf{p}, \varepsilon \longrightarrow 0)$ until ε exceeds the characteristic FC energy $\varepsilon_{FC} \sim \eta\varepsilon_F^0$ evaluated by comparison of $\delta\gamma_C(\varepsilon)$ and $\gamma_C(\varepsilon) \sim \beta^{-1}(\eta\varepsilon_F^0\varepsilon)^{1/2}$.

At energies $\varepsilon \geq \varepsilon_{FC}$, corrections exhibit themselves in full force, so Eq. (2) should be solved numerically in conjunction with the Kramers–Krönig relation, employed to connect $\gamma(\varepsilon)$ and $\sigma(\varepsilon)$. This is performed with the aid of an iteration procedure, which converges rapidly. In Fig. 1, we display results from these calculations. Two different η values, specifying the fraction of the Brillouin zone occupied by the FC, were considered: (a) $\eta = 0.1$, close to the maximum η value in the model of fermion condensation driven by antiferromagnetic fluctuations [18], and (b) $\eta = 0.01$. In spite of the simplicity of the interaction adopted, the salient features of ARPES data [3, 6, 15] are reproduced, including the shape of the curve $\text{Im}\Sigma_R(\mathbf{p} \in \text{M}, x, T)/T$ as a

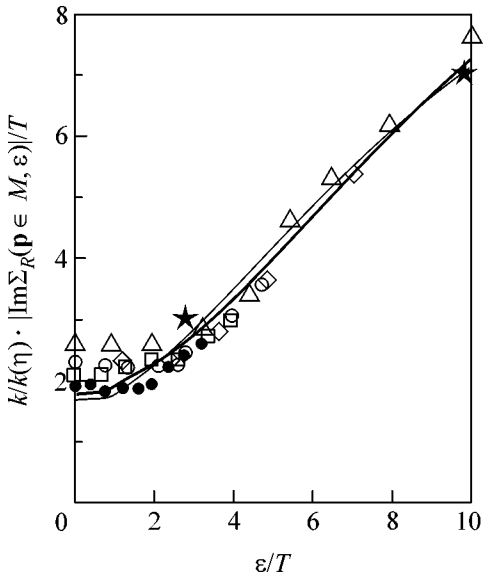

Fig. 2. The ratio $|\mathrm{Im}\Sigma_R(\varepsilon)|/T$ around the diagonal of the Brillouin zone as a function of ε/T, calculated for η = (solid line) 0.1 and (thin line) 0.01 and normalized to the same slope $k = 0.75$, i.e., multiplied by the factor $k/k(\eta)$, where $k(\eta) = |\partial \mathrm{Im}\Sigma_R(\mathbf{p} \in \mathrm{M}, \varepsilon, T; \eta)/\partial\varepsilon|$. The experimental data for the optimally doped cuprate $Bi_2Sr_2CaCu_2O_{8+\delta}$ [3] are shown by open and solid circles (T = 300 K), triangles and squares (T = 90 K), and diamonds and stars (T = 48 K).

function of $x = \varepsilon/T$ measured in [3] for the optimally doped cuprate $Bi_2Sr_2CaCu_2O_{8+\delta}$, provided the proper normalization of the results is done. Moreover, our theory predicts the same behavior of $\mathrm{Im}\Sigma_R(\mathbf{p} \in \mathrm{M}, x)/T$ in different compounds. This can be seen from Fig. 2, where two curves of $\mathrm{Im}\Sigma_R(\mathbf{p} \in \mathrm{M}, x, T)/T$ evaluated at $\eta = 0.1$ and $\eta = 0.01$ and normalized at $x \gg 1$ to the same slope are compared to each other and to experimental data [3]. At the same time, as seen from the above formula $\gamma_C(x, T) = \gamma_C\sqrt{T\varepsilon_F^0}D(x)$, the linearity of $\mathrm{Im}\Sigma_R(T)$ with T at a given x uncovered in [3] is destroyed in the FC region, and, instead, this function displays $\sqrt{T}$ dependence.

The above scenario, in which the fermion condensation precedes the antiferromagnetic phase transition, does apply in the three-dimensional case, although the range of the FC region shrinks markedly. Along the same lines, one can analyze the situation with fermion condensation in the vicinity of other second-order phase transitions, such as charge-density-wave instability [12]. So far, the feedback of the FC on the scattering amplitude r has been ignored. However, the simplest FC diagram, i.e., a loop evaluated with the FC Green's function (4), diverges logarithmically. As a result, we are led to a familiar problem of the parquet-diagram summation, the solution to which will be reported in a separate paper.

Summing up the results of our analysis, we infer that electron systems with a fermion condensate, irrespective of the dimensionality, do not admit Landau quasiparticles, since the renormalization factor $z = (1 - \partial\Sigma/\partial\varepsilon)_F^{-1}$ determining the quasiparticle weight in the SP state vanishes in all regions of the Brillouin zone. The model of fermion condensation presented here allows one to explain basic features of the spectral functions of normal states of high-T_c superconductors, including (i) the marginal Fermi liquid behavior of the damping of SP states around the diagonals of the Brillouin zone (the M region) and (ii) the suppression of the peaks in APRES data in the immediate vicinity of the van Hove points (the C region). The universal behavior of the ratio $\mathrm{Im}\Sigma_R(\mathbf{p} \in M, T, x)/T$, where $x = \varepsilon/T$, as established in the M region in [3], is also reproduced in this model. Moreover, our model predicts that all data for $\mathrm{Im}\Sigma_R(\mathbf{p} \in M, T, x)/T$, when properly normalized, should collapse on the same curve. However, as we have seen, this universal behavior is destroyed in the C region.

We are grateful to P.W. Anderson, J.C. Campuzano, J.W. Clark, L.P. Gor'kov, K.A. Kikoin, G. Kotliar, A.J. Millis, J. Mesot, N. Nafari, M.R. Norman, E.E. Saperstein, and G.E. Volovik for many stimulating discussions. This work was supported in part by the NSF (Grant no. PHY-9900713), the McDonnell Center for the Space Sciences (VAK), and the Russian Foundation for Basic Research (project no. 00-15-96590). VAK is grateful to J.W. Clark for kind hospitality at Washington University in St. Louis.

REFERENCES

1. L. D. Landau, Zh. Éksp. Teor. Fiz. **30**, 1058 (1956) [Sov. Phys. JETP **3**, 920 (1956)]; Zh. Éksp. Teor. Fiz. **35**, 97 (1958) [Sov. Phys. JETP **8**, 70 (1958)].
2. A. Kaminski, J. Mesot, H. Fretwell, *et al.*, cond-mat/9904390.
3. T. Valla, A. V. Fedorov, P. D. Johnson, *et al.*, Science **285**, 2110 (1999).
4. Z.-X. Shen and J. R. Schrieffer, Phys. Rev. Lett. **78**, 1771 (1997).
5. M. R. Norman, H. Ding, H. Fretwell, *et al.*, Phys. Rev. B **60**, 7585 (1999).
6. Z. Yusof, B. O. Wells, T. Valla, *et al.*, cond-mat/0104367.
7. V. A. Khodel and V. R. Shaginyan, Pis'ma Zh. Éksp. Teor. Fiz. **51**, 488 (1990) [JETP Lett. **51**, 553 (1990)]; Condens. Matter Theor. **12**, 222 (1997).
8. G. E. Volovik, Pis'ma Zh. Éksp. Teor. Fiz. **53**, 208 (1991) [JETP Lett. **53**, 222 (1991)]; Pis'ma Zh. Éksp. Teor. Fiz. **59**, 798 (1994) [JETP Lett. **59**, 830 (1994)].
9. P. Nozieres, J. Phys. I **2**, 443 (1992).
10. V. A. Khodel, V. V. Khodel, and V. R. Shaginyan, Phys. Rep. **249**, 1 (1994).
11. V. A. Khodel, J. W. Clark, and V. R. Shaginyan, Solid State Commun. **96**, 353 (1995).

12. V. A. Khodel, V. R. Shaginyan, and M. V. Zverev, Pis'ma Zh. Éksp. Teor. Fiz. **65**, 242 (1997) [JETP Lett. **65**, 253 (1997)].
13. J. Dukelsky, V. A. Khodel, P. Schuck, and V. R. Shaginyan, Z. Phys. B **102**, 245 (1997).
14. M. V. Zverev and M. Baldo, Zh. Éksp. Teor. Fiz. **114**, 2078 (1998) [JETP **87**, 1129 (1998)]; J. Phys.: Condens. Matter **11**, 2059 (1999).
15. M. R. Norman, in *High Temperature Superconductivity*, Ed. by S. E. Barnes, J. Ashkenazi, J. L. Cohn, and F. Zuo (American Inst. of Physics, Woodbury, 1999), p. 298.
16. V. A. Khodel and M. V. Zverev, Pis'ma Zh. Éksp. Teor. Fiz. **70**, 759 (1999) [JETP Lett. **70**, 772 (1999)].
17. M. V. Zverev, V. A. Khodel, and M. Baldo, Pis'ma Zh. Éksp. Teor. Fiz. **72**, 183 (2000) [JETP Lett. **72**, 126 (2000)].
18. M. V. Zverev, V. A. Khodel, and J. W. Clark, Pis'ma Zh. Éksp. Teor. Fiz. **74**, 48 (2001) [JETP Lett. **74**, 46 (2001)].
19. A. A. Abrikosov, L. P. Gor'kov, and I. E. Dzyaloshinskii, in *Methods of Quantum Field Theory in Statistical Physics* (Fizmatgiz, Moscow, 1962; Prentice-Hall, Englewood Cliffs, 1965), p. 172.
20. A. J. Millis, H. Monien, and D. Pines, Phys. Rev. B **42**, 167 (1990).
21. C. M. Varma, P. B. Littlewood, S. Schmitt-Rink, *et al.*, Phys. Rev. Lett. **63**, 1996 (1989).

JETP Letters, Vol. 74, No. 10, 2001, pp. 507–511. Translated from Pis'ma v Zhurnal Éksperimental'noĭ i Teoretichesko ĭ Fiziki, Vol. 74, No. 10, 2001, pp. 570–574.

Shot Noise in Mesoscopic Systems with Resonance Andreev Tunneling

A. V. Lebedev and G. B. Lesovik

Landau Institute for Theoretical Physics, Russian Academy of Sciences, ul. Kosygina 2, Moscow, 117334 Russia

Received November 1, 2001

The general scattering-matrix formalism is suggested for the description of shot noise in single-channel quantum NS contacts in the presence of smeared Andreev levels in the $eV < \Delta$ regime. It is shown that the noise spectral density as a function of frequency shows a number of characteristic features due to the presence of the Andreev resonances in the system. It turns out that, by analyzing these singularities, one can determine the relative phases of the Andreev reflection amplitudes corresponding to the neighboring resonances. © *2001 MAIK "Nauka/Interperiodica".*

PACS numbers: 72.70.+m; 73.23.-b

Shot noise in normal and superconducting systems is an interesting phenomenon, because it can be used to examine those features of electron transport which do not affect quantities of the type of current–voltage characteristic.

For example, the noise spectral density $S(\omega)$ of a normal quantum conductor has a singularity at frequency $\omega = eV/\hbar$ specified by the contact voltage [1, 2]. At the same time, shot noise of an ideal NS contact in the $eV < \Delta$ regime has a singularity at the Josephson frequency $\hbar\omega = 2eV$ [3, 4]. Since both these systems have well-defined linear current–voltage characteristics, it seems quite unexpected that the noise has a certain "intrinsic" frequency. This frequency is caused by a peculiar kind of two-particle interference, and it is precisely for this reason that it appears in the noise and not in conductance. In the $eV > \Delta$ regime, the noise shows additional features at frequencies $\hbar\omega = 2\Delta$ and $eV \pm \Delta$(see [5, 6]) related to the singularity in the conductance at $eV = \Delta$.

The noise singularities at a finite frequency ω_0 can also be revealed by studying the experimentally more accessible low-frequency noise in the presence of an additional ac voltage at frequencies $\Omega = \omega_0/n$ with integer n's. For the normal contact and $eV = n\hbar\Omega$, singularities in the zero-frequency noise spectral density $S(0, V)$ were found in [2] in the presence of ac voltage at frequency Ω (this was confirmed experimentally in [7]). Similarly, $S(0, V)$ for an NS contact also shows singularities in the presence of ac voltage at frequency Ω, but now $2eV = n\hbar\Omega$ [4], which was demonstrated experimentally in [8].

In [2, 4, 5], noise was studied using the scattering matrix formalism. However, this matrix was assumed to be independent of the particle energy.

In this work, we consider shot noise in superconducting systems in the Andreev regime $eV < \Delta$ at zero temperature, when the smeared Andreev energy levels (resonances) may be present, so that the scattering matrix of the system may *depend explicitly on energy.* It is found that the noise singularities can appear in this case at frequencies $(eV \pm \epsilon_n)/\hbar$ and $(\epsilon_n \pm \epsilon_m)/\hbar$.

It is remarkable (and unexpected) that the relative phases of the resonances can be judged from the presence of singularities at frequencies $(\epsilon_n \pm \epsilon_m)/\hbar$. Note that the problem of relative phases is not all that trivial. Experiments [9] demonstrate that the relative phase of the transmission amplitudes corresponding to two neighboring resonances in a quantum dot is a multiple of 2π, instead of expected π (a plausible explanation of this experiment is given in [10]). The revelation of the fact that the relative phases can be measured and the development of the general formalism for the description of noise in the presence of Andreev resonances are the major results of this work.

Moreover, in the particular case of the Andreev resonance near the Fermi level, a singularity appears at $\omega \simeq eV/\hbar$, which is typical of a normal conductor. This was likely observed experimentally in [11]. Our calculations show that the appearance of the frequency $\omega \simeq eV/\hbar$ in this case does not necessarily means that there is a transition to normal conductivity.

Both in the stationary case and in the presence of ac voltage, the calculation of noise using the scattering matrix technique is the well-known procedure and can be found in many works, so we will not go into the details of this calculation (see, e.g., [1, 2, 4, 5, 12] and references therein). We will assume that a single nor-

mal metal contact is attached to the mesoscopic system under study. To calculate noise, one has to determine the scattering matrix for the contact. In the electron–hole space, this matrix has the form

$$\hat{\mathbf{S}}(\epsilon) = \begin{pmatrix} s_{ee}(\epsilon) & s_{eh}(\epsilon) \\ s_{he}(\epsilon) & s_{hh}(\epsilon) \end{pmatrix}. \quad (1)$$

We will not describe the internal organization of the mesoscopic system in detail but merely construct the scattering matrix using the unitarity and the electron–hole symmetry conditions (the latter follows from the Bogoliubov equation), assuming that the widths and positions of resonances are given by $E_n = \epsilon_n - i\Gamma_n/2$:

$$s_{ee}(\epsilon) = s_{hh}^*(-\epsilon), \quad s_{eh}(\epsilon) = -s_{he}^*(-\epsilon), \quad |s_{he}(\epsilon)| = |s_{eh}(\epsilon)|. \quad (2)$$

Since all resonances E_n are simple poles of the $\hat{\mathbf{S}}$ matrix, the scattering matrix can be sought in the form

$$\hat{\mathbf{S}}(\epsilon) = \hat{\mathbf{S}}_0 + \sum_n \left(\frac{\hat{\mathbf{S}}_{-n}}{\epsilon - E_{-n}} + \frac{\hat{\mathbf{S}}_n}{\epsilon - E_n} \right), \quad (3)$$

where $\hat{\mathbf{S}}_0$ and $\hat{\mathbf{S}}_n$ are the constant 2×2 matrices, and $E_{\pm n} = \epsilon_n - i\Gamma_n/2$ are the resonances symmetric about zero.

Using symmetry conditions (2), one obtains the following relations between the matrix elements of $\hat{\mathbf{S}}_n$ and $\hat{\mathbf{S}}_0$:

$$\hat{\mathbf{S}}_0 = \begin{pmatrix} a_0 & b_0 \\ -b_0^* & a_0^* \end{pmatrix}, \quad \hat{\mathbf{S}}_n = \begin{pmatrix} a_n & b_n \\ b_{-n}^* & -a_{-n}^* \end{pmatrix}, \quad (4)$$

$$a_{-n}a_0^* = -a_n^* a_0; \quad b_{-n}b_0^* = -b_n^* b_0. \quad (5)$$

In turn, the unitarity condition gives $\hat{\mathbf{S}}_0^+ \hat{\mathbf{S}}_0 = \hat{\mathbf{1}}$ and

$$b_{-n}\left(a_0 + \sum_m \mathbf{A}_{nm} a_m \right) = a_{-n}\left(b_0 + \sum_m \mathbf{A}_{nm} b_m \right), \quad (6)$$

$$b_n^*\left(a_0 + \sum_m \mathbf{A}_{nm} a_m \right) = -a_n^*\left(b_0 + \sum_m \mathbf{A}_{nm} b_m \right), \quad (7)$$

where $\mathbf{A}_{nm} = 1/(E_n^* - E_m)$.

Let none of the numbers a_n and b_n be zero. By introducing the parameters $\alpha_n = b_n/a_n \neq 0$, one obtains from Eqs. (6) and (7) the following equations for the coefficients of the scattering matrix:

$$\alpha_n \alpha_{-n}^* = -1, \quad \sum_m \mathbf{B}_{nm} a_m + a_0 + b_0 \alpha_n^* = 0, \quad \forall n \quad (8)$$

where $\mathbf{B}_{nm} = \mathbf{A}_{nm}(1 + \alpha_n^* \alpha_m)$. One can rigorously show that, if $\forall \alpha_n \neq 0$, then the matrix $\mathbf{B}$ always has its inverse; i.e., Eq. (8) always has a solution for the a_n numbers.

Using relationships (5), one can verify that the parameters α_n are not arbitrary but equal to

$$\alpha_{\pm n} = \pm \lambda_n e^{i\phi}, \quad (9)$$

where $\lambda_n = \pm 1$, and $e^{i\phi} = i\sqrt{(b_0/b_0^*)(a_0^*/a_0)}$ is a constant phase factor.

Equation (8) and condition (9) completely solve the problem of constructing the scattering matrix. Let $2N$ symmetric resonances $E_{\pm n} = \pm\epsilon_n - i\Gamma_n/2$ occur near the Fermi level. Then, by choosing n numbers $\lambda_n = \pm 1$ for each of the N resonances on one side of the Fermi level and specifying the unitary matrix $\hat{\mathbf{S}}_0$, one uniquely finds all coefficients of the matrices $\hat{\mathbf{S}}_n$ using Eq. (8) and conditions (4):

$$\hat{\mathbf{S}}_n = a_n \begin{pmatrix} 1 & \lambda_n e^{i\phi} \\ \lambda_n e^{-i\phi} & 1 \end{pmatrix}. \quad (10)$$

In the case of narrow resonances, i.e., if $|\epsilon_n - \epsilon_m| \ll \Gamma_n, \Gamma_m \ \forall n, m$, the parameterization using numbers λ_n has a clear meaning: if $\lambda_n \lambda_{n+1} = \mp 1$ for two neighboring well-separated resonances ϵ_n and ϵ_{n+1}, then the phase of the Andreev reflection amplitude s_{he} or s_{eh} changes, respectively, by π or 2π upon going from one resonance to another.

Let us consider a noise at positive frequencies. One can obtain the following expression for the noise at $0 < \omega < 2eV/\hbar$ [$S(\omega) = 0$ at $\omega > 2eV/\hbar$] in terms of the Andreev and normal reflection amplitudes:

$$S(\omega) = \frac{2e^2}{h} \times \int_{\hbar\omega - eV}^{eV} (R_N(\epsilon)R_A(\hbar\omega - \epsilon) + K(\epsilon)K^*(\hbar\omega - \epsilon))d\epsilon, \quad (11)$$

where $R_A(\epsilon) = |s_{he}(\epsilon)|^2$, $R_N(\epsilon) = |s_{ee}(\epsilon)|^2$, and $K(\epsilon) = s_{ee}^*(\epsilon)\, s_{he}(\epsilon)$.

Using Eq. (10), one obtains the following expression for the noise:

$$S(\omega) = 2\frac{e^2}{h}\int_{\hbar\omega - eV}^{eV} d\epsilon \times\left\{R_A(\epsilon) - \left(\sum_{nm}\frac{\chi_n\chi_m(1+\lambda_n\lambda_m)}{(\epsilon - E_n^*)(\hbar\omega - \epsilon - E_m^*)} + \text{c.c.}\right)\right. \quad (12)$$
$$\left. + \left(\sum_{nm}\frac{\chi_n^*\chi_m(1-\lambda_n\lambda_m)}{(\epsilon - E_n)(\hbar\omega - \epsilon - E_m^*)} + \text{c.c.}\right)\right\},$$

where $\chi_n = a_n^* \sum_m A_{nm}\lambda_m a_m$ is a constant factor and eV is the contact voltage. Although the integral in Eq. (12) can be elementarily evaluated, we will not present here the results, because the corresponding expressions are rather cumbersome and uninformative.

Certain general conclusions can be drawn for the narrow resonances. Indeed, for $|\epsilon_n - \epsilon_m| \ll \Gamma_n, \Gamma_m\ \forall n, m$, one can set $a_0 = 1$ and $b_0 = 0$ in the $\hat{\mathbf{S}}_0$ matrix. Such a choice for $\hat{\mathbf{S}}_0$ corresponds to the case where the Andreev reflection probability in the resonance is unity, as can easily be seen if one uses the well-known Breit–Wigner formula and expands $\hat{\mathbf{S}}(\epsilon)$ near the respective resonance. Then $a_n = -i\Gamma_n/2$ and $\chi_n = -(i/4)\lambda_n\Gamma_n\ \forall n$. Taking also into account that the terms in the second sum of Eq. (12) are the products of two poles located on one side of the real axis and, hence, make a negligible contribution to the integral, one can obtain the following approximate formula for the noise at $\omega > 0$:

$$S(\omega) = 2\pi\frac{e^2}{h}\left\{\sum_n\frac{\Gamma_n}{2}\right. \quad (13)$$
$$\left. - \frac{1}{8}\sum_{n,m}\frac{(1+\lambda_n\lambda_m)\Gamma_n\Gamma_m(\Gamma_n+\Gamma_m)}{(\hbar\omega - \epsilon_n - \epsilon_m)^2 + (\Gamma_n+\Gamma_m)^2/4}\right\},$$

where the summation is over only those resonances for which $\hbar\omega - eV < \epsilon_n < eV$.

It follows that the finite-frequency noise has singularities of two characteristic types: "steps" at frequencies $\hbar\omega_n = eV \pm \epsilon_n$ and "dips" with widths $\Gamma_n + \Gamma_m$ at frequencies $\omega_{nm} = (\epsilon_n + \epsilon_m)/\hbar > 0$ such that $\lambda_n\lambda_m = 1$, where the noise is partially suppressed (in some cases, almost to zero; see below). Inasmuch as $\lambda_n^2 = 1\ \forall n$, the singularity at $\omega_{nn} > 0$ is always of the second type, whereas the appearance of such singularities at frequencies ω_{nm} depends on the relative phase of the Andreev reflection amplitudes for the nth and mth resonances.

If $\lambda_n\lambda_m = -1$ (relative phase of the Andreev reflection amplitudes for the corresponding resonances is a multiple of π; i.e., resonances are "in antiphase"), then the dip appears at frequency $\omega = |\epsilon_n - \epsilon_m|/\hbar$; in turn, if $\lambda_n\lambda_m = 1$ (relative phase is a multiple of 2π; i.e., the resonances are "in phase"), then noise is suppressed at frequency $\omega_{nm} = (\epsilon_n + \epsilon_m)/\hbar$.

As for steps, the singularities of this type are always present, regardless of the relative phase of resonances. Although function (13) has discontinuities at $\omega_n = (eV + \epsilon_n)/\hbar$, the noise is continuous at these frequencies, because steps have finite widths of order Γ_n. Therefore, Eq. (13) properly describes the behavior of noise away from steps, i.e., at $eV + \epsilon_n < \hbar\omega < eV + \epsilon_{n+1}$.

One can show that the noise singularities at negative frequencies are exactly the same as at $\omega > 0$. Likewise, the positions of noise singularities of the second type (dips) are determined by the relative phases of Andreev resonances. For this reason, the symmetrized current correlator $S_{\text{sym}}(\omega) = 1/2(S(\omega) + S(-\omega))$ must show the same singularities and the same dependence of their positions on the relative phases of resonances. Therefore, noise measurements can provide information not only on the position of resonances but also on their relative phases, which cannot be done by measuring only the conductance of a mesoscopic system.

If all resonances have almost the same widths and are arranged periodically (within the widths Γ_n and Γ_{n+1} of the corresponding resonances), i.e., if $\epsilon_{n+1} - \epsilon_n \approx \Delta_\epsilon$, and if, moreover, any two neighboring resonances are in antiphase, then, as follows from Eq. (13), the noise at positive frequencies $\omega_n = n\Delta_\epsilon/\hbar$ is suppressed almost to zero because of the superposition of singularities at frequencies $\omega_{nn} = (\epsilon_n + \epsilon_n)/\hbar \approx (2n - 1)\Delta_\epsilon/\hbar$ and $\omega_{ij} = (\epsilon_i + \epsilon_j)/\hbar \approx \omega_{nn}$ such that $\lambda_i\lambda_j = 1$. This situation occurs, for example, in a ballistic NINS contact if the NS interface is close to ideal.

We illustrate this by a particular case where only two resonances, $E_1 = \epsilon_1 - i\Gamma_1/2$ and $E_2 = \epsilon_2 - i\Gamma_2/2$, fall within the eV interval (if there are several resonances in the system, we assume that their energies $\epsilon_n \gg eV$, i.e., that they do not affect the noise behavior at frequencies $|\omega| \le 2eV/\hbar$). All characteristic frequencies can conveniently be schematized by the energy diagram shown in Fig. 1. In this case, the scattering matrix can be parameterized only in two ways: $\lambda_1 = \lambda_2 = 1$ (in-phase resonances) and $\lambda_1 = -\lambda_2 = 1$ (antiphase resonances). The results of numerical calculation of the noise at positive frequencies are presented for each of the parameterizations in Fig. 2, where the singularities are clearly seen at all characteristic frequencies shown in Fig. 1. One can see from Fig. 1 that (cf. [11]), in the presence of a resonance near ϵ_F, a step appears at frequency $\omega \simeq eV/\hbar$, which is not associated with any normal (nonsuperconducting) transport regime.

We now describe qualitatively how a finite temperature influences the noise singularities. At $T \neq 0$, the Fermi step is smeared; i.e., the characteristic energy eV

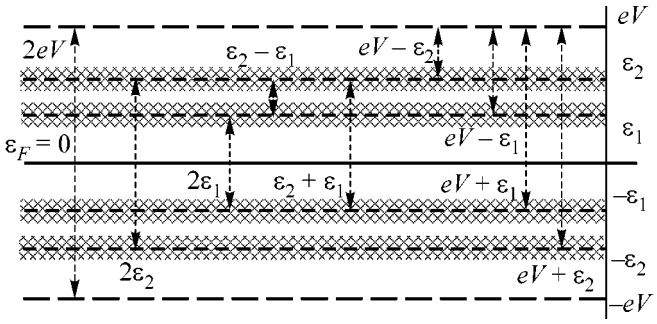

Fig. 1. Diagram of the characteristic energy intervals in the system. The corresponding frequencies are indicated by arrows, and the resonance widths are cross-hatched (scale is not kept).

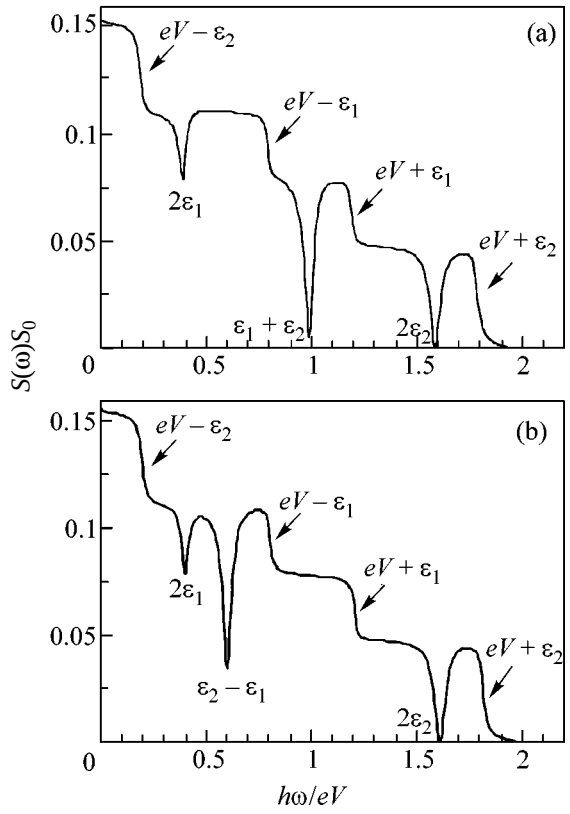

Fig. 2. Noise at positive frequencies in units of $S_0 = 2(e^2/h)eV$ for (a) in-phase levels and (b) antiphase levels: $\epsilon_1 = 0.2$ eV, $\epsilon_2 = 0.8$ eV, $\Gamma_1 = 0.02$ eV, and $\Gamma_2 = 0.03$ eV.

in the diagram in Fig. 1 is smeared by $\sim T$ (similar to the smearing of the resonances by $\sim\Gamma$). At $T \ll \min|\epsilon_n - \epsilon_m|$, the steps at frequencies $(eV \ll \epsilon_n)/\hbar$ are broadened to $\Gamma_n + T$ (Fig. 1), and the singularity at the Josephson frequency $2eV/\hbar$ acquires a width of $\sim 2T$. As for the singularities of the second type (dips) at frequencies $(\epsilon_n + \epsilon_m)/\hbar$, $\epsilon_n, \epsilon_m \ll eV$), their widths and shapes should not change at temperatures $T \ll \min|\epsilon_n - \epsilon_m|$.

One can see that the noise has no zero-frequency singularities in the case of narrow resonances. Now let any two neighboring resonances, ϵ_1 and ϵ_2, be in antiphase and separated by a distance which cannot be regarded as small (i.e., $\epsilon_2 - \epsilon_1 \sim \Gamma_1, \Gamma_2$), but both them are away from the Fermi level ($\epsilon = 0$). In this case, one cannot use the Breit–Wigner formula for calculating the scattering amplitudes near ϵ_1 and ϵ_2. Whereas $R_A(\epsilon)$ for narrow resonances has maxima exactly at ϵ_n, such is not the case for two closely spaced resonances. These resonances merge; i.e., the maxima of $R_A(\epsilon)$ start to approach each other and occur at the points $(1/2)(\epsilon_1 + \epsilon_2) \pm (1/2)\sqrt{(\epsilon_2 - \epsilon_1)^2 - \Gamma_1\Gamma_2}$ separated by a distance smaller than the distance between the corresponding quasi-discrete energy levels. The resonances fully merge at $\Delta = \epsilon_2 - \epsilon_1 = \sqrt{\Gamma_1\Gamma_2}$, resulting in a single maximum (equal unity) of $R_A(\epsilon)$ at $\epsilon = (\epsilon_1 + \epsilon_2)/2$. On further decrease in Δ, this maximum decreases to zero. Therefore, after the resonances fully merge, measurement of conductance alone will not give an answer to the question as to whether two closely spaced quasi-discrete levels or only one level occur at $(\epsilon_1 + \epsilon_2)/2$.

One should expect that if the Δ distance becomes too small ($\Delta \sim \sqrt{\Gamma_1\Gamma_2}$), then the corresponding noise singularities at frequencies $2\epsilon_{1,2}/\hbar$, $(eV + 2\epsilon_{1,2})/\hbar$, etc., also merge. In particular, the singularity at $(\epsilon_2 - \epsilon_1)/\hbar$ shifts exactly to zero. The analytic expression for the low-frequency noise at $(\epsilon_1 + \epsilon_2)/2 \ll eV$ has the form

$$S(\omega) = 4\pi\frac{e^2}{h}\Gamma_+\frac{\Delta^2 + \Gamma_-^2}{\Delta^2 + \Gamma_+^2} \times\left\{1 - \frac{\Gamma_1\Gamma_2}{2\Gamma_+}\left(\frac{\Gamma_+\cos 2\phi + (\hbar\omega + \Delta)\sin 2\phi}{(\hbar\omega + \Delta)^2 + \Gamma_+^2}\right.\right. \quad (14)$$
$$\left.\left. + \frac{\Gamma_+\cos 2\phi + (\Delta - \hbar\omega)\sin 2\phi}{(\hbar\omega - \Delta)^2 + \Gamma_+^2}\right)\right\},$$

where $\Gamma_+ = (\Gamma_1 + \Gamma_2)/2$, $\Gamma_- = (\Gamma_1 - \Gamma_2)/2$, and $\phi = \arctan(\Gamma_+/\Delta)$. The results of the numerical calculation of the noise near zero frequency are presented in Fig. 3 as functions of the ratio Γ_+/Δ. One can see that, at $\Gamma_+/\Delta < 1$ ("near-narrow" resonances), noise has a minimum near (but not at) zero; at $\Gamma_+/\Delta \sim 1$ the minimum shifts to zero; and at $\Gamma_+/\Delta \gg 1$ the noise has a maximum at zero.

Let us now briefly consider the nonstationary case with an alternating vector potential $A_x(t) = A_x\sin\Omega t$ applied to a restricted region of width d near the contact. We are interested in the dependence of the zero-

frequency noise $S_0(\Omega, V)$ on the frequency of ac potential and the contact voltage. Assuming that electrons passing through the region with ac potential gain an additional phase $\Phi(t) = \Phi\sin\Omega t$ ($\Phi = 2\pi\int dx A_x/\Phi_0$) and that the potential $A_x(t)$ weakly changes in a time of electron passage through the scattering region, one can obtain

$$S_0(\Omega, V) = \sum_{n=-\infty}^{\infty}\left(1 - 2\Theta\left(n - \frac{2eV}{\hbar\Omega}\right)\right)J_n^2(2\Phi)F(n\Omega), \quad (15)$$

where $J_n(x)$ is the Bessel function and $F(\omega) = 2e^2/h\int_{\hbar\omega - eV}^{eV}(R_A(\hbar\omega - \epsilon)R_N(\epsilon) + K(\epsilon)K^*(\hbar\omega - \epsilon))\,d\epsilon$ [see Eq. (11)]. Since $F(2eV) = 0$, the first derivative of the noise with respect to the voltage is equal to

$$\frac{\partial S_0(V, \Omega)}{\partial V} = \sum_{n=-\infty}^{\infty}\left(1 - 2\Theta\left(n - \frac{2eV}{\hbar\Omega}\right)\right) \times J_n^2(2\Phi)\frac{\partial F(n\Omega)}{\partial V}. \quad (16)$$

It is seen that the derivative $\partial S_0/\partial V$ as a function of V has discontinuities (steps) at $2eV = n\Omega$. This result was obtained in [2] for the nonresonant case. In the resonance case, additional features appear as small peaks at $eV = \epsilon_i$ and $eV = n\Omega \pm \epsilon_i$, with widths Γ_i and heights given by the Bessel function squared $J_n^2(2\Phi)$. It should be noted that both the step heights at $2eV = n\hbar\Omega$ and the peak heights at $eV = \epsilon_i$ and $n\hbar\Omega \pm \epsilon_i$ are sensitive to the phase incursion during the electron (hole) passage through the region with the ac potential.

This calculation is formally valid only if $\hbar\Omega \ll \Gamma$ (the ac potential weakly changes during the scattering time). Because of this, the results obtained are formally invalid at $\hbar\Omega > \Gamma$. However, we believe that, at a qualitative level, they correctly describe the behavior of $\partial S(0)/\partial V$ in this case as well (at least, this relates to the positions of the peak and step singularities).

We thank the participants in the seminar of the Quantum Mesoscopics Division of the Institute for Theoretical Physics RAS for discussions. This work was supported by the Russian Foundation for Basic Research (project no. 00-02-16617), the Ministry of Science (project "Physical Principles of Quantum Calculations"), the Dutch Scientific Foundation (grant for collaboration with Russia), and the Swiss Scientific Foundation.

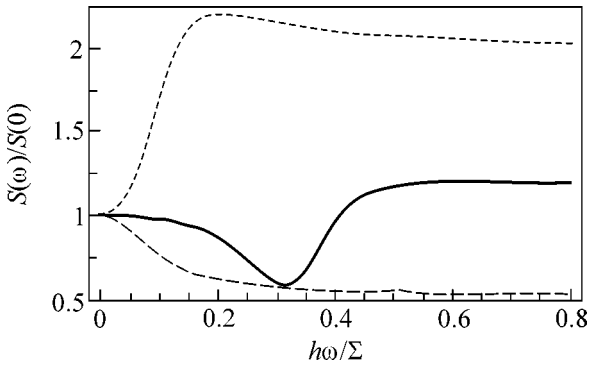

Fig. 3. Noise near $\omega = 0$ for the case of closely spaced levels $\Gamma_1 = \Gamma_2 = 0.1\Sigma$, where $\Sigma = (\epsilon_1 + \epsilon_2)/2$: $\Gamma_+/\Delta =$ (solid line) 0.25, (finely dashed line) 1, and (coarse-dashed line) 10.

REFERENCES

1. G. B. Lesovik, Pis'ma Zh. Éksp. Teor. Fiz. **70**, 209 (1999) [JETP Lett. **70**, 208 (1999)]; S.-R. Eric Yang, Solid State Commun. **81**, 375 (1992).
2. G. B. Lesovik and L. S. Levitov, Phys. Rev. Lett. **72**, 538 (1994).
3. V. A. Khlus, Zh. Éksp. Teor. Fiz. **93**, 2179 (1987) [Sov. Phys. JETP **66**, 1243 (1987)].
4. G. B. Lesovik, T. Martin, and J. Torres, Phys. Rev. B **60**, 11935 (1999).
5. J. Torries, T. Martin, and G. B. Lesovik, Phys. Rev. B **63**, 134517 (2001).
6. K. E. Nagaev and M. Büttiker, Phys. Rev. B **63**, 081301 (2001).
7. R. J. Schoelkopf, A. A. Kozhevnikov, D. E. Prober, and M. J. Rooks, Phys. Rev. Lett. **80**, 2437 (1998).
8. A. A. Kozhevnikov, R. J. Schoelkopf, and D. E. Prober, Phys. Rev. Lett. **84**, 3398 (2000).
9. A. Yacobi, M. Helblum, D. Mahalu, and H. Shtrikman, Phys. Rev. Lett. **74**, 4047 (1995).
10. C. Bruder, R. Fazio, and H. Schoeller, Phys. Rev. Lett. **76**, 114 (1996); T. Taniguchi and M. Büttiker, Phys. Rev. B **60**, 13814 (1999).
11. A. A. Kozhevnikov, Ph.D. Thesis (Yale, 2001).
12. M. P. Anantram and S. Datta, Phys. Rev. B **53**, 16390 (1996).

Translated by V. Sakun

JETP Letters, Vol. 74, No. 10, 2001, pp. 512–516. Translated from Pis'ma v Zhurnal Éksperimental'noĭ i Teoreticheskoĭ Fiziki, Vol. 74, No. 10, 2001, pp. 575–579.

Quantum Coherence between States with Even and Odd Numbers of Electrons

A. F. Andreev

Kapitza Institute for Physical Problems, Russian Academy of Sciences, ul. Kosygina 2, Moscow, 117334 Russia
e-mail: andreev@kapitza.ras.ru

Received October 19, 2001

Systems with variable numbers of electrons are described in which the states representing coherent superpositions of states with even and odd numbers of electrons may occur. An experiment is suggested which generalizes the experiment of Nakamura *et al.* and may provide direct evidence of such coherence and, thereby, justify the reality of a superspace. © *2001 MAIK "Nauka/Interperiodica"*.

PACS numbers: 03.65.-w; 05.30.Fk

In 1952, Wick, Wightman, and Wigner [1] claimed that the coherent linear superpositions of states with even and odd numbers of fermions are incompatible with the Lorentz invariance and introduced the superselection rule, according to which such linear superpositions are physically impossible. In actuality (as was pointed out in [2, 3]), the superselection rule is the alternative to the existence, along with *x, y, z,* and *t,* of additional spinor coordinates, which, in fact, are introduced in quantum field theory to account for supersymmetry.

The point is that the vector $|\text{odd}\rangle$ of any state with an odd number of fermions, being spinor of the odd rank, is multiplied by (–1) upon the rotations $\mathbf{O}(2\pi)$ of the coordinate system through an angle of 2π about any axis and upon the double time reversal $\mathbf{R}^2$. The vectors $|\text{even}\rangle$ of the states with an even number of fermions do not change under the $\mathbf{O}(2\pi)$ and $\mathbf{R}^2$ transformations. For this reason, the existence of a coherent linear superposition $a|\text{even}\rangle + b|\text{odd}\rangle$ (a and b are nonzero complex coefficients) implies the existence of a state physically changing under the $\mathbf{O}(2\pi)$ and $\mathbf{R}^2$ transformations, because the corresponding change of the state vector does not amount to the appearance of a common phase factor.

If *x, y, z,* and t completely characterize the space–time, then the $\mathbf{O}(2\pi)$ and $\mathbf{R}^2$ transformations coincide with the identical transformation, which can change nothing physically. The superselection rule is necessary in this case. If, in addition to *x, y, z,* and *t,* the spinor coordinates exist, $\mathbf{O}(2\pi)$ and $\mathbf{R}^2$ are physically real transformations changing the sign of the additional coordinates. In this case, the superselection rule is not required. Thus, the proof of the possible existence of states corresponding to the coherent superpositions of states with even and odd numbers of fermions is simultaneously the proof of the existence of a superspace with additional spinor coordinates. It should be emphasized that these arguments are not pertinent to the supersymmetry itself, which involves simultaneously the additional spinor coordinates and the superselection rule (see [4]).

In this work, it is proved theoretically that the superselection rule is, generally, not self-consistent. Namely, simple realistic systems with variable numbers of electrons are considered, which are governed by the Hamiltonians whose eigenvectors are all coherent superpositions of the states with even and odd numbers of electrons. The idea of the proof is as follows.

The number of electrons is a conserved quantity which is analogous, in this respect, to the momentum and the angular momentum. Physical systems with Hamiltonians whose eigenvectors are all coherent superpositions of the states with different momenta are well known. A particle in an external potential field depending on the particle coordinate is the simplest system of this type. In fact, this particle is part of an isolated system consisting of the particle and a certain massive body, the interaction with which can be described as an external field acting on the particle. As known, this is justified only if certain requirements are fulfilled. For example, the states of a massive body must adiabatically adjust to the changes in the particle coordinate in order to prevent excitation of the body degrees of freedom.

Below, the systems with variable numbers of electrons are considered which form, together with the environment, an isolated common system with a fixed number of electrons. The interaction of the system with the environment (an analogue of a massive body in the above-mentioned example) can be described as an external field acting on the system. In the case considered, this field does not commute with the electron operators in the system (by analogy with the fact that

the potential energy of interaction between a particle and a massive body does not commute with the particle momentum operator). Moreover, this field has the spinor character; i.e., it changes sign under the $\mathbf{O}(2\pi)$ and $\mathbf{R}^2$ transformations. All eigenfunctions of the Hamiltonian of the system are coherent superpositions of the states with even and odd numbers of electrons.

Below, an experiment will also be proposed which generalizes the Nakamura *et al.* experiment [5] on the observation of quantum coherence between the states with different (but even in both cases) numbers of electrons. The implementation of this experiment will directly demonstrate the coherence between the states with even and odd numbers of electrons.

1. Let us consider two typical examples where the interaction of the two parts of a total closed system can be described in terms of spinor external fields.

Let there be two quantum dots and one electron which can occur with close energies in either of the dots and has a certain spin projection, specified once and for all. The quantum dots have gates, whose electric potentials can be varied to move the electron energy levels. In the second quantization representation, a complete set of system states $|n, N\rangle$ consists of two states:

$$|0, 1\rangle, \quad |1, 0\rangle. \tag{1}$$

Here, n and N are the numbers of electrons in the first dot (which will be referred to as system) and the second dot (referred to as environment), respectively. The characteristic feature of states (1) is that the set of environment quantum numbers N is uniquely determined by the quantum numbers of the system: $N = 1 - n$. It is this property that allows the interaction of the system with environment to be treated as an external field acting on the system. Indeed, the state of a system comprising a part of the total closed system is generally described by the density matrix

$$|q'\rangle\langle q| = \sum_Q |q', Q\rangle\langle Q, q|,$$

where q and Q are the sets of quantum numbers, respectively, of the system and environment, and the summation is over all Q's which are possible for a given q and q'. In the case considered, no more than one term is nonzero in the sums, and the density matrix of the system, in actuality, corresponds to the pure state $|n\rangle = |n, 1 - n\rangle$.

With allowance made for electron tunneling between the quantum dots, the Hamiltonian of the total system is

$$H = H_0 + H_t, \tag{2}$$

where

$$H_0 = e(n) + E(N). \tag{3}$$

In Eq. (3), $e(n)$ and $E(N)$ are the energies of quantum dots in the gate potentials without tunneling, and

$$H_t = VaA^+ - V^*a^+A, \tag{4}$$

where V is the tunneling amplitude; a, a^+ and A, A^+ are the operators of electron annihilation and creation in the system and the environment, respectively. In the usual representation (see [6], Sec. 65), the action of the operators A and A^+ on vectors (1) is given by the formulas (if the result is nonzero)

$$A|0, 1\rangle = |0, 0\rangle, \quad A^+|1, 0\rangle = -|1, 1\rangle. \tag{5}$$

The substitution of Eqs. (5) into Hamiltonian (4) shows that the tunneling Hamiltonian in the case of interest is equivalent to the following interaction Hamiltonian involving only the system operators:

$$H_\eta = \eta a + \eta^* a^+. \tag{6}$$

Here, the operators a and a^+ act on the vectors $|n\rangle$ by the usual rules of an isolated system, and η is the external field equal to $-V$ in the representation used. The total Hamiltonian of the system is then

$$H = e(n) + E(1 - n) + H_\eta, \tag{7}$$

so that the total interaction energy is the sum of the second and third terms in Eq. (7). Under the $\mathbf{O}(2\pi)$ and $\mathbf{R}^2$ transformations, the field η, as well as the operators a and other spinor quantities, change sign so that, for a given field value, Hamiltonian (6) is not invariant about these transformations. Due to the presence of terms linear in electron operators, all eigenstates of the Hamiltonian are coherent superpositions of the states with even and odd numbers of electrons.

2. Let us consider a more complicated system, which generalizes the system used in the experiments of Nakamura *et al.* [5]. Let a single-Cooper-pair box B [5] be connected through tunneling contacts to a macroscopic superconductor (Cooper-pair reservoir) S and a quantum dot d. Our system differs from the system of Nakamura *et al.* by the presence of quantum dot d. Moreover, the sizes of box B must be such that the single-electron level spacing in it (on the order of $\delta \sim E_F/N$, where E_F is the Fermi energy and N is the total number of electrons in the box) is large compared both to temperature and to the amplitudes of electron tunneling from the box to d and S. In this sense, the box should be similar to the systems used in the experiments of Ralph *et al.* [7]. The box B and the quantum dot d have gates whose potentials U_B and U_d can be varied to vary the relative positions of energy levels. Let $|0\rangle$ be the box ground state with energy e_0 corresponding to the presence of a certain number of electron pairs in it (in the absence of tunneling). The number n of electrons in B is reckoned from its value in the $|0\rangle$ state. By varying

U_B, the energy e_2 of the box single-pair state $|2\rangle$ can be made close (on the δ scale) to e_0. In this case, the ground-state energy e_1 for $n = 1$ will not be close to e_0.

Assume that the quantum dot d may be either empty or contain one electron with an arbitrary spin projection (the energy of the two-electron state with opposite electron-spin projections is large because of the Coulomb interaction of electrons). Denote the corresponding energies by E_0 and E_1. By varying U_d, the sum $e_1 + E_1$ can be made close to $e_2 + E_0$. Therefore, the total system composed of the box B and its environment ($S + d$) can occur in four states with close energies (and zero total spin projection). In the second quantization representation $|n_1, n_2; N_1, N_2\rangle$, where n_α and N_α are the numbers of electrons with spin projections $\alpha = 1$ and 2 in the box and the dot, respectively, these are

$$|0, 0; 0, 0\rangle,\ |1, 0; 0, 1\rangle,\ |0, 1; 1, 0\rangle,\ |1, 1; 0, 0\rangle. \quad (8)$$

Inasmuch as the macroscopic superconductor S contains a Cooper-pair condensate, its state does not change upon changing the number of pairs by unity. As to the single electrons, they cannot appear in the superconductor, because the energy gap is assumed to be larger than δ.

In the states (8), the environment quantum numbers N_α are uniquely determined by the box quantum numbers n_α:

$$N_1 = (1 - n_1)n_2, \quad N_2 = (1 - n_2)n_1. \quad (9)$$

For this reason, the Hamiltonian

$$H_t = Va_\alpha A_\alpha^+ - V^* a_\alpha^+ A_\alpha, \quad (10)$$

(V is the tunneling amplitude, and a_α, a_α^+ and A_α, A_α^+ are the electron operators in the box and quantum dot, respectively) describing the tunneling interaction of B and d is equivalent to the Hamiltonian

$$H_\zeta = V(a_1 n_2 + a_2 n_1) + \text{h.c.}, \quad (11)$$

containing only the box operators. Indeed, one can directly verify that all matrix elements of Hamiltonian (10) between the states (8) are equal to the respective matrix elements of Hamiltonian (11) between the states

$$|n_1, n_2\rangle = |n_1, n_2; (1 - n_1)n_2, (1 - n_2)n_1\rangle.$$

Note that Hamiltonian (10) has nonzero matrix elements between the states (8) and the states with $N_1 = N_2 = 1$, whose energies, as mentioned above, are very high. The Hamiltonian (11), being the effective Hamiltonian of a system with the four energetically closely spaced states, naturally, has no such matrix elements.

After simple mathematics, Eq. (11) can be brought to the form

$$H_\zeta = \zeta n(a_1 + a_2) + \text{h.c.}, \quad (12)$$

where $n = n_1 + n_2$ and $\zeta = V$ is an external spinor field. It should be emphasized that Eqs. (12) and (6) are written in the form that is, evidently, not invariant about the spin rotations. The matter is that all the above considerations are not invariant about these transformations, because the original sets of states (1) and (8) are not invariant [the set (8) contains both singlet $|1, 0; 0, 1\rangle - |0, 1; 1, 0\rangle$ and triplet $|1, 0; 0, 1\rangle + |0, 1; 1, 0\rangle$ combinations]. Both (1) and (8) are complete sets of degenerate (in the absence of tunneling) states if the system is placed in an external magnetic field. This is of no significance when one is interested in the symmetry about the $\mathbf{O}(2\pi)$ and $\mathbf{R}^2$ transformations.

Due to the insensitivity of the state of superconductor S to a change in the number of Cooper pairs by unity, the tunneling interaction of the box B with superconductor S can also be described as the action of a scalar external field J on B. The interaction Hamiltonian is given by the well-known formula

$$H_J = Ja_2 a_2 + \text{h.c.} \quad (13)$$

The field magnitude $|J|$ is equal to a half of the Josephson energy, and the J phase is determined by the phase of the superconductor order parameter.

The total Hamiltonian of the box can be represented as

$$H = \left(2\epsilon_1 - \frac{\epsilon_2}{2}\right)n + \left(\frac{\epsilon_2}{2} - \epsilon_1\right)n^2 + H_\zeta + H_J, \quad (14)$$

where $\epsilon_1 = e_1 + E_1$ and $\epsilon_2 = e_2 + E_0$ are the energies of the states with one ($n = 1$) and two ($n = 2$) electrons; the energy origin is chosen so that the energy $e_0 + E_0$ of the ground state with $n = 0$ is zero.

The spinor external fields were considered in my work [2] without, however, specifying the exact conditions under which the interaction of a system with environment could be described using external fields. The one-electron example considered above was, in fact, also discussed earlier (see [8, 9], Chap. 5) and used in [2, 3, 8, 9] to draw the conclusion about non-self-consistency of the concept of the superselection rule.

3. Thus, the introduction of additional spinor space–time coordinates is the only way to attack the problem. Assuming that these coordinates are the nonrelativistic limit of the coordinates introduced in the field theory to account for the supersymmetry, one obtains [2, 3] additional anticommuting $\{\theta_\alpha, \theta_\beta\} = 0$ spinor coordinates θ_α, with $\alpha = 1$ and 2. Whatever the actual superspace structure is in the relativistic case, this simplest possibility should exist for every particular fermionic system in the nonrelativistic limit. This situation is analogous to that occurring for the Dirac bispinors or any other relativistic fermionic fields, which leave, in the nonrelativistic limit for spin 1/2, only the universal Pauli spinors. As was pointed out in [2, 3], the degrees of freedom of the systems considered above and in [2, 3]

possessing a set of several states with close energies correspond, at low temperatures where all usual spatial degrees of freedom are completely frozen out, to the "motion" of the system "as a whole" along the additional coordinates θ_α. In this case, the operators a_α^+ and a_α in the Hamiltonians of the types (6), (12), and (13) play the role of collective fermion coordinates and momenta: $a_\alpha^+ = \theta_\alpha$ and $a_\alpha = \partial/\partial\theta_\alpha$.

4. If the energy of one-electron states of the system described by Eq. (14) is far above all other energies, i.e., if $\epsilon_1 \gg \epsilon_2$, $|J|$, $|V|$, it becomes a two-level system considered by Nakamura *et al.* [5] obeying the time-dependent Shrödinger equations

$$i\dot{a} = \tau b, \quad i\dot{b} = \epsilon b + \tau^* a, \tag{15}$$

where $\tau = J$ and $\epsilon = \epsilon_2$. The general state of this two-level system is a superposition $a|0, 0\rangle + b|1, 1\rangle$ of states with different, but even, numbers of electrons.

In the limiting case $\epsilon_2 \gg \epsilon_1$, $|J|$, $|V|$, system (14) transforms to a two-level system of the second type obeying Eqs. (15) with $\epsilon = \epsilon_1 - 2|V|^2/\epsilon_2 + |J|^2/\epsilon_2$ and $\tau = \sqrt{2}\,JV^*/\epsilon_2$. Its general state is a superposition $a|0, 0\rangle + (b/\sqrt{2})(|1, 0\rangle + |0, 1\rangle)$ of states with even and odd numbers of electrons in the box.

The system considered in paragraph **1** is also a two-level system of the second type. The corresponding parameters are $\tau = -V$ and $\epsilon = e(1) - e(0) + E(0) - E(1)$, and the general state is $a|0\rangle + b|1\rangle$.

The experiment of Nakamura *et al.* [5] is as follows. Before the initial time ($t = 0$), a two-level system was in the ground state with the gate potential such that $\epsilon \gg \tau$. Accordingly, $a = 1$ and $b = 0$. At $t = 0$, the gate potential rapidly changes to a value for which $\epsilon = 0$. Then, the potential remains constant for a time Δt, after which it rapidly regains its initial value. On the time interval between $t = 0$ and $t = \Delta t$, the system obeys Eqs. (15) with $\epsilon = 0$ and initial conditions $a(t = 0) = 1$ and $b(t = 0) = 0$. Then $a(t) = \cos|\tau|t$ and $\bar{b}(t) = \sin|\tau|t$, where $\bar{b} \equiv (i\tau/|\tau|)b$ so that $|\bar{b}| = |b|$. At $t = \Delta t + 0$, one measures the excited-state population

$$|b(\Delta t)|^2 = \frac{1}{2}(1 - \cos 2|\tau|\Delta t) \tag{16}$$

as a function of pulse duration Δt. This can be done (as in the experiment of Nakamura *et al.* [5]) using a probe electrode connected to the box through a tunneling contact or (as in the experiment of Aassime *et al.* [10]) using a probe electrometer based on a single-electron transistor. The observed oscillations indicate that the system coherently oscillates between the states with electron numbers 0 and 2 on the time interval $(0, \Delta t)$. If such an experiment had been performed with a two-level system of the second type, it would have been proved that the corresponding systems coherently oscillate between the states with electron numbers 0 and 1. It should be emphasized that this interpretation of the oscillations is essentially based on the description of the system by the Hamiltonians (7) and (14), which account for the interaction with environment by introducing the fields J, ζ, and η. As pointed out in paragraph **3**, the systems considered are oscillators moving along the fermionic spatial coordinates θ_α. However, if one interprets oscillations (16) as a phenomenon occurring in the total closed system, then they are evidence only of the oscillatory electron transitions between different parts of the system. According to this interpretation, the oscillation frequency is proportional to $|\tau|$, i.e., to the tunneling amplitudes. One may note, in this connection, that the experiment of Nakamura *et al.* and the other experiments of this type can be refined by passing from the single-pulse to two-pulse technique.

As above, let the two-level system be at $t < 0$ in the ground state $a = 1$ and $b = 0$ ($\epsilon \gg |\tau|$). The amplitude of the first gate-potential rectangular pulse is the same as above (i.e., corresponds to $\epsilon = 0$), but its duration is fixed at $t_1 = \pi/4|\tau|$. Immediately after the pulse at $t = t_1 + 0$, the system is in the state with $a = b = 1/\sqrt{2}$. In the interval between $t = t_1$ and $t = t_1 + \Delta t$, the potential is equal to its initial value corresponding to $\epsilon \gg |\tau|$. Under these conditions, the tunneling interaction of the system with environment can be ignored and it behaves as a closed system in its pure state. In this case, $a(t) = 1/\sqrt{2}$ and $\bar{b}(t) = (1/\sqrt{2})\exp(i\phi(t))$, with the relative phase of the ground and excited states linearly depending on time: $\phi(t) = -\epsilon(t - t_1)$.

However, it would be incorrect to conceive that the environment is also in the pure state and the state vector of the total system is the product of the state vectors of its parts. In this case, the total system occurs in the so-called entangled state (see [11]).

The second gate-potential pulse with parameters of the first pulse is switched on at time $t_1 + \Delta t$. Using Eqs. (15), one can see that, after completion of the second pulse at time $2t_1 + \Delta t$ ($\Delta t \ll t_1$ because $\epsilon \gg |\tau|$), the population of the excited state is

$$|b|^2 = \frac{1}{2}(1 + \cos\epsilon\Delta t). \tag{17}$$

The observation of oscillations (17) as a function of time delay Δt between the pulses would demonstrate that the relative phase of the states with different numbers of electrons in a closed system has a definite value $\phi(t)$ linearly depending on time. For the two-level systems of the second type, this would be direct proof of the quantum coherence between the states with even and odd numbers of electrons.

This work was done during my visit to the Chalmers University. I am grateful to T. Claeson, A. Danilov,

L. Kuzmin, and R. Shekhter for hospitality and helpful discussions.

REFERENCES

1. G. C. Wick, A. S. Wightman, and E. P. Wigner, Phys. Rev. **88**, 101 (1952).
2. A. F. Andreev, Pis'ma Zh. Éksp. Teor. Fiz. **68**, 638 (1998) [JETP Lett. **68**, 673 (1998)].
3. A. F. Andreev, Physica B (Amsterdam) **280**, 440 (2000).
4. P. G. O. Freund, in *Introduction to Supersymmetry* (Cambridge Univ. Press, Cambridge, 1986), p. 7.
5. Y. Nakamura, Yu. A. Pashkin, and J. S. Tsai, Nature **398**, 786 (1999).
6. L. D. Landau and E. M. Lifshitz, *Course of Theoretical Physics*, Vol. 3: *Quantum Mechanics: Non-Relativistic Theory* (Nauka, Moscow, 1989, 4th ed.; Pergamon, New York, 1977, 3rd ed.).
7. D. C. Ralph, C. T. Black, and M. Tinkham, Phys. Rev. Lett. **74**, 3241 (1995); **76**, 688 (1996); **78**, 4087 (1997).
8. A. F. Andreev, Usp. Fiz. Nauk **168**, 655 (1998) [Phys. Usp. **41**, 581 (1998)].
9. A. F. Andreev, J. Supercond. **12**, 197 (1999).
10. A. Aassime, G. Johansson, G. Wendin, *et al.*, Phys. Rev. Lett. **86**, 3376 (2001).
11. J. M. Raimond, M. Brune, and S. Haroche, Rev. Mod. Phys. **73**, 565 (2001).

Translated by V. Sakun

JETP Letters, Vol. 74, No. 10, 2001, pp. 517–521. Translated from Pis'ma v Zhurnal Éksperimental'noĭ i Teoretichesko ĭ Fiziki, Vol. 74, No. 10, 2001, pp. 580–585.

The Efficiency of Repeaters Based on the Einstein–Podolsky–Rosen Effect for Quantum Cryptography in a Damping Channel

S. N. Molotkov

Institute of Solid State Physics, Russian Academy of Sciences, Chernogolovka, Moscow region, 142432 Russia

Received October 30, 2001

Based on the fundamental Holevo inequality and on the direct calculations, it is argued that the number of commitments required per one bit in a key in a damping channel increases exponentially with channel length. It is shown that the conclusion drawn recently by Duan *et al.* [4] that the exponential increase in resources for quantum cryptography in a damping channel can be reduced to the polynomial law by generating a through Einstein–Podolsky–Rosen pair is erroneous. Therefore, the results of [4] do not solve the fundamental problem restricting practical application of quantum cryptography at distances larger than the damping length. © *2001 MAIK "Nauka/Interperiodica".*

PACS numbers: 03.67.Dd; 03.65.Ud

Quantum cryptography can, in principle, ensure the ultimate security of key distribution between distant participants [1, 2]. One of the basic restrictions for practical application of quantum cryptosystems at large distances is damping in an optical fiber. For standard optical fiber lines, the distance at which quantum cryptosystems can operate is restricted to several tens of kilometers [3]. The exponential increase in the number of commitments per one bit at the receiving end with an increase in the channel length is unacceptable for practical application. Duan *et al.* recently proposed a quantum cryptosystem with repeaters based on the Einstein–Podolsky–Rosen (EPR) states and claimed that it requires only the polynomial increase in resources with increasing distance [4]. If such were the case, the problem of using quantum cryptography at large distances would, in principle, be solved. Unfortunately, this conclusion, in my opinion, is erroneous. In classical optical-fiber communication systems, the problem of damping is solved by using repeaters, whose action reduces to measuring a classical signal, creating a copy with higher intensity (amplification), and transmitting it to the next site. In the quantum case, copying is impossible if information states belong to a nonorthogonal basis [5]. Therefore, the transmission of a key along a chain from one site to another leads to the exponential decrease in its length even in an ideal channel. This conclusion follows from the Holevo inequality [6]. The mutual information about the key between two sites is fundamentally restricted by the inequality

$$I(x; y) \le \mathrm{Tr}\{\rho \log \rho\} - \sum_i p_i \mathrm{Tr}\{\rho_i \log \rho_i\}, \qquad (1)$$

where p_i is the prior information about the appearance of the i symbol (ρ_i state) from the alphabet at the entry. For a binary channel (the alphabet x, y consists of two symbols 0 and 1), the mutual information between the entry and the exit of a communication channel satisfies the inequality

$$I(x; y) \le 1, \qquad (2)$$

where equality is achieved if and only if the states ρ_i commute with each other (for pure states, this means that they are orthogonal). Therefore, when a key is transmitted along a chain from one site to another, the mutual information (key length) decreases exponentially even in an ideal channel:

$$I(n) \propto (I(x; y))^n, \qquad (3)$$

where n is the number of sites.

In relativistic quantum cryptography, orthogonal states can be used [7, 8]. In this case, the transmission of a key along a chain in an ideal channel does not lead to a decrease in the key length because $I(x; y) = 1$. For this reason, relativistic quantum cryptosystems can eventually be more efficient in applications. Thus, the maximal mutual information is achieved for orthogonal states, because they are classical in terms of distinguishability. Mutual information for nonorthogonal states is always smaller than unity. For this reason, let us consider a damping channel for orthogonal states; i.e., a channel where noise acts so that orthogonal states arrive at the exit with certain probability depending on the length. The capacity of a binary communication channel (the number of bits that can be transmitted with

0021-3640/01/7410-0517$21.00

an error as small as desired) is defined as the maximal of mutual information for all possible entrance states:

$$C_H = \max_{\{p_i, \rho_i\}} I(x; y). \quad (4)$$

Here, the mutual information is determined as

$$I(x; y) = S(x) - H(p), \quad (5)$$

where

$$S(x) = -\sum_{x = 0, 1} p(x)\log_2 p(x) = 1, \qquad p(0) = p(1) = \frac{1}{2} \quad (6)$$

is the entrance Shannon information, and

$$H(p) = -p\log_2 p - (1 - p)\log_2(1 - p) \quad (7)$$

is the entropy function with the conditional probability p defined as

$$p(x = 0|y = 0) = p(x = 1|y = 1) = 1 - p = \frac{1}{2}(1 + p(L)),$$
$$p(x = 0|y = 1) = p(x = 1|y = 0) = p = \frac{1}{2}(1 - p(L)), \quad (8)$$

where $p(L) = 1\exp(-L)$ is the probability of reaching the receiving end and L is the length of the communication channel. The conditional probability, say, $p(x = 0|y = 0)$ in Eq. (8) is the probability $1p(L) + (1/2)(1 - p(L))$ of correctly detecting the zero sent state. In the first term, the probability p(L) of arriving at the receiving end is multiplied by the probability of correct distinction, which is equal to unity for orthogonal states. The second term describes the case where the state does not reach the receiving end [probability is $1 - p(L)$]. In this case, the probability of correct identification in the absence of the state at the exit is equal to 1/2, i.e., to the probability of simple guessing. The determination of other conditional probabilities in Eq. (8) is similar. The channel capacity depends on length as

$$C_H(L) = 1 - H(p) = -\frac{1}{2}[(1 + p(L))\log_2(1 + p(L)) + (1 - p(L))\log_2(1 - p(L))] \approx p^2(L) = e^{-2L}. \quad (9)$$

The error at the receiving end is, in fact, associated with the absence of a state. Because of the exponentially low channel capacity for large L, the exponentially large number of entrance states should be transmitted per one bit at the receiving end. This channel capacity (dictated by the Holevo inequality) refers to the case where states are directly sent through the communication channel. In the presence of an EPR pair preliminarily distributed between the entrance and receiving ends, the channel capacity may be different (see, e.g., [9, 10]). Duan *et al.* [4] suggested that an EPR pair be propagated between the entry and exit of the channel through entanglement transfer along a chain between the neighboring EPR pairs generated at intermediate sites. In that work, the authors erroneously stated that this process requires resources increasing polynomially rather than exponentially with length. The matter is that, even if the channel is free from decoherence processes other than damping and even if EPR pairs are generated with unit probability at each intermediate site, the generation of the resulting EPR pair between the channel ends requires exponentially large number of attempts. This is due to the fact that pairs of photons from the left and right EPR pairs should be measured jointly if entanglement transfer occurs between two neighboring segments. The measurement is successful if each photon arrives at a detector. The probability that both photons from neighboring EPR pairs reach the detector is equal to the product of the probabilities p_1 for individual photons. Because of damping, this probability depends exponentially on the length of segments; i.e., $p_1 \propto \exp(-L_s)$. For the successful generation of a through EPR pair between the entry and exit, measurements realizing entanglement transfer must be successful for *all* segments. As a result, the probability that a through EPR pair is successfully generated is $\propto \exp(-nL_s)$ (n is the number of segments and $nL_s = L$ is the entire channel length). The concept of exponential damping with increasing communication channel length implies local measurements in the coordinate space. More precisely, the characteristic dimensions of a region where measurements are carried out should be much smaller than the damping length. For the classical case, this means that these local measurements of a signal in the vicinities of points spaced at a certain distance yield the outcome whose probability decreases exponentially with increasing distance between these points. Quantum states described by vectors in the Hilbert space must be "locked" to the Minkowski space–time. If measurements in small spatial regions are considered without such an explicit locking, i.e., only within the Hilbert space (as was done, e.g., in [4]), the concept of exponential damping with an increase in length also cannot be introduced. Let us consider a one-dimensional case. A one-particle state of a massless relativistic particle (photon) is generated by the generalized operator-valued functions $\varphi^+(\hat{x})$ [11] satisfying the commutation relations

$$[\varphi^-(\hat{x}), \varphi^+(\hat{x}')] = 0, \quad (10)$$

if $\hat{x} \sim \hat{x}'$ are spacelike. The normalized physical states ($|\psi\rangle \in \mathcal{H}$) are defined as the result of smoothing the

generalized operator functions with the basic functions $\psi(\hat{x})$ (for details, see [11]):

$$|\psi\rangle = \int d\hat{x}\psi(\hat{x})\varphi^+(\hat{x})|0\rangle = \int_{-\infty}^{\infty}\frac{dk}{k_0}\psi(k, k_0 = |k|)|\hat{k}\rangle,$$
$$\varphi^+(\hat{x}) = \frac{1}{\sqrt{2\pi}}\int d\hat{k}e^{i\hat{k}\hat{x}}\delta(\hat{k}^2)\theta(k_0)a^+(\hat{k}), \quad (11)$$
$$\psi(\hat{k}) = \psi(k, k_0) = \int d\hat{x}e^{-i\hat{k}\hat{x}}\psi(\hat{x}),$$
$$a^+(\hat{k})|0\rangle = |\hat{k}\rangle, \quad \langle\hat{k}|\hat{k}'\rangle = k_0\delta(k-k').$$

For the states propagating in one direction and transmitting information through the communication channels, the amplitude $\psi(k, k_0 = |k|)$ on the mass surface includes only the components with $k > 0$. The polarization structure of states is ignored for a while.

The evolution of states in an ideal communication channel is represented as the translation in the Minkowski space–time ($\hat{x} = (x, x_0)$); it is described by the translation operator in the Poincaré group and is an analogue of the time evolution operator $U(t) = \exp(-iHt)$ in the nonrelativistic case. The translation of a state by a vector $\hat{a} = (a, a_0)$ is expressed as

$$|\psi(\hat{a})\rangle = \hat{\mathbf{T}}(\hat{a})|\psi\rangle = \int d\hat{x}\psi(\hat{x})\hat{\mathbf{T}}(\hat{a})\varphi^+(\hat{x})\hat{\mathbf{T}}^{-1}(\hat{a})\hat{\mathbf{T}}(\hat{a})|0\rangle. \quad (12)$$

Taking into account that the vacuum vector is invariant, i.e., that $\hat{\mathbf{T}}(\hat{a})|0\rangle = |0\rangle$, we obtain

$$\hat{\mathbf{T}}(\hat{a})\varphi^+(\hat{x})\hat{\mathbf{T}}^{-1}(\hat{a}) = \varphi(\hat{x}+\hat{a}),$$
$$\hat{\mathbf{T}}(\hat{a})a^+(\hat{k})\hat{\mathbf{T}}^{-1}(\hat{a}) = e^{i\hat{k}\hat{a}}a^+(\hat{k}). \quad (13)$$

The measurement associated with finding a particle in the vicinity $(x, x + dx)$ at time x_0 is described by the expansion of unity

$$I = \int_{-\infty}^{\infty}dx\left(\int_{-\infty}^{\infty}\frac{dk}{\sqrt{k_0}}e^{-i\hat{k}\hat{x}}|\hat{k}\rangle\right)$$
$$\times\left(\int_{-\infty}^{\infty}\frac{dk'}{\sqrt{k_0'}}\langle\hat{k}'|e^{i\hat{k}'\hat{x}}\right) = \int_{-\infty}^{\infty}\mathcal{M}(\hat{x}, dx). \quad (14)$$

Accordingly, the probability is

$$\Pr\{\hat{x}, dx\} = \mathrm{Tr}\{\mathcal{M}(\hat{x}, dx)|\psi(\hat{a})\rangle\langle\psi(\hat{a})|\}$$
$$= |\psi(\hat{x}+\hat{a})|^2dx,$$
$$\psi(\hat{x}+\hat{a}) = \int_0^{\infty}\frac{dk}{\sqrt{k_0}}\psi(k, k_0 = |k|)e^{i\hat{k}(\hat{x}+\hat{a})}. \quad (15)$$

For states propagating in one direction ($k > 0$, $k_0 = k$), the probability depends only on the difference $x - x_0$:

$$\Pr\{x - x_0, dx\} = |\psi(x - x_0 + (a - a_0))|^2dx,$$
$$\psi(x - x_0) = \int_0^{\infty}\frac{dk}{\sqrt{k}}e^{ik(x-x_0)}\psi(k, k). \quad (16)$$

For a damping channel, the translation operator in Eqs. (12) and (13) should be replaced by the $\hat{\mathbf{S}}(\hat{a})$ matrix, an analogue of a nonrelativistic instrument (superoperator). In an ideal channel, the $\hat{\mathbf{S}}(\hat{a})$ matrix coincides with the translation operator. The superoperator can be represented as [12]

$$\hat{\mathcal{T}}_{\hat{a}}[\ldots] = \hat{\mathbf{S}}(\hat{a})[\ldots]\hat{\mathbf{S}}^+(\hat{a}). \quad (17)$$

The action of $\hat{\mathbf{S}}^+(\hat{a})$ on the $|\psi\rangle$ state, in the case of translation in a channel with exponential damping, implies that the matrix elements of $\hat{\mathbf{S}}(\hat{a})$ can be represented as

$$\langle\hat{k}|\hat{\mathbf{S}}(\hat{a})|\hat{k}'\rangle = e^{-\gamma|a-a_0|+i\hat{k}\hat{a}}k_0\delta(k-k'). \quad (18)$$

In contrast, the matrix elements of the $\hat{\mathbf{S}}(\hat{a})$ matrix [translation operator (13)] in an ideal channel have the form

$$\langle\hat{k}|\hat{\mathbf{T}}(\hat{a})|\hat{k}'\rangle = e^{i\hat{k}\hat{a}}k_0\delta(k-k'). \quad (19)$$

In this case, the probability of finding a particle in the vicinity $(x, x + dx)$ at time x_0 is

$$\Pr_{\mathrm{decay}}(\hat{x}, dx) = e^{-\gamma a}|\psi(\hat{x}-\hat{a})|^2dx$$
$$= e^{-\gamma|a-a_0|}\Pr\{\hat{x}, dx\}; \quad (20)$$

i.e., the probability of finding decreases exponentially relative to the corresponding probability (15) in an ideal channel. Let us turn to the two-particle EPR state. A polarization-entangled two-particle state can be represented as

$$|\psi_{\mathrm{EPR}}\rangle = \frac{1}{\sqrt{2}}\int\int d\hat{x}_1d\hat{x}_2\psi(\hat{x}_1, \hat{x}_2)$$
$$\times[\varphi^+(\hat{x}_1, +)\varphi^+(\hat{x}_2, -)\varphi^+(\hat{x}_1, -)\varphi^+(\hat{x}_2, +)]|0\rangle$$
$$= \frac{1}{\sqrt{2}}\int\int d\hat{k}_1d\hat{k}_2\psi(\hat{k}_1, \hat{k}_2)\delta(\hat{k}_1^2)\delta(\hat{k}_2^2)\theta(k_{01})\theta(k_{02})$$
$$\times[a^+(\hat{k}_1+)a^+(\hat{k}_2-) + a^+(\hat{k}_1-)a^+(\hat{k}_2+)]|0\rangle \quad (21)$$
$$= \frac{1}{\sqrt{2}}\int\int\frac{dk_1dk_2}{k_{01}k_{02}}\psi(k_1, k_{01} = |k_1|; k_2, k_{02} = |k_2|)$$
$$\times(|\hat{k}_1+, \hat{k}_2-\rangle + |\hat{k}_1-, \hat{k}_2+\rangle),$$

where $\varphi^+(\hat{x}, \pm)$ are the field creation operators for the states with polarizations $\pm$. Strictly speaking, because

of the presence of a common vacuum vector in the system of identical particles, the measurement of a two-particle state cannot generally be represented as a tensor product [13]. However, if individual subsystems have "marks," the measurement of individual subsystems is meaningful, although the unity expansion describing the measurement cannot be represented as a tensor product. In the case under consideration, the wave vector may be such a mark. Let us assume that $k_1 > 0$ and $k_2 < 0$ (photons of an EPR pair propagate in opposite directions). A measurement described by the projection onto a certain polarization state is nonlocal in the coordinate space; i.e., the outcome with the probability as close to unity as desired can be obtained if the spatial region where the measurement is carried out entirely covers the spatial part of state amplitude. For two observers carrying out measurements in bounded spatial regions, the EPR correlations for polarizations are described by the following expansion of unity

$$I_2 = \sum_{s_1, s_2 = \pm} \int_{-\infty}^{\infty}\int_{-\infty}^{\infty} \frac{dk_1 dk_2}{k_{01}k_{02}} |\hat{k}_1 s_1, \hat{k}_2 s_2\rangle\langle \hat{k}_2 s_2, \hat{k}_1 s_1|$$
$$= \sum_{s_{1,2} = \pm} \int_{-\infty}^{\infty}\int_{-\infty}^{\infty} dx_1 dx_2 \mathcal{M}(\hat{x}_1 s_1, \hat{x}_2 s_2),$$

where

$$\mathcal{M}(\hat{x}_1 s_1, \hat{x}_2 s_2) \tag{22}$$
$$= \left(\int_{-\infty}^{\infty}\int_{-\infty}^{\infty} \frac{dk_1 dk_2}{k_{01}k_{02}} e^{-i(\hat{k}_1\hat{x}_1 + \hat{k}_2\hat{x}_2)} |\hat{k}_1 s_1, \hat{k}_2 s_2\rangle\right)$$
$$\times \left(\int_{-\infty}^{\infty}\int_{-\infty}^{\infty} \frac{dk_1' dk_2'}{k_{01'}k_{02}'} e^{i(\hat{k}_1'\hat{x}_1 + \hat{k}_2'\hat{x}_2)} \langle \hat{k}_1' s_1, \hat{k}_2' s_2|\right).$$

The probability that one and two observers obtain the outcome in polarization channels σ_1 and σ_2 in the vicinities $(x_1, x_1 + dx_1)$ and $(x_2, x_2 + dx_2)$ at time instants x_{01} and x_{02}, respectively, is defined as

$$\Pr\{\hat{x}_1\sigma_1, \hat{x}_2\sigma_2\} dx_1 dx_2$$
$$= \mathrm{Tr}\{\mathcal{M}(\hat{x}_1\sigma_1, \hat{x}_2\sigma_2)|\psi_{EPR}\rangle\langle\psi_{EPR}|\} \tag{23}$$
$$= (\delta_{\sigma_1,+}\delta_{\sigma_2,-} + \delta_{\sigma_1,-}\delta_{\sigma_2,-})|\psi(\hat{x}_1, \hat{x}_2)|^2 dx_1 dx_2,$$

where

$$\psi(\hat{x}_1, \hat{x}_2) = \int_0^{\infty}\int_0^{\infty} \frac{dk_1 dk_2}{\sqrt{k_{01}k_{02}}} e^{ik_1(x_1 - x_{01})} \tag{24}$$
$$\times e^{-ik_2(x_2 - x_{02})} \psi(k_1, k_1, -k_2, -k_2).$$

The first factor in Eq. (23) describes the EPR correlations of polarizations, and the second factor takes into account the fraction corresponding to the spatial part of the state. There are no formal exclusions to the selection of the spatial amplitude in such a way that it is strongly localized. Measurements carried out in bounded regions will provide full correlation between the polarization states [the factor responsible in Eq. (23) for the spatial part of the state is always close to unity if the integration goes over as small an observation region as desired; i.e., $\iint dx_1 dx_2 |\psi(\hat{x}_1, \hat{x}_2)|^2 \approx 1$]. If the extended (almost monochromatic [4]) states are used, the second factor in Eq. (23) will diminish the probability of correlations for the measurements in bounded spatial regions smaller than the effective extent of the state. The amplitude is assumed to be strongly localized. Let the EPR pairs be generated in the vicinity of certain sites x_i at time x_0 and then propagate to sites for the measurements associated with entanglement transfer. We have

$$|\psi_{i,i+1}\rangle = \frac{1}{\sqrt{2}} \iint d\hat{x}_1 d\hat{x}_2 \psi(\hat{x}_1 - \hat{x}_i, \hat{x}_2 - \hat{x}_i) \tag{25}$$
$$\times [\varphi^+(\hat{x}_1+)\varphi^+(\hat{x}_2-) + \varphi^+(\hat{x}_1-)\varphi^+(\hat{x}_2+)]|0\rangle,$$

where the time argument of $\hat{x}_i = (x_i, x_{0i})$ is assumed to be identical for all $i = 1, 2, \ldots, n$ (EPR pairs are generated simultaneously). This assumption is insignificant and simplifies the calculations. All distances between the neighboring sites are also assumed to be identical. Measurements of the entanglement transfer between the neighboring i and $i + 1$ EPR states are carried out in the small vicinities of sites $\hat{y}_{i,i+1} = (y_{i,i+1}, y_0)$. The favorable outcome of the measurement can be obtained only at time y_0 (because of a strong localization of the spatial amplitude), which is determined by the time it takes for particles to travel from sites where the EPR pair is generated to sites where measurements on entanglement transfer are carried out. The measurements on entanglement transfer in the vicinities of points $\hat{y}_{i,i+1}$ are given by the expansion of unity

$$I_2 = \frac{1}{2} \sum_{s_{1,2}, \alpha = \pm} \int_{-\infty}^{\infty}\int_{-\infty}^{\infty} dy_1 dy_2 \left(\iint \frac{dk_1 dk_2}{\sqrt{k_{01}k_{02}}}\right.$$
$$\times e^{-i\hat{k}_1(\hat{y}_1 - \hat{y}_{i,i+1}) - i\hat{k}_2(\hat{y}_2 - \hat{y}_{i,i+1})}$$
$$\left.\times (|k_{i+1}s_1, \hat{k}_{i+2}s_2\rangle + \alpha|k_{i+1} - s_1, \hat{k}_{i+2} - s_2\rangle)\right)$$
$$\times \left(\iint \frac{dk_1' dk_2'}{\sqrt{k_{01}'k_{02}'}} e^{i\hat{k}_1'(\hat{y}_1 - \hat{y}_{i,i+1}) + i\hat{k}_2'(\hat{y}_2 - \hat{y}_{i,i+1})}\right. \tag{26}$$
$$\left.\times (\langle s_1\hat{k}_{i+1}, s_2\hat{k}_{i+2}| + \alpha\langle -s_1\hat{k}_{i+1}, -s_2\hat{k}_{i+2}|)\right)$$

$$= \int_{-\infty}^{\infty}\int_{-\infty}^{\infty} \mathcal{M}(\hat{y}_1 - \hat{y}_{i,i+1}, \hat{y}_2 - \hat{y}_{i,i+1}, dy_1 dy_2).$$

The evolution of states in the damping channel is obtained by the action of an instrument on either of the particles in the EPR pairs similarly to Eqs. (17) and (19). Taking into account the structure of $\psi(\hat{x}_1, \hat{x}_2)$, one can reduce this action to

$$\hat{\mathbf{S}}_2(-\hat{a}, \hat{a})|\psi_{i,i+1}\rangle = \frac{1}{\sqrt{2}}\int_0^\infty\int_0^\infty \frac{dk_1 dk_2}{\sqrt{k_{01}k_{02}}}\psi_1(k_1, k_1) \times \psi_1(k_2, k_2) e^{ik_1[(x_1+a)-(x_0+a_0)]-\gamma|a-a_0|} \times e^{-ik_2[(x_2+a)-(x_0+a_0)]-\gamma|a+a_0|}(|\hat{k}_1+, \hat{k}_2-\rangle + |\hat{k}_1-, \hat{k}_2+\rangle), \tag{27}$$

which corresponds to the damping translation of one particle in the positive direction of the x axis and the other in the negative direction. The through EPR pair is formed due to the entanglement transfer between all neighboring pairs only in the case where the measurements at all intermediate sites yield the favorable outcome, whose probability is given as

$$\begin{aligned}&\Pr\{\hat{x}_2 - \hat{y}_{2,3}, \hat{x}_3 - \hat{y}_{2,3}, \ldots, \hat{x}_{n-1} - \hat{y}_{n-2,n-1}\}dx_2 dx_3 \ldots dx_{n-2} dx_{n-1}\\ &= \mathrm{Tr}\{(\hat{\mathbf{S}}_2\rho_{1,2}\hat{\mathbf{S}}_2^+)(\hat{\mathbf{S}}_2\rho_{3,4}\hat{\mathbf{S}}_2^+)\ldots(\hat{\mathbf{S}}_2\rho_{n-1,n-2}\hat{\mathbf{S}}_2^+)\mathcal{M}(\hat{x}_2 - \hat{y}_{2,3}\hat{x}_3 - \hat{y}_{2,3}, dx_2 dx_3)\ldots\\ &\quad\times \mathcal{M}(\hat{x}_{n-2} - \hat{y}_{n-2,n-1}, \hat{x}_{n-1} - \hat{y}_{n-2,n-1}, dx_{n-2}dx_{n-1})\}\\ &= (e^{-\gamma a}|\psi_2(x_2 - y_{2,3} - (x_0 - y_0))|^2 dx_2)\ldots(e^{-\gamma a}|\psi_{n-1}(x_{n-1} - y_{n-2,n-1} - (x_0 - y_0))|^2 dx_{n-1}).\end{aligned} \tag{28}$$

It is assumed that the outer particles 1 and n are not subjected to measurements and remain free (the trace over these states is taken with unity operator). Each factor describes the probability of a pair of particles from neighboring EPR pairs being detected at intermediate sites. The favorable outcome takes place only if *all* detectors operate. The probability of this outcome is

$$\Pr \propto e^{-n\gamma a} = e^{-\gamma L}, \quad L = na, \tag{29}$$

and decreases exponentially with increasing channel length, in contrast to the power-law decrease stated by Duan *et al.* [4]. This implies that an exponentially large number of attempts at generating intermediate EPR pairs is required to form a through EPR pair. The only method for applying quantum cryptography at large distances likely consists in the production of communication channels based on new materials whose damping constant is smaller than those in the available optical fiber systems.

I am grateful to S.S. Nazin for stimulating discussions and useful remarks. This work was supported by the projects "Physical Foundations of Quantum Calculations," "Electron States," and by the Russian Foundation for Basic Research (project no. 02-02-16289).

REFERENCES

1. C. H. Bennett and G. Brassard, in *Proceedings of IEEE International Conference on Computer Systems and Signal Processing, Bangalore, India, 1984*, p. 175.
2. A. K. Ekert, Phys. Rev. Lett. **67**, 661 (1991).
3. N. Gisin, G. Ribordy, W. Tittel, and H. Zbinden, quant-ph/0101098.
4. L.-M. Duan, M. Lukin, J. I. Cirac, and P. Zoller, quant-ph/0105105.
5. C. H. Bennett, Phys. Rev. Lett. **68**, 3121 (1992); C. H. Bennett, G. Brassard, and N. D. Mermin, Phys. Rev. Lett. **68**, 557 (1992).
6. A. S. Kholevo, Probl. Inf. Transm. **9**, 177 (1973).
7. L. Goldenberg and L. Vaidman, Phys. Rev. Lett. **75**, 1239 (1995); quant-ph/9506030.
8. S. N. Molotkov and S. S. Nazin, quant-ph/0008008; Pis'ma Zh. Éksp. Teor. Fiz. **73**, 767 (2001) [JETP Lett. **73**, 682 (2001)].
9. C. H. Bennett, P. W. Shor, J. A. Smolin, and A. V. Thapliya, quant-ph/0160052.
10. A. S. Holevo, quant-ph/0106075.
11. N. N. Bogolyubov, A. A. Logunov, A. I. Oksak, and I. T. Todorov, *General Principles of Quantum Field Theory* (Nauka, Moscow, 1987).
12. K. Kraus, *States, Effects and Operations* (Springer-Verlag, Berlin, 1983).
13. R. Laiho, S. N. Molotkov, and S. S. Nazin, Phys. Lett. A **275**, 36 (2000); Phys. Lett. A **278**, 9 (2000).

Translated by R. Tyapaev